A STABLE ISOTOPE APPROACH TO NEOTROPICAL CLOUD FOREST PALEOCLIMATOLOGY

by

Kevin John Anchukaitis

A Dissertation Submitted to the Faculty of the

DEPARTMENT OF GEOSCIENCES

In Partial Fulfillment of the Requirements

For the Degree of

DOCTOR OF PHILOSOPHY

In the Graduate College

THE UNIVERSITY OF ARIZONA

2 0 0 7

THE UNIVERSITY OF ARIZONA
GRADUATE COLLEGE

As members of the Final Examination Committee, we certify that we have read the dissertation prepared by Kevin John Anchukaitis
entitled A Stable Isotope Approach to Neotropical Cloud Forest Paleoclimatology
and recommend that it be accepted as fulfilling the dissertation requirement for the Degree of Doctor of Philosophy.

Michael N. Evans — Date: 23 April 2007

Julio L. Betancourt — Date: 23 April 2007

Malcolm K. Hughes — Date: 23 April 2007

Julie E. Cole — Date: 23 April 2007

Jonathan T. Overpeck — Date: 23 April 2007

Final approval and acceptance of this dissertation is contingent upon the candidate's submission of the final copies of the dissertation to the Graduate College.

I hereby certify that I have read this dissertation prepared under my direction and recommend that it be accepted as fulfilling the dissertation requirement.

Dissertation Director: Michael N. Evans — Date: 23 April 2007

STATEMENT BY AUTHOR

This dissertation has been submitted in partial fulfillment of requirements for an advanced degree at The University of Arizona and is deposited in the University Library to be made available to borrowers under rules of the Library.

Brief quotations from this dissertation are allowable without special permission, provided that accurate acknowledgment of source is made. Requests for permission for extended quotation from or reproduction of this manuscript in whole or in part may be granted by the head of the major department or the Dean of the Graduate College when in his or her judgment the proposed use of the material is in the interests of scholarship. In all other instances, however, permission must be obtained from the author.

SIGNED: Kevin John Anchukaitis

ACKNOWLEDGEMENTS

There are dozens of people that have helped make this research a reality. First and foremost, I owe a debt of gratitude to my advisor, Mike Evans, for allowing me to come to Arizona to work with him on tropical dendroclimatology and paleoclimatology. Throughout my years at Arizona, Mike has provided me with unlimited opportunities to expand my education and research experience. He has been unwavering in his optimism and support, always willing to give me the latitude to explore new ideas but diligent in his guidance. It has been my extremely good fortune to have him as my mentor. Julio Betancourt and Malcolm Hughes have been incredibly generous with their wisdom and their time, and have been unfailingly positive and encouraging. I will miss very much their enthusiasm and our conversations. Julie Cole and Jonathan Overpeck have always kept my eye on the larger context of my research.

Laboratory portions of this research were made possible by the diligence, knowledge, and creative thinking of John Buchanan, MC Foo, Lisa Wade, Greg Eischeid, Heidi Barnett, Rex Adams, Brooke Rabe, Brianna Muhlenkamp, Chris Jones, Jim Burns, Bruno Lavettre, David Dettman, Dave Steinke, Ben McElhaney, and Martin Munro. In Costa Rica, I benefitted tremendously from the assistance of Frank Joyce, Koky Porras, Alan Pounds, Eladio Cruz, and Arturo Cruz. Access to Monteverde was facilitated through the Tropical Science Center (Rafael Bolanos, Carlos Hernndez) and the Organization for Tropical Studies. My collaborators Nat Wheelwright, Dan Schrag, Todd Lange, Dave Smith, and Steve Leavitt have all contributed important advice, ideas, and data to various aspects of this work. I also thank Todd Dawson, David Killick, and Henry Diaz for their continued support of me and of this research.

My housemates, Mary Good, Jerome Guynn, and Tim Shanahan, all of them talented scholars as well as good friends, have been instrumental in keeping me optimistic, happy, and sane. I have been very fortunate to be surrounded by a wonderful, supportive group of friends and colleagues including Toby Ault, Jessica Conroy, Tom Damassa, Matt Devitt, Nathan English, Anna Felton, Nicole Flowers, Andy Frassetto, Camille Holmgren, Kevin Jones, Dave Keeler, Lynnette Kleinsasser, Susan Mentzer, Maarten de Moor, Christa Placzek, Dan Potts, Jessica Rowland, Britt Starkovich, Scott St. George, Aly Thibodeau, and many others. Indeed, the graduate students, faculty, and staff of the Laboratory of Tree-Ring Research and Department of Geosciences have given me five wonderful years in an amazing and generous academic community.

Mary Gagen – my colleague, friend, and partner – has been a constant source of support, expertise, wisdom, and love, and I would never have made it without her. My parents, Melanie and Stephen, and my brother, Jeff, have supported me through 25 years of education with patience, humor, and unquestioning love. This thesis is dedicated to all of them.

This research was made possible by generous funding from the National Science Foundation and the Department of Energy. Specific grants and fellowships are acknowledged individually in the attached appendices to this dissertation.

DEDICATION

This dissertation is dedicated to my parents, Melanie and Stephen, and to my brother, Jeff, for their patience, love, and unyielding support.

TABLE OF CONTENTS

TABLE OF CONTENTS – *Continued*

TABLE OF CONTENTS – *Continued*

LIST OF FIGURES

LIST OF FIGURES – *Continued*

LIST OF TABLES

ABSTRACT

Many tropical trees do not form reliable annual growth rings, making it a challenge to develop tree-ring width chronologies for application to paleoclimatology in these regions. Here, I seek to establish high-resolution proxy climate records from trees without rings from the Monteverde Cloud Forest in Costa Rica using stable isotope dendroclimatology. Neotropical cloud forest ecosystems are associated with a relatively narrow range of geographic and hydroclimatic conditions, and are potentially sensitive to climate variability and change at time scales from annual to centennial and longer.

My approach takes advantage of seasonal changes in the δ^{18}O of water sources used by trees over a year, a signature that is imparted to the radial growth and provides the necessary chronological control. A rapid wood extraction technique is evaluated and found to produce cellulose with δ^{18}O values indistinguishable from conventional approaches, although its application to radiocarbon requires a statistical correction. Analyses of plantation-grown *Ocotea tenera* reveal coherent annual δ^{18}O cycles up to 9‰. The width of these cycles corresponds to observed basal growth increments. Interannual variability in δ^{18}O at this site is correlated with wet season precipitation anomalies. At higher elevations within the orographic cloud bank, year-to-year changes in the amplitude of oxygen isotope cycles show a relationship with dry season climate.

Longer δ^{18}O chronologies from mature *Pouteria* (Sapotacae) reveal that dry season hydroclimatology is controlled at interannual time scales by variability in the eastern equatorial Pacific (ENSO) and the Western Hemisphere Warm Pool (WHWP), which are correlated with trade wind strength and local air temperature. A change in the late

1960s toward enhanced annual $\delta^{18}O$ amplitude may reflect low frequency changes in the Atlantic and Pacific ocean-atmosphere system. This study establishes the basis for cloud forest isotope dendroclimatology and demonstrates that the local climate of neotropical cloud forests is sensitive to interannual, and perhaps, multidecadal changes in important large-scale modes of climate variability.

CHAPTER 1

INTRODUCTION

1.1 Statement of the Problem

The tropical ocean-atmosphere system influences climate and weather at a global scale, and variability in the system across a range of time scales results in anomalous patterns of both temperature and precipitation around the world. The result can be the disruption or destruction of habitat, transportation, agriculture, and infrastructure, and the concomitant economic, political, environmental, and social costs of recovery. Despite this, considerable uncertainty exists regarding both the potential behavior of and controls on tropical climate system variability at time scales from years to centuries and longer. This uncertainty extends to interactions between the Pacific and Atlantic Oceans as well as the range of potential responses to radiative forcing. Substantial uncertainties also exist for predictions of spatiotemporal changes in regional hydroclimatology due to anthropogenic greenhouse gas emissions and the accompanying alterations to the global energy balance [c.f. *Douville*, 2006; *Douville et al.*, 2006; *Neelin et al.*, 2006].

Uncertainties concerning tropical climate system state and behavior arise due in part to the lack of long-term meteorological records from these regions. Even where continuous climate records exist, they often cover too limited a time span to resolve ocean-atmosphere variability or feedbacks which may have preferred timescales of decades or longer. Paleoclimate reconstructions of precipitation and temperature can help alleviate the limitation of the instrumental, observational record for interpreting tropical climate dynamics and the potential range of natural variability; however, high-

resolution paleoclimate proxies from the *terrestrial* tropics are thus far mostly limited to comparatively few speleothem, ice core, and varved lake sediment records.

1.2 Background

1.2.1 The Tropics

1.2.1.1 The Pacific

The El Niño Southern Oscillation (ENSO), a coupled interaction between the ocean and atmosphere of the tropical Pacific Ocean, is the leading mode of global interannual climate variability [*Cane*, 2005]. During warm ENSO events, anomalously warm waters move toward the east along the equator into the normally colder waters associated with deep ocean upwelling and a shallow thermocline. Accompanying the changes in sea surface temperatures (SST), sea level pressures also shift, with low pressure anomalies over the eastern tropical Pacific, and anomalously high pressure descending on the western Pacific, Indonesia, and eastern Australia [*Rasmusson and Wallace*, 1983; *Diaz and Kiladis*, 1992].

These changes result in anomalous zonal atmospheric circulation and wind patterns, bringing drought to the western Pacific, and heavy rains to the west coast of South America. Through concurrent changes in atmospheric circulation, the effect of ENSO are also felt around the globe. During canonical ENSO events, the southwestern and southeastern United States experiences a wetter winter, while the northwest and northern Prairies are dry [*Diaz et al.*, 2001]. Canonical teleconnections, however, may conceal more complicated seasonal to interdecadal spatiotemporal patterns. On the southeastern coast of the United States, for instance, warm ENSO events are associated not only with a wetter winter, but also a subsequently drier summer [*Diaz et al.*, 2001]. In the Caribbean

and Central America, warm ENSO events are associated typically with wetter boreal winter dry seasons and drier summer wet seasons [*Diaz et al.*, 2001], but the sign of the correlation depends on the modulating influence of the Atlantic Ocean, as well as whether the Pacific or Caribbean side of the Central American cordillera is considered [*Giannini et al.*, 2001a].

Decadal-scale variability can be detected within the interannual behavior of the ENSO system. It is commonly characterized by periods of lesser or greater tropical SST anomaly (SSTA) amplitudes [*Urban et al.*, 2000; *Yeh and Kirtman*, 2005], and has a basin-wide expression [*Garreaud and Battisti*, 1999; *Tomita et al.*, 2001; *Evans et al.*, 2001; *Newman et al.*, 2003]. The wavelet-based spectral analysis of *Torrence and Webster* [1999] identified periods of high canonical ENSO wavelength variance from 1875 to 1920 and from 1960 to 1990. A period of low ENSO variance occurred from 1920 to 1960. Periods of low and high variance in the canonical ENSO band as identified in *Torrence and Webster* [1999] agree with those seen in evolutionary spectral analysis of reconstructed NINO 3.4 SST records by *Urban et al.* [2000]. The tree-ring based reconstruction of ENSO by *Stahle et al.* [1998] also shows decadal-scale fluctuations in the amplitude of the canonical ENSO frequencies.

There have been a number of attempts to explicitly reconstruct decadal modes of both tropical and extratropical Pacific climate variability using high resolution proxies. *Evans et al.* [2001], *Biondi et al.* [2001], *D'Arrigo et al.* [2001] and *MacDonald and Case* [2005] have used tree-ring chronologies from western North and South America to develop reconstructions extending back as far as AD 1000. Stable isotope proxies from corals have also been successfully used to identify decadal patterns of SST variability [*Linsley et al.*, 2000; *Urban et al.*, 2000]. The reconstructions are not, however, identical. In fact, in many cases the independent reconstructions show little coherency prior to the current

century [*Gedalof et al.*, 2002]. *Evans et al.* [2002] further point out that reconstructed (coral and tree-ring) and instrumental Pacific sea surface temperatures show different spectral power at low frequencies. With existing proxy records, largely extratropical tree rings and marine corals, it is still difficult to estimate what the magnitude and preferred time scale of interannual to multidecadal variability in the Pacific may have been over the last several centuries.

1.2.1.2 The Atlantic

The tropical Atlantic also displays variability over a range of time scales. High-frequency interannual variations in the equatorial Atlantic are associated with the so-called Atlantic Niño [c.f *Chang et al.*, 2006] and the North American Oscillation [NAO; *Seager et al.*, 2000]. Since the NAO is related to the strength of the subtropical high pressure cell in the Atlantic, it also has an influence on trade wind strength and SSTs in the subtropical and tropical Atlantic and Caribbean [*Seager et al.*, 2000]. Both the Atlantic Nino and NAO may reflect the influence of remote Indo-Pacific tropical forcing [*Hoerling et al.*, 2001; *Hoerling and Kumar*, 2003; *Chang et al.*, 2006]. The cross-equatorial SST gradient between northern and southern tropical Atlantic influences the position of the ITCZ and tropical trade wind strength at interannual time scales as well, and therefore both rainfall and sea-air latent heat feedbacks on both SST anomalies and wind [*Wang and Carton*, 2003; *Xie and Carton*, 2004].

At multidecadal timescales, both tropical and extratropical Atlantic variability is prominently related to the Atlantic Multidecadal Oscillation (AMO), which is centered on the North Atlantic and characterized by relatively rapid multidecadal shifts between warmer and colder conditions [*Enfield et al.*, 2001]. From approximately 1930 to 1970, the Atlantic was in a warm phase. From 1970 to 1995, the Atlantic shifted to a cold phase

[*Enfield et al.*, 2001]. The warm phase of the AMO is related to spatiotemporal SST patterns similar to those that exist during prolonged negative phases of the NAO [*Grosfeld et al.*, 2007]. *Gray et al.* [2004] used tree-ring chronologies from North America, Europe, and North Africa to reconstruct the index of the AMO over the period 1567 to 1990, which demonstrated significant mulitdecadal power over nearly the entire period. Evidence for robust multidecadal variability in the Atlantic coupled with long GCM simulations have been used to suggest that the AMO is the result of periodic changes in thermohaline circulation and meridional overturning circulation (MOC) in the North Atlantic [*Knight et al.*, 2005].

Interaction between the Pacific and Atlantic Oceans at decadal time scales appears to play an important role in extratropical climate as well. *Cole et al.* [2002] found that some major North American droughts, including that of the 1950s, corresponded to La Niña (cold) conditions in the Pacific, while other droughts, including the 1930s Dust Bowl, were only marginally correlated with Pacific SSTs. In their analysis, *McCabe et al.* [2004] used instrumental PDSI measurements to hypothesize that patterns of severe drought were related to the interaction between Pacific and Atlantic SST forcing, with severe drought occurring when the Atlantic Ocean was in a cold (negative) phase. Modeling studies have also suggested that Pacific SST anomalies alone are not sufficient to force droughts with the spatial and temporal characteristics of the Dust Bowl [*Schubert et al.*, 2004]. The Atlantic could therefore be an important determinant of extratropical climate at decadal-scales or longer, in addition to potentially mediating the canonical teleconnections associated with ENSO. However, *Mann and Emanuel* [2006] have shown that the residual sea surface temperature signal from the tropical Atlantic after accounting for global SST patterns does not have a robust multidecadal signal similar to the AMO. This finding suggests that observed multidecadal trends in the tropical Atlantic are

primarily related to greenhouse gas and aerosol forcing over the 20th century. Whether endogenous multidecadal tropical variability exists in the Atlantic is difficult to determine over the period of instrumental and historical observations, since it is inextricable linked to global scale forcing.

It is an active research question whether variability in the Pacific drives changes in the Atlantic, or whether multidecadal variability in the Atlantic, perhaps arising from changes in ocean circulation in the North Atlantic [*Knight et al.*, 2005] can influence the amplitude of interannual and interdecadal variability in the Pacific. For instance, *Dong et al.* [2006] used a coupled ocean-atmosphere GCM with an imposed Atlantic SSTA forcing to mimic the AMO. In these simulations, easterly surface wind anomalies over the central and western Pacific forced by latent heat flux in the tropical North Atlantic deepened the western Pacific themocline, stabilizing the ocean-atmosphere coupled instability in the tropical Pacific and reducing ENSO variance. The more common view has been that ENSO influences the Atlantic via atmospheric teleconnections [c.f. *Latif*, 2001]. *Wang and Enfield* [2001] have shown that warm ENSO anomalies influence the Western Hemisphere Warm Pool via the connection of anomalous Walker circulation to changes in the Atlantic subtropical high. Similarly, *Giannini et al.* [2001b] hypothesized that ENSO influenced the tropical Atlantic variability through the stabilization of the tropical atmosphere via the propagation of the warming signal through the troposphere. These and numerous other studies point to extant uncertainties regarding the forcing mechanisms for the observed association between Atlantic and Pacific variability at a variety of time scales.

1.2.2 Tropical climate change: phenomenology and dynamics

At least three important research questions arise out of observations and modeling of the Pacific and Atlantic ocean-atmosphere variability discussed above. First, there are outstanding issues regarding the preferred time scale and stability of decadal scale variability in the tropical Pacific [*Cane and Evans*, 2000; *Evans et al.*, 2001], which might be better resolved by an expanded network of high resolution tropical proxy records. Second, similar questions exist regarding tropical North Atlantic variability and its characteristic natural and forced time scales and variability. Removing the global sea surface temperature signal from the tropical Atlantic reveals no significant multidecadal variance. However, as *Mann and Emanuel* [2006] note, this is based on the assumption that the tropical Atlantic signal does not project significantly onto the global mean. Whether this assumption is valid over longer time scales than considered by *Mann and Emanuel* [2006], or even under current transient forcing, is difficult to resolve using the instrumental record alone. Finally, understanding the interactions and feedbacks between the Atlantic and Pacific is critical for interpreting variability in the paleoclimate record and understanding potential global teleconnections associated with both the tropics and North Atlantic. For instance, if ocean circulation in the Atlantic forces multidecadal or longer changes in the Pacific through changes in sea surface temperatures and circulation anomalies generated in the tropics, this has substantial implications for feedbacks between thermohaline circulation and the Asian monsoon, and could help explain how regional signals associated with the MOC can propagate globally. There is clear evidence that variability across a range of time scales between the Atlantic and Pacific are linked. However, the mechanisms, stability, and directionality of those linkages remain unclear and in some cases contradictory. [*Schwing et al.*, 2003] found that North Atlantic and North Pacific variability at decadal scales was positively correlated until the 1950s, and

negatively correlated after that time. The stability of interbasin interactions may therefore be a function of other, low frequency components of their variability.

1.2.3 Why tropical dendroclimatology?

Hundreds of tree-ring width and density chronologies provide a spatially extensive data network for high resolution paleoclimate reconstructions in temperate regions. Because they have annual or seasonal resolution and are exactly dated, these records can be empirically calibrated against existing instrumental data in order to develop quantitative reconstructions of past climatic variables. Relatively few such tree-ring chronologies, however, have been developed in tropical regions. Despite some notable exceptions [c.f. *Worbes*, 2002; *Fichtler et al.*, 2004; *D'Arrigo et al.*, 2006], many trees in the tropics do not develop reliably annual rings whose variability reflects the influence of climate variability and can be utilized for paleoclimate reconstructions. Even when they appear to form annual increment bands, patterns of ring width variability may be incoherent between individual trees, making both chronology development and climate signal detection difficult [*Worbes and Junk*, 1989; *February and Stock*, 1998; *Dünisch et al.*, 2002; *Speer et al.*, 2004; *Robertson et al.*, 2004; *Bauch et al.*, 2006]. As a consequence, high-resolution, long terrestrial proxy climate records from the tropics remain sparse compared to temperate regions.

1.2.4 Neotropical montane cloud forests

Tropical montane cloud forests cover as much as 50 million hectares worldwide [*Stadtmüller*, 1987], about half of which is found in Latin America [*Brown and Kappelle*, 2001]. Cloud forests are characterized by frequent or persistent ground-level clouds and fog (horizontal or 'occult' precipitation) and have a multicanopy forest laden

with epiphytes [*Stadtmüller*, 1987; *Haber*, 2000]. These forests have high rates of endemism [*Brown and Kappelle*, 2001] and are important in regional hydrology, since they intercept cloud moisture, increasing available water and influencing biogeochemistry within catchments and in areas downstream.

Tropical cloud forests are ecosystems found within a relatively narrow set of both geographic and meteorological conditions, and as a consequence, they are particularly sensitive to climate change [*Loope and Giambelluca*, 1998; *Foster*, 2001; *Bush*, 2002]. Computer modeling of climate under doubled CO2 conditions predict higher lifting condensation levels and reduced cloud contact for tropical montane cloud forests as global temperatures rise [*Still et al.*, 1999]. Analysis of observational data also suggests that warmer eastern tropical Pacific sea surface temperatures (SSTs) are related to interannual decreases in cloud cover at Monteverde [*Pounds et al.*, 1999], but that there also exists a longer-term trend of reduced moisture potentially related to tropical surface and sea surface temperature increases. Increases in global temperature may fundamentally alter the suite of climatic and biophysical conditions that maintain cloud forests environments [*Pounds et al.*, 1999; *Still et al.*, 1999]. The observed and modeled sensitivity of the hydroclimatology of tropical cloud forests to broad-scale climate variability and change indicates that they may be optimal locations at which to develop proxies for paleoclimate reconstructions.

1.2.5 The stable isotope approach to tropical dendroclimatology

Stable oxygen isotope ratios (δ^{18}O) offer an analytical approach to resolving both chronology and climate signal in tropical trees [*Evans and Schrag*, 2004]. The advantage of this approach to tropical dendrochronology is that it does not rely on the formation nor width variations of annual growth rings, which in tropical trees can be absent or may not

reflect local climate variability. I hypothesize that the $\delta^{18}O$ value of cellulose in tropical montane cloud forest trees from Central America preserves a record of plant water use that reflects regular seasonal changes in hydroclimatology. These cycles can be used for chronological control in the absence of rings. Annual oxygen isotope cycles have been previously identified in lowland rainforests [*Evans and Schrag*, 2004; *Poussart et al.*, 2004; *Verheyden et al.*, 2004].

The $\delta^{18}O$ of cellulose in the stem of a tree reflects the original oxygen isotope composition of the source water (precipitation or cloud water), the isotopic enrichment via transpiration in the leaves, and the fractionation associated with the synthesis of α-cellulose from sucrose [*Roden et al.*, 2000; *Barbour et al.*, 2004; *McCarroll and Loader*, 2004]. Assuming the latter is constant, cellulose in cloud forest trees should therefore reflect both the amount of rainfall received and climatic influences on the rate of evapotranspiration from the leaf. On annual time scales in this conceptual model, cellulose $\delta^{18}O$ is controlled by the seasonal change in $\delta^{18}O$ of source water as determined by the amount of rainfall and the utilization by trees of available cloud water. On interannual time scales, departures from the mean annual cycle are likely to result from anomalous rainfall and changes in temperature, relative humidity, and evapotranspiration.

My selection of tropical cloud forests as a site for tropical paleoclimate reconstruction parallels, in a somewhat paradoxical manner, the approach of classical dendroclimatology in seeking out sampling locations where trees are likely to be sensitive to relatively small changes in annual climate. In temperate regions and for trees with regular annual changes in morphology or wood density, these are typically dry or cold sites at the limits of a species range. For tropical isotope dendroclimatology, however, I seek a research site which is wet enough to allow trees to grow throughout the year, yet is subject to regular seasonal changes in the stable oxygen isotope composition of available moisture that

provides the means of establishing annual chronology. In cloud forest environments, the largest interannual changes of interest are likely to be wet season rainfall and dry season cloudiness. As such, site selection for tropical isotope dendroclimatology is very different from that of classical field approaches in dendrochronology in terms of climate regimes, but the guiding principle is the same.

1.2.6 Monteverde, Costa Rica

My study focuses on the Monteverde Cloud Forest in Costa Rica where environmental and meteorological data available over the last 20 years provides the data necessary to validate this hypothesis. The existing environmental data from Monteverde also reveal that its local climatology reflects interannual variability in the Pacific related to ENSO, as well as apparent long-term trends potentially related to similar trends in tropical air and sea surface temperatures.

Several recent publications [*Still et al.*, 1999; *Pounds et al.*, 1999; *Lawton et al.*, 2001] have explored the specific issue of the impact of climate variability and global environmental chance on these tropical montane cloud forests in Costa Rica. The impetus for this research was the population crash and eventual extinction of the Monteverde Golden Toad after the 1987 El Niño event, as well as population declines in other anuran and lizard populations, and observed changes in the elevational range of several bird species [*Pounds and Crump*, 1994; *Pounds et al.*, 1997, 1999; *Pounds and Puschendorf*, 2004; *Pounds et al.*, 2006]. *Still et al.* [1999] used the GENESIS GCM to simulate relative humidity and lifting condensation levels (LCL) for doubled CO_2 conditions. Using both calculated relative humidity surfaces and warmth index values, they concluded that anthropogenic global warming could shift the altitude of cloud forests upward by more than 200 meters. Other studies have found that LCLs at cloud forest sites could

shift upward by as much as 400 to 500 meters [*Foster*, 2001]. *Pounds et al.* [1999] found that dry season mist and cloud frequency at Monteverde was negatively correlated with Pacific SSTs. A positive trend in dry days (increasing number of dry days/year) remained even when taking into account the influences of warm ENSO events, apparently indicated some longer-term trend underlying interannual variability. An earlier study of the relationship between precipitation at Monteverde and ENSO events [*Pounds and Crump*, 1994] had found higher temperatures and lower seasonal rainfall during the 1982-83 and 1986-87 El Niño events, indicating that warmer SSTs were inducing warmer, drier conditions. Because they occupy an altitudinal range and topography associated with very specific climatic conditions, tropical montane cloud forests may also be some of the first ecosystems to unequivocally show the consequences of anthropogenic global warming, and may provide early indications of the impacts of global temperature rise.

1.3 Research Approach

My focus on the application of tropical stable isotope dendroclimatology in the cloud forests of Monteverde in Costa Rica accomplish several complementary goals. First and foremost, it does not require the identification of trees with reliable annual growth rings, instead using the isotope hydroclimatology of the cloud forest for both chronology and paleoclimate signal. Second, I am able to take advantage of the sensitivity of the local climate of these forests to broad-scale forcing in order to develop the basis for using cloud forest trees to develop proxy records of past ocean-atmosphere variability. Finally, a reconstruction of the local, dry season climate conditions at Monteverde allows recent changes identified from the short instrumental record to be interpreted in the context of interannual variability and trends over several decades.

CHAPTER 2

PRESENT STUDY

The research presented in this dissertation is focused on the development and application of a stable isotope approach to extracting annually-resolved climate information from trees without rings in tropical cloud forests in Central America. Specifically, I first investigated the purity and isotopic composition of cellulose extracted from whole wood using a rapid chemical processing procedure. Using this sample preparation method and analytical protocols for tropical isotope dendroclimatology [*Evans and Schrag*, 2004], I then established the basis for developing high resolution $\delta^{18}O$ records from cloud forest trees at Monteverde. I used a calibration study to test my hypothesized age model and identify the existence of a wet season precipitation signal in the isotope time series. I also conducted an additional pilot survey along an elevation transect to identify promising candidate species and sites for long climate reconstructions from the upper cloud forest and transition zone. I identified and selected mature canopy *Sapotaceae* from above 1500m and used analyses of these trees to develop a longer $\delta^{18}O$ chronology and to investigate the link between local climate at Monteverde and broad-scale ocean atmosphere forcing. The methods, results and conclusions of this research are presented in the papers appended to this dissertation and the following is a summary of the methods used and the most significant results.

2.1 Evaluation of a rapid α-cellulose extraction protocol

I used Fourier Transform Infrared Spectroscopy (FTIR), radiocarbon assays, and stable oxygen isotope analyses to evaluate a rapid cellulose preparation protocol for wood samples from tropical trees. Paired comparison of replicate $\delta^{18}O$ measurements on sets of laboratory standard wood powders and α-cellulose established that there was no statistically significant difference between samples processed using traditional methods [*Leavitt and Danzer*, 1993] and those prepared using the Brendel method [*Brendel et al.*, 2000]. Radiocarbon dating, however, revealed a small degree of contamination sufficient to significantly bias absolute age estimates. My analysis of FTIR spectra revealed that the contamination was cellulose acetate formed during acid delignification. FTIR and radiocarbon analysis suggested that contaminant acetyl groups were not removed by strong alkali saponification, nor by other methods used to prevent acetylation. However, I proposed a statistical correction to allow wood samples processed to α-cellulose using the Brendel technique to be corrected for contamination and utilized for chronology development. My study design enabled me to establish that the Brendel technique could be used for stable oxygen isotope analysis, to identify the cause and consequences of sample contamination during processing, and to develop a correction to allow the technique to be reasonably to radiocarbon dating. My assessment of the Brendel method for applications in high resolution tropical isotope dendroclimatology is contained in the article manuscript attached as Appendix A.

2.2 Stable oxygen isotope chronology and climate signal calibration from *Ocotea tenera*

I used high-resolution stable oxygen isotope analysis on wood from planted and monitored *Ocotea tenera* in order to demonstrate that chronological control in trees without annual rings could be established using $\delta^{18}O$ cycles imparted to the xylem

of cloud forest trees due to seasonal changes in the moisture regime. Cores that I collected from these plantation trees were microsampled, extracted to α-cellulose using the Brendel technique, and their $\delta^{18}O$ was measured by continuous flow isotope ratio mass spectrometer. I identified regular $\delta^{18}O$ cycles in wood of up to 9‰, which were associated as I had hypothesized with the seasonal changes in precipitation and moisture sources. The calculated annual growth rates I derived from the isotope time series match those observed from long-term basal growth measurements, confirming my hypothesized age model. My statistical analysis of the interannual anomalies in the amplitude of the oxygen isotope cycles in *Ocotea tenera* revealed that, at this site, they are primarily controlled to interannual changes in summer precipitation. I also used a forward mechanistic model of the relationship between monthly climate (precipitation, temperature, and relative humidity) to independently confirm the detection and identification of the annual $\delta^{18}O$ and their relationship to climate.

I sought to identify trees from which I could potentially develop longer $\delta^{18}O$ chronologies for paleoclimate analysis using a pilot isotopic survey of nine additional trees along an elevational transect from the transitional lower forest zone up to the continental divide. Trees from elevations above the orographic cloud bank showed larger interannual variability, but less consistently showed coherent annual cycles. The confirmation of annual chronology and sensitivity to interannual climate anomalies verified my heuristic, conceptual model of the seasonal, annual, and interannual controls on cloud forest tree xylem $\delta^{18}O$. These data further indicated that trees from higher elevation sites within the persistent orographic cloud bank at Monteverde could preserve a record of past variability in dry season climate. My calibration study establishing the basis for tropical isotope dendroclimatology in the cloud forests of Costa Rica is contained in the article manuscript attached as Appendix B.

2.3 Reconstructing dry season climate variability from *Sapotaceae*

Following my validation of the annual chronology and climate signal from the lower forest plantations, I applied this same analytical approach to mature *Sapotaceae* trees from the upper elevation cloud forest. High-resolution isotope measurements along the growth radius of these trees revealed coherent annual cycles in $\delta^{18}O$ that I then used to establish annual chronological control in the absence of growth rings. I also used radiocarbon dates to verify the age models established using the $\delta^{18}O$ time series, including the identification of a growth hiatus not evident from the $\delta^{18}O$ data alone. The annual maxima and amplitude of the oxygen isotope cycles reflected interannual variability in dry season orographic cloud cover, moisture advection, and temperature. The minima of the annual $\delta^{18}O$ reflected summer precipitation anomalies. Positive dry season $\delta^{18}O$ anomalies are associated with El Niño events and weaker northeasterly trade winds. I interpreted lower frequency (multidecadal) variability in the amplitude of the $\delta^{18}O$ time series be potentially related to climate trends in the tropical Atlantic and changes in the frequency of ENSO events in the tropical Pacific. According to my oxygen isotope chronology from cloud forest *Sapotaceae*, the extinction of the Monteverde Golden Toad after 1987 occurred during one of the driest periods in the last 50 years, and potentially in the last century. The development of longer isotope chronologies from *Sapotaceae* and my analysis of these records in the context of local and global patterns of climate variability are contained in the article manuscript attached as Appendix C.

REFERENCES

Barbour, M. M., J. S. Roden, G. D. Farquhar, and J. R. Ehleringer (2004), Expressing leaf water and cellulose oxygen isotope ratios as enrichment above source water reveals evidence of a Peclet effect, *Oecologia*, *138*(3), 426–435.

Bauch, J., L. Quiros, G. Noldt, and P. Schmidt (2006), Study on the wood anatomy, annual wood increment and intra-annual growth dynamics of *Podocarpus oleifolius* var. *macrostachyus* from Costa Rica, *Journal of Applied Botany and Food Quality*, *80*(1), 19–24.

Biondi, F., A. Gershunov, and D. R. Cayan (2001), North Pacific decadal climate variability since 1661, *J. Climate*, *14*, 5–10.

Brendel, O., P. P. M. Iannetta, and D. Stewart (2000), A rapid and simple method to isolate pure α-cellulose, *Phytochemical Analysis*, *11*, 7–10.

Brown, A. D., and M. Kappelle (2001), Introducción a los bosques nublados del neotrópico: una síntesis regional, in *Bosques nublados del neotrópico*, edited by M. Kappelle and A. D. Brown, pp. 25–40.

Bush, M. B. (2002), Distributional change and conservation on the Andean flank: a palaeoecological perspective, *Global Ecology And Biogeography*, *11*, 463–473.

Cane, M. A. (2005), The evolution of El Nino, past and future, *Earth Planet. Sci. Lett.*, *230*(3-4), 227–240.

Cane, M. A., and M. N. Evans (2000), Do the Tropics Rule?, *Science*, *290*, 1107–1108.

Chang, P., Y. Fang, R. Saravanan, L. Ji, and H. Seidel (2006), The cause of the fragile relationship between the Pacific El Nino and the Atlantic Nino., *Nature*, *443*(7109), 324–8.

Cole, J. E., J. T. Overpeck, and E. R. Cook (2002), Multiyear La Niña events and persistent drought in the contiguous United States, *Geophys. Res. Lett.*, *29*.

D'Arrigo, R., R. Villalba, and G. Wiles (2001), Tree-ring estimates of Pacific decadal climate variability, *Clim. Dynam.*, *18*, 219–224.

D'Arrigo, R., R. Wilson, J. Palmer, P. Krusic, A. Curtis, J. Sakulich, S. Bijaksana, S. Zulaikah, and L. O. Ngkoimani (2006), Monsoon drought over Java, Indonesia, during the past two centuries, *Geophys. Res. Lett.*, *33*, 4709.

Diaz, H., M. Hoerling, and J. Eischeid (2001), ENSO variability, teleconnections, and climate change, *Int. J. Climatol.*, *21*, 1845–1862.

Diaz, H., and G. Kiladis (1992), Atmospheric teleconnections associated with the extreme phases of the Southern Oscillation, in *El Niño: Historical and Paleoclimatic Aspects of the Southern Oscillation*, edited by H. Diaz and V. Markgraf, Cambridge University Press, Cambridge, UK.

Dong, B., R. Sutton, and A. Scaife (2006), Multidecadal modulation of El Niño-Southern Oscillation (ENSO) variance by Atlantic Ocean sea surface temperatures, *Geophys. Res. Lett.*, *8*, 03,405.

Douville, H. (2006), Detection-attribution of global warming at the regional scale: How to deal with precipitation variability?, *Geophys. Res. Lett.*, *33*, 2701.

Douville, H., D. Salas-Melia, and S. Tyteca (2006), On the tropical origin of uncertainties in the global land precipitation reponse to global warming, *Clim. Dynam.*, *26*, 367–385.

Dünisch, O., J. Bauch, and L. Gasparotto (2002), Formation of increment zones and intraannual growth dynamics in the xylem of Swietenia macrophylla, Carapa guianensis, and Cedrela odorata (Meliaceae), *IAWA Journal*, *23*, 101–119.

Enfield, D. B., A. M. Mestas-Nunez, and P. J. Trimble (2001), The Atlantic Multidecadal Oscillation and its relation to rainfall and river flows in the continental US, *Geophys. Res. Lett.*, *28*, 2077–2080.

Evans, M. N., and D. P. Schrag (2004), A stable isotope-based approach to tropical dendroclimatology, *Geochim. Cosmochim. Acta*.

Evans, M. N., M. A. Cane, D. P. Schrag, A. Kaplan, B. K. Linsley, R. Villalba, and G. M. Wellington (2001), Support for tropically-driven Pacific decadal variability based on paleoproxy evidence, *Geophys. Res. Lett.*, *28*, 3689–3692.

Evans, M. N., A. Kaplan, and M. A. Cane (2002), Pacific sea surface temperature field reconstruction from coral δ^{18}O data using reduced space objective analysis, *Paleoceanography*, *17*.

February, E. C., and W. D. Stock (1998), An assessment of the dendrochronological potential of two *Podocarpus* species, *The Holocene*, *8*(6), 747.

Fichtler, E., V. Trouet, H. Beeckman, P. Coppin, and M. Worbes (2004), Climatic signals in tree rings of *Burkea africana* and *Pterocarpus angolensis* from semiarid forests in Namibia, *Trees - Structure and Function*, *18*(4), 442–451.

Foster, P. (2001), The potential negative impacts of global climate change on tropical montane cloud forests, *Earth Science Reviews*, *55*, 73–106.

Garreaud, R. D., and D. S. Battisti (1999), Interannual (ENSO) and interdecadal (ENSO-like) variability in the Southern Hemisphere tropospheric circulation, *J. Climate*, *12*, 2113–2123.

Gedalof, Z., N. J. Mantua, and D. L. Peterson (2002), A multi-century perspective of variability in the Pacific Decadal Oscillation: new insights from tree rings and coral, *Geophys. Res. Lett.*, *29*, doi:10.1029/2002GL015824.

Giannini, A., M. A. Cane, and Y. Kushnir (2001a), Interdecadal changes in the ENSO teleconnection to the Caribbean region and the North Atlantic oscillation, *J. Climate*, *14*(13), 2867–2879.

Giannini, A., J. Chiang, M. A. Cane, Y. Kushnir, and R. Seager (2001b), The ENSO teleconnection to the tropical Atlantic Ocean: contributions of the remote and local SSTs to rainfall variability in the tropical Americas, *J. Climate*, *14*(24), 4530–4544.

Gray, S., L. Graumlich, J. Betancourt, and G. Pederson (2004), A tree-ring based reconstruction of the Atlantic Multidecadal Oscillation since 1567 AD, *Geophysical Research Letters*, *31*(12).

Grosfeld, K., G. Lohmann, N. Rimbu, K. Fraedrich, and F. Lunkeit (2007), Atmospheric multidecadal variations in the North Atlantic realm: proxy data, observations, and atmospheric circulation model studies, *Climate of the Past*, *3*(1), 39–50.

Haber, W. A. (2000), Plants and vegetation, in *Monteverde: Ecology and Conservation of a Tropical Cloud Forest*, edited by N. M. Nadkarni and N. T. Wheelwright, pp. 39–70, Oxford University Press, Oxford, United Kingdom.

Hoerling, M. P., and A. Kumar (2003), The perfect ocean for drought, *Science*, *299*, 691–694.

Hoerling, M. P., J. W. Hurrell, and T. Xu (2001), Tropical origins for recent North Atlantic climate change, *Science*, *292*, 90–92.

Knight, J., R. Allan, C. Folland, M. Vellinga, and M. Mann (2005), A signature of persistent natural thermohaline circulation cycles in observed climate, *Geophys. Res. Lett.*, *32*.

Lawton, R. O., U. S. Nair, R. A. Pielke, and R. M. Welch (2001), Climatic impact of tropical lowland deforestation on nearby montane cloud forests, *Science*, *294*, 584–587.

Leavitt, S. W., and S. R. Danzer (1993), Method for batch processing small wood smaples to holocellulose for stable carbon isotope analysis, *Analytical Chemistry*, *65*, 87–89.

Linsley, B. K., L. Ren, R. B. Dunbar, and S. S. Howe (2000), ENSO and decadal-scale climate variability at 10^{o}N in the Eastern Pacific from 1893-1994: A coral-based reconstruction from Clipperton Atoll, *Paleoceanography*, *15*, 322–325.

Loope, L. L., and T. W. Giambelluca (1998), Vulnerability of island tropical montane cloud forests to climate change, with special reference to East Maui, Hawaii, *Clim. Change*, *39*, 503–517.

MacDonald, G. M., and R. A. Case (2005), Variations in the pacific oscillation over the past millennium, *Geophys. Res. Lett.*, *32*.

Mann, M. E., and K. A. Emanuel (2006), Alantic hurricane trends linked to climate change, *Eos*, *87*(24), 233–244.

McCabe, G. J., M. A. Palecki, and J. Betancourt (2004), Pacific and Atlantic Ocean influences on multidecadal drought frequency in the United States, *Proc. U. S. Natl. Acad. Sci.*, *101*(12), 4136–4141.

McCarroll, D., and N. J. Loader (2004), Stable isotopes in tree rings, *Quat. Sci. Rev.*, *23*(7-8), 771–801.

Neelin, J. D., M. Munnich, H. Su, J. E. Meyerson, and C. E. Holloway (2006), Tropical drying trends in global warming models and observations, *Proc. National Acad. Sciences United States Am.*, *103*(16), 6110–6115.

Newman, M., G. P. Compo, and M. A. Alexander (2003), ENSO-forced variability of the Pacific decadal oscillation, *J. Climate*, *16*, 3853–3857.

Pounds, J. A., and M. L. Crump (1994), Amphibian declines and climate disturbance - the case of the golden toad and the harlequin frog, *Conservation Biology*, *8*, 72–85.

Pounds, J. A., and R. Puschendorf (2004), Clouded futures, *Nature*, *427*, 107–109.

Pounds, J. A., M. Fogden, J. M. Savage, and G. C. Gorman (1997), Tests of null models for amphibian declines on a tropical mountain, *Conservation Biology*, *11*, 1307–1322.

Pounds, J. A., M. Fogden, and J. H. Campbell (1999), Biological response to climate change on a tropical mountain, *Nature*, *398*, 611–615.

Pounds, J. A., et al. (2006), Widespread amphibian extinctions from epidemic disease driven by global warming, *Nature*, *439*(7073), 161–167.

Poussart, P. F., M. N. Evans, and D. P. Schrag (2004), Resolving seasonality in tropical trees: multi-decade, high-resolution oxygen and carbon isotope records from Indonesia and Thailand, *Earth Planet. Sci. Lett.*, *218*(3-4), 301–316.

Rasmusson, E. M., and J. M. Wallace (1983), Meteorological aspects of the El Niño-Southern Oscillation, *Science, 222*, 1195–1202.

Robertson, I., C. A. Froyd, R. P. D. Walsh, D. M. Newbery, S. Woodborne, and R. C. Ong (2004), The dating of dipterocarp tree rings: establishing a record of carbon cycling and climatic change in the tropics, *J. Quaternary Science*, *19*, 657–664.

Roden, J. S., G. Lin, and J. R. Ehleringer (2000), A mechanistic model for interpretation of hydrogen and oxygen ratios in tree-ring cellulose, *Geochim. Cosmochim. Acta*, *64*, 21–35.

Schubert, S. D., M. J. Suarez, P. J. Pegion, R. D. Koster, and J. Bacmeister (2004), On the cause of the 1930s Dust Bowl, *Science*, *303*(5665), 1855–1859.

Schwing, F. B., J. M. Jiang, and R. Mendelssohn (2003), Coherency of multi-scale abrupt changes between the NAO, NPI, and PDO, *Geophys. Res. Lett.*, *30*.

Seager, R., A. C. Clement, and M. A. Cane (2000), Glacial cooling in the tropics: Exploring the roles of tropospheric water vapor, surface wind speed, and boundary layer processes, *Journal of The Atmospheric Sciences*, *57*(13), 2144–2157.

Seager, R., Y. Kushnir, M. Visbeck, N. Naik, J. Miller, G. Krahmann, and H. Cullen (2000), Causes of Atlantic Ocean Climate Variability between 1958 and 1998, *J. Climate*, *13*, 2845–2862.

Speer, J. H., K. H. Orvis, H. D. Grissino-Mayer, L. M. Kennedy, and S. P. Horn (2004), Assessing the dendrochronological potential of *Pinus occidentalis* Swartz in the Cordillera Central of the Dominican Republic, *The Holocene*, *14*(4), 563.

Stadtmüller, T. (1987), *Cloud forests in the humid tropics*, United Nations University.

Stahle, D., et al. (1998), Experimental dendroclimatic reconstruction of the Southern Oscillation, *Bulletin of the American Meteorological Society*, *79*(10), 2137–2152.

Still, C., P. Foster, and S. Schneider (1999), Simulating the effects of climate change on tropical montane cloud forests, *Nature*, *398*, 608–610.

Tomita, T., B. Wang, T. Yasunari, and H. Nakamura (2001), Global patterns of decadal-scale variability observed in sea surface temperature and lower-tropospheric circulation fields, *J. Geophys. Res.*, *106*, 26,805–26,815.

Torrence, C., and P. J. Webster (1999), Interdecadal Changes in the ENSO–Monsoon System, *J. Climate*, *12*, 2679–2690.

Urban, F. E., J. E. Cole, and J. T. Overpeck (2000), Influence of mean climate change on climate variability from a 155-year tropical pacific coral record, *Nature*, *407*, 989–993.

Verheyden, A., G. Helle, G. H. Schleser, F. Dehairs, H. Beeckman, and N. Koedam (2004), Annual cyclicity in high-resolution stable carbon and oxygen isotope ratios in the wood of the mangrove tree Rhizophora mucronata, *Plant Cell Environment*, *27*, 1525–1536.

Wang, C., and D. Enfield (2001), The tropical Western Hemisphere warm pool, *Geophys. Res. Lett.*, *28*, 1635–1638.

Wang, J., and J. Carton (2003), Modeling climate variability in the tropical Atlantic atmosphere, *Journal of Climate*, *16*(23), 3858–3876.

Worbes, M. (2002), One hundred years of tree-ring research in the tropics – a brief history and an outlook to future challenges, *Dendrochronologia*, *20*(1-2), 217–231.

Worbes, M., and W. Junk (1989), Dating tropical trees by means of C14 from bomb tests, *Ecology*, *70*, 503–507.

Xie, S.-P., and J. A. Carton (2004), Tropical Atlantic Variability: Patterns, Mechanisms, and Impacts, in *Earth Climate: The Ocean-Atmosphere Interaction*, edited by C. Wang, S.-P. Xie, and J. A. Carton, Geophysical Monograph, AGU, AGU, Washington, DC.

Yeh, S.-W., and B. P. Kirtman (2005), Pacific decadal variability and decadal ENSO amplitude modulation, *Geophys. Res. Lett.*, *32*.

APPENDIX A

PURITY AND ISOTOPIC RESULTS FROM A RAPID CELLULOSE EXTRACTION METHOD FOR HIGH-RESOLUTION ISOTOPE DENDROCLIMATOLOGY

Manuscript for submission to *Analytical Chemistry*

Purity and isotopic results from a rapid cellulose extraction method for high-resolution isotope dendroclimatology

Kevin J. Anchukaitis[1,2], Michael N. Evans[1,2], Todd Lange[3], David R. Smith[4], Daniel P. Schrag[5], and Steve W. Leavitt[1]

1. Laboratory of Tree-Ring Research, The University of Arizona, Tucson, AZ
2. Department of Geosciences, The University of Arizona, Tucson, AZ
3. Accelerator Mass Spectrometry Laboratory, The University of Arizona, Tucson AZ
4. Department of Chemistry, The University of Arizona, Tucson AZ
5. Department of Earth and Planetary Sciences, Harvard University, Cambridge, MA

A.1 Abstract

Light stable isotope analyses are increasingly becoming part of multiproxy, high-resolution approaches to the reconstruction of past climates from trees. The extraction of α-cellulose from whole wood is now the primary time-limiting factor in the development of long and well-replicated tree-ring isotope chronologies. Here, we use infrared, radiocarbon, and stable isotope analyses to investigate a rapid processing technique for extracting cellulose from whole wood for isotope dendroclimatology. Replicate laboratory standards processed using the standard Brendel method are not significantly different with respect to δ^{18}O from those prepared using traditional techniques, although the process does result in a slight acetylation of the wood samples. Radiocarbon comparisons, however, show significant differences. We conclude that the Brendel method is appropriate for developing stable isotope time series for high-resolution isotope dendroclimatology, but must be used with caution for precision radiocarbon measurements. We propose a simple statistical correction for those instances where Brendel must be used for radiocarbon analyses.

A.2 Introduction

Stable isotope analysis of tree-rings for the study of paleoenvironmental and plant physiological processes has typically focused on the α-cellulose component of wood, necessitating the removal of resins, lignins and non-celluloic polysaccharides, or hemicellulose, prior to measurement. α-cellulose is by definition the components of a cellulosic material which are insoluble in a 17.5% solution of NaOH at 20^{o}C, which includes primarily cellulose but also small amounts of lignin, hemicellulose, and extractives which cannot be removed even under these conditions [*Green*, 1963; *Leavitt and Danzer*, 1993; *Gaudinski et al.*, 2005]. The goal of extracting cellulose for stable isotope analysis is not, however, to arrive at α-cellulose simply by processual definition, but rather to remove as much of the unstable, translocated, or exchangeable noncellulosic components as possible in order to consistently isolate the most stable component of the wood.

The use of specific wood components is often preferred because the noncellulosic compounds can be deposited after the time the ring itself is formed, may be radially translocated, and have different isotopic signatures [*Gray and Thompson*, 1977; *de Water et al.*, 1994]. While recent studies suggest that for both stable carbon and oxygen isotopes the climate signal is preserved in whole wood [*Borella et al.*, 1999; *Saurer et al.*, 2000; *Barbour et al.*, 2001; *Saurer et al.*, 2002; *Loader et al.*, 2003; *Verheyden et al.*, 2005], analysis of specific compounds is still desirable or necessary in some applications, including radiocarbon analysis [*Hoper et al.*, 1998], analyses of fossil wood that may have experienced heterogeneous decomposition [*Schleser et al.*, 1999; *Poole et al.*, 2004], and those instances where mechanistic models of α-cellulose synthesis will be used to interpret the climatic influence on stable isotope ratios [*Roden et al.*, 2000; *Evans*, 2007]. Analyses using α-cellulose may also be preferable to avoid potential biases in isotope

time series as a function of spatiotemporal changes in the relative contribution in whole wood from lignins, hemicellulose, and α-cellulose.

Here, we investigate a procedure for rapidly producing α-cellulose for use in high-resolution stable isotope dendrochronology. The Brendel method [*Brendel et al.*, 2000; *Evans and Schrag*, 2004] allows on average 100 samples per day to be extracted to α-cellulose and prepared for analysis the following day. In its modified form [*Evans and Schrag*, 2004], it also permits the use of very small initial wood samples ($\sim$400 μg). Furthermore, the Brendel method also uses smaller quantities of less toxic reagents, reducing both chemical waste (less than 1.5 mL of waste per sample) and the potential hazards to laboratory personnel. Unlike traditional extraction procedures, however, it uses a hot nitric-acetic acid step to simultaneously remove both lignins and hemicellulose from wood samples. It is important to understand how cellulose extracted using the Brendel procedure compares to samples prepared using traditional techniques [*Green*, 1963; *Leavitt and Danzer*, 1993; *Loader et al.*, 1997] and to determine the efficacy of the procedure in removing extractives, lignins, and hemicellulose. Potential biases introduced by alternative chemical preprocessing protocols could include a difference in means or a reduction in variance [*Gaudinski et al.*, 2005]. The former could complicate intercomparison with other studies, while the latter might lead to underestimation of environmental variability as reflected in isotope time series.

A.3 Methods

A.3.1 Sample preparation

We used three laboratory wood and alpha cellulose standards in this study. We prepared our Arizona/Peruvian *Prosopis* (APP) laboratory wood standard by repeatedly grinding a radial cross section collected in 2001 from a living *Prosopis sp.* near Piura, Peru,

until the wood powder could pass through a $125\mu m$ sieve. The Alaska White Spruce (AWS) standard was previously prepared by grinding to $250\mu m$ a cross-section (UA-BCLV-132) of *Picea glauca* with a total of 172 annual rings collected in the early 1990s. We used Sigma-Aldrich (Batch 024K0329) Alpha Cellulose (SAC) for our α-cellulose control standard.

Samples (8 mg) of the whole wood standards (APP and AWS) were homogenized and separated using a microsplitter (ACS Scientific, Jamestown, RI) and sealed in commercial digestion pouches (ANKOM Technology, Boston, MA). These were processed to holocellulose in a soxhlet apparatus [*Sheu and Chiu*, 1995; *Hoper et al.*, 1998] using a modified Jayme-Wise procedure [*Green*, 1963; *Leavitt and Danzer*, 1993]. Samples were progressively extracted with toluene/ethanol, ethanol, and boiling deionized water. They were then delignified in an sodium chlorite-acetic acid solution at 70^oC and thoroughly rinsed in deionized water. The resulting holocellulose samples were then converted to α-cellulose by treatment in a 17% NaOH solution [*Green*, 1963; *Borella et al.*, 1998] and dried in a warm oven.

Replicate samples (1 – 1.5 mg) of the whole wood and industrial α-cellulose (APP, AWS, and SAC) were processed following the standard Brendel method [*Brendel et al.*, 2000] as modified for small sample processing [*Evans and Schrag*, 2004, , hereafter 'SBrendel']. Samples were heated at 120^oC in a 10:1 mixture of 80% acetic acid and 70% nitric for 30 minutes. Samples were then washed with 100% ethanol and de-ionized water and subsequently dehydrated with consecutive additional washes of pure ethanol and acetone. Samples were dried for 30 minutes in a warm oven, and then overnight in a vacuum desiccator [*Evans and Schrag*, 2004].

We also processed a set of 1 to 1.5mg wood and cellulose samples (SAC, APP, and AWS) using the 'Modified Brendel' method [*Gaudinski et al.*, 2005, , hereafter,

'MBrendel'], which adds a 10 minute 17% NaOH extraction and several additional water rinses to the published Brendel procedure [*Brendel et al.*, 2000; *Evans and Schrag*, 2004].

A.3.2 Stable isotope and infrared analysis

For stable oxygen isotope analysis, 100 to 150 μg cellulose samples were loaded in silver capsules and converted to CO online by pyrolysis in a ThermoFinnigan Thermal Conversion/Elemental Analyzer (TC/EA) at 1450^{o}C. The stable isotopic composition of the CO was then analysed on a ThermoFinnigan Delta Plus XL continuous flow isotope ratio mass spectrometer. Data are reported relative to Vienna Standard Mean Ocean Water (VSMOW). External precision for oxygen isotopic measurements during these experiments based on a Baker α-cellulose standard was 0.45‰ (VSMOW).

For radiocarbon analysis, carbon was extracted from the samples in the form of CO_2 using conventional combustion methods. The volume of the evolved and purified gas was measured and the CO_2 was reduced to an iron carbide powder over hot zinc. Radiocarbon measurement was performed on a National Electrostatics Accelerator Mass Spectrometer at the University of Arizona-NSF AMS Facility [*Donahue et al.*, 1990].

Fourier Transform Infrared Spectroscopy (FTIR) [*Putzig et al.*, 1994; *Moore and Owen*, 2001] was performed using a Thermoelectron (Nicolet) Avatar spectrometer at a resolution of 4 cm^{-1}. The spectra were all obtained using a single-bounce diamond Attenuated Total Reflectance (ATR) accessory. At least two duplicate spectra were obtained in every case to verify the results.

A.4 Results

A.4.1 Stable isotopes and radiocarbon

Stable oxygen isotope measurements on the paired groups of replicate laboratory wood and cellulose standards shows no statistically significant difference (two-tailed t-test, α = 0.05) between those processed using the SBrendel method and those extracted using the Leavitt-Danzer procedure (Figure A.1, Table A.1), although the intercomparison for the industrial Sigma Alpha Cellulose is statistically different at a lower significance threshold (α = 0.10). Significant differences are observed (Figure A.2), however, in the fraction of modern radiocarbon (FMC) measured in replicate samples processed using SBrendel and MBrendel, Leavitt-Danzer, and a standard acid-base-acid (hydrochloric and sodium hydroxide) [*DeVries and Barendsen*, 1954] procedure. Wood and cellulose samples processed using Leavitt-Danzer and acid-base-acid (ABA) pretreatments have consistently higher fractions of modern carbon (FMC), whereas samples processed using SBrendel and MBrendel have reduced FMC, indicating contamination by radiocarbon-depleted sources. For both wood and cellulose standards, the offset between Leavitt-Danzer and SBrendel is consistently 0.07 to 0.08. Wood samples processed with MBrendel show FMC values inconsistently intermediate between SBrendel and Leavitt-Danzer and ABA (0.05 to 0.14). The Sigma Alpha-Cellulose processed with MBrendel actually shows further decreases in FMC relative to Leavitt-Danzer/ABA.

A.4.2 Infrared analysis of compounds

Figures A.3, A.4, and A.5 show the FTIR spectra for in-house wood and α-cellulose samples. Consistent with previous studies [*Brendel et al.*, 2002], SBrendel-processed whole wood shows removal of resins (Figure 3, Peak 1; $\sim$1600 cm^{-1}), lignin (Figure 3,

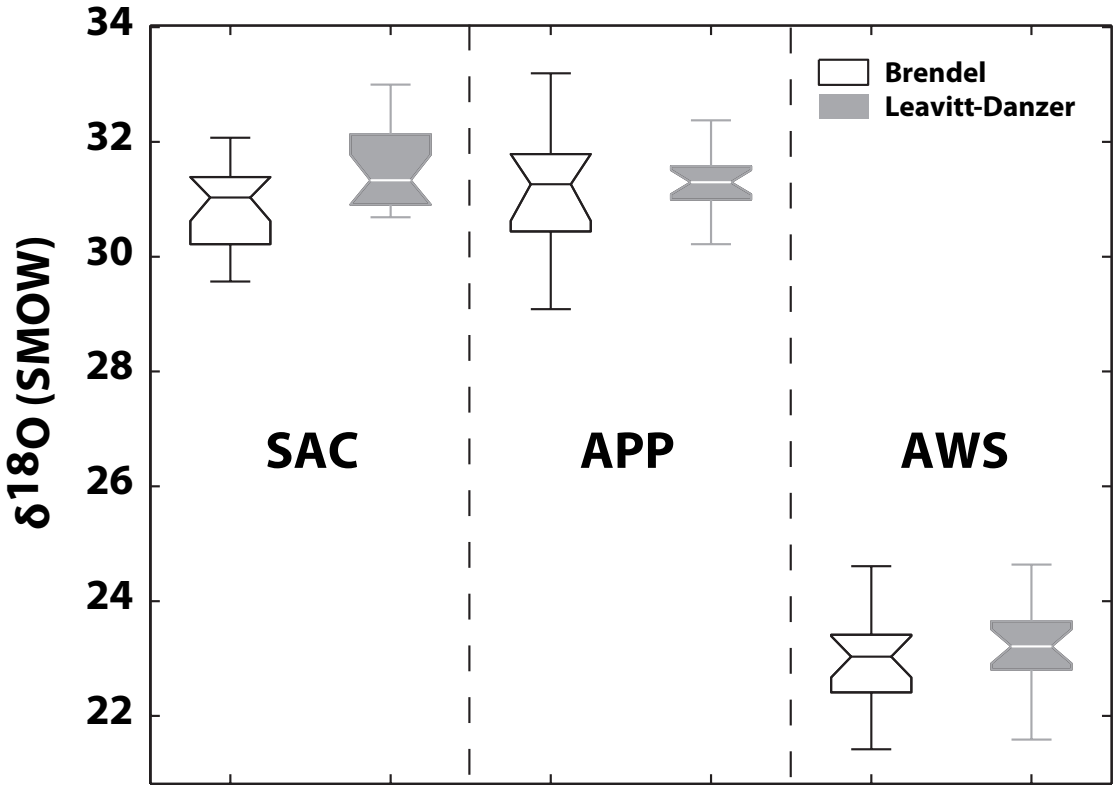

Figure A.1: Boxplots for δ^{18}O measurements on replicate Sigma Alpha-Cellulose (SAC), Arizona/Peruvian *Prosopis* (APP), and Alaska White Spruce (AWS) laboratory standards prepared with Leavitt-Danzer and SBrendel techniques. Following Tukey [*Tukey*, 1977], boxes show the interquartile range, with the notch-line indicating the median. Whiskers demarcate values within 1.5 times the interquartile range. In all three cases, there is no significant difference (two-tailed t-test, 95% significance level) between the samples processed by the two methods.

Standard Material	$\bar{x}_B$(‰)	$\bar{x}_{LD}$(‰)	*d.f.*	*t-statistic*	*p-value*
SAC	30.99	31.51	37	-1.99	0.054
APP	31.26	31.16	28	0.25	0.808
AWS	23.03	23.26	37	-0.88	0.387

Table A.1: Statistical intercomparison of wood and cellulose prepared with SBrendel and Leavitt-Danzer techniques. $\bar{x}_B$ is the mean of the samples processed using the SBrendel technique, $\bar{x}_{LD}$ is the mean of those processed using Leavitt-Danzer, *d.f.* is the number degrees of freedom, which is based on the number of samples measured that passed data quality control for minimum voltage. Also shown are the result of the Student's t-test and the significance level ($p > 0.05$ indicates no statistically significant difference in the means).

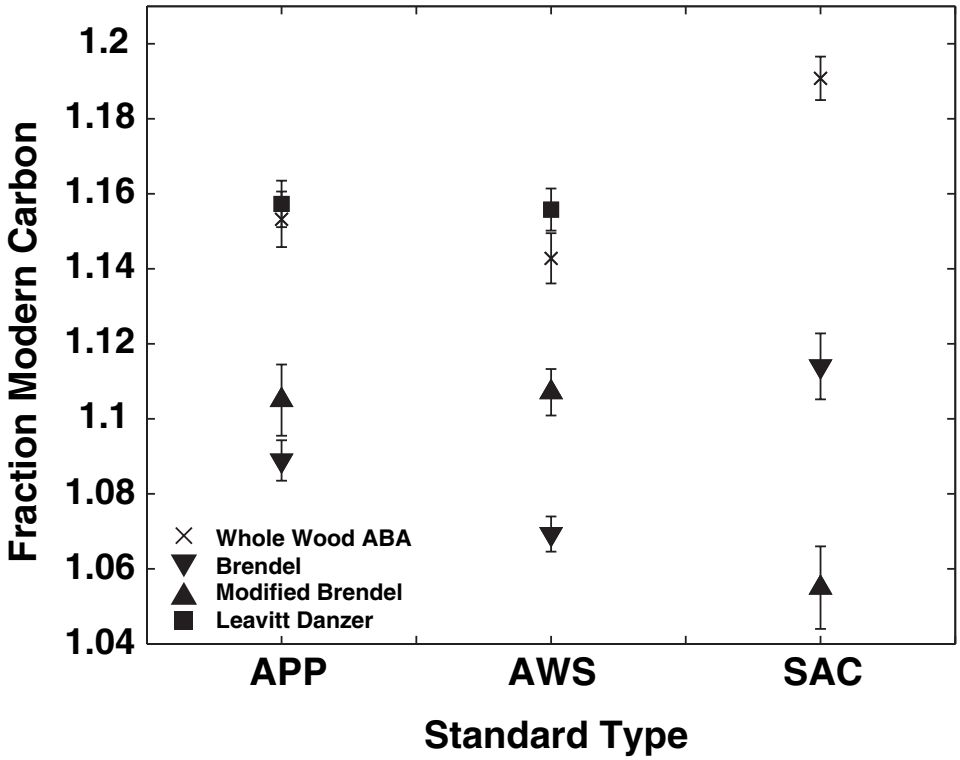

Figure A.2: Fraction modern carbon determinations (FMC) from AMS radiocarbon assays at the University of Arizona's Accelerator Mass Spectrometry Laboratory. SBrendel-processed samples are consistently offset from Raw, ABA, and Leavitt-Danzer processed samples suggesting a 6% contribution of ^{14}C dead carbon from a contaminant, most like acetyl groups inherited for acetic acid). MBrendel-processed methods show an inconsistent offset.

Peak 2; 1550 to 1450 cm^{-1}) and noncelluloic polysaccharides (Figure 3, Peak 3; 1230-1180 cm^{-1}) (Figure A.3a) However, samples (both wood and α-cellulose) processed with the SBrendel method are characterized by infrared spectra with 3 peaks that are not present in wood or cellulose processed using Leavitt-Danzer at ~1720, 1245, and 1110 cm^{-1} (Figure A.3, Peaks 4, 5, 7, and 8). Additionally, the peak near ~900 cm^{-1} (Figure 3, Peak 9) seen in all samples is less distinct in those processed using SBrendel.

The peak near 1720 cm^{-1} is reduced and shifted toward a maximum near 1710 cm^{-1}, but is not fully removed by the MBrendel NaOH extraction (Figure A.3b, A.4, A.5). This peak reduction and shift is consistently detected despite being close to instrument wavelength resolution. The NaOH wash does appear to sharpen the peak near 900 cm^{-1}, but interestingly also removes the peak near 1430 cm^{-1}, which is present in both the unprocessed and SBrendel-processed SAC samples, and adds an additional peak near 3430 cm^{-1}, something which is also seen in the Leavitt-Danzer processed samples (not shown). For the samples that were put through the additional 17% NaOH wash, the peaks at 1245 and 1110 cm^{-1} also disappear (Figure A.3b).

A.5 Analysis and Discussion

A.5.1 Stable isotopes and infrared spectra

Statistical analysis of the stable oxygen isotope measurements on laboratory standard material reveals that no significant bias ($p < 0.05$) is introduced by our small-sample SBrendel method for $\delta^{18}O$ analysis. This finding is consistent with previously reported results [*Evans and Schrag*, 2004] for a small set of $\delta^{18}O$ samples, as well as for $\delta^{13}C$ as reported by *Brendel et al.* [2000], but differs from the conclusions of Gaudinski et al. (2005) [*Gaudinski et al.*, 2005]. This discrepancy may be the result of comparing different techniques across tissue types, (leaves, wood, roots), instead of considering xylem wood

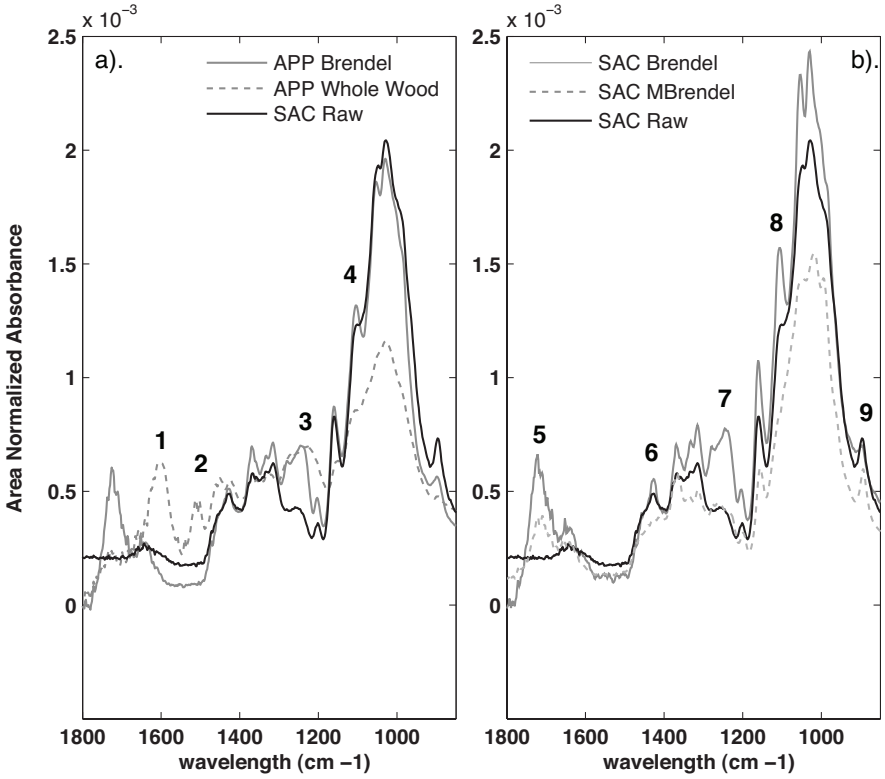

Figure A.3: Area normalized absorbance spectra derived from ATR FTIR analysis of (a) unprocessed and SBrendel-processed Arizona/Peruvian *Prosopis* (APP), compared against Sigma Alpha Cellulose (SAC), and (b) SBrendel- and MBrendel-processed as well as unprocessed SAC. Number labeled spectral peaks or bands show characteristic wavelengths [*Putzig et al.*, 1994; *Stewart et al.*, 1995; *Krasovskii et al.*, 1996; *Vazquez et al.*, 1997; *Pandey*, 1999; *Brendel et al.*, 2000; *Adebajo and Frost*, 2004b; *Sun and Tomkinson*, 2004; *Silverstein et al.*, 2005; *Rinne et al.*, 2005] for (1) resin, (2) lignins, (3) hemicellulose and cellulose acetate/acetic acid, (4,8-9) soluble cellulose acetate/acetic acid, and (5) insoluble cellulose acetate. Peak (6) is removed by the Leavitt-Danzer method, even though it is still present in SBrendel-processed and raw α-cellulose(See Figure 4 and 5). Slight differences in the normalized area under the curve reflect between-sample differences in cellulose adsorbed water, whose bands (not shown) are disproportionately strong and vary with relative humidity.

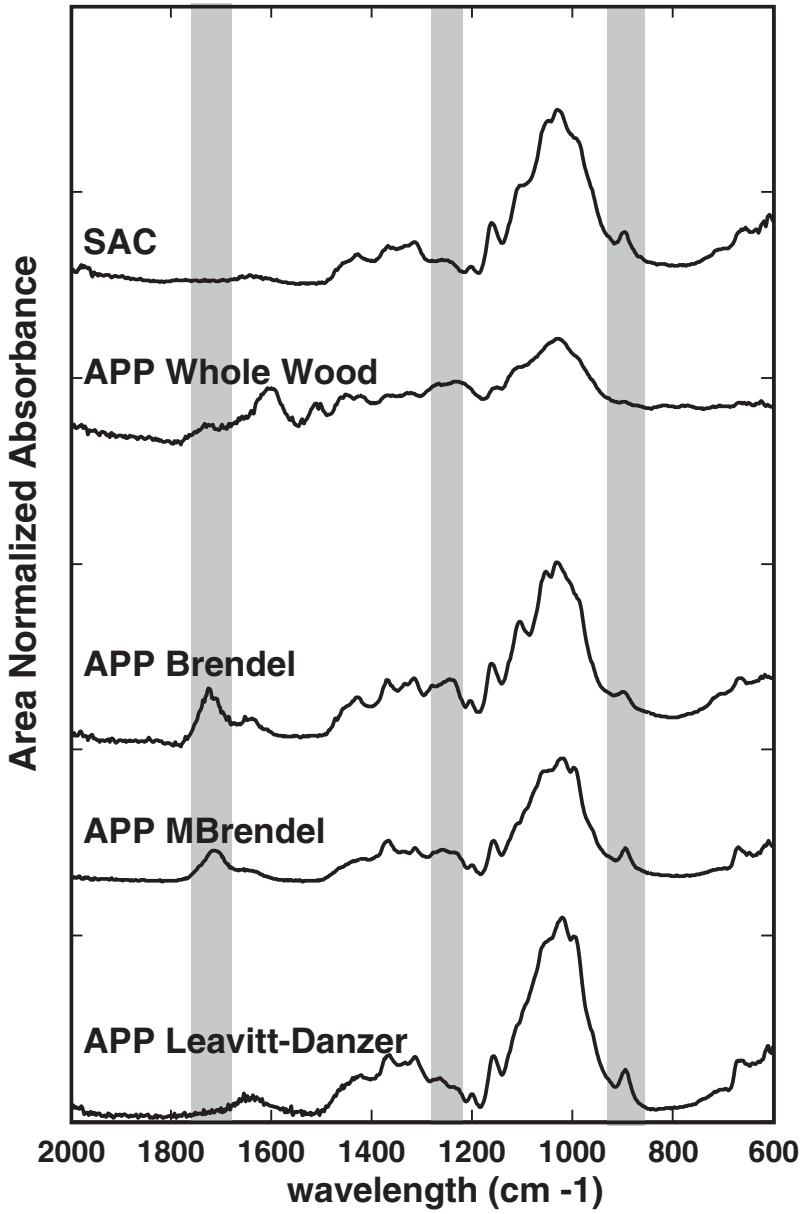

Figure A.4: Area normalized absorbance spectra derived from ATR FTIR analysis of Arizona/Peruvian *Prosopis* (APP) processed using SBrendel, Leavitt-Danzer and MBrendel. Spectra from untreated Sigma Alpha Cellulose (SAC) and Arizona-Peruvian *Prosopis* (APP) are shown for comparison. Shaded vertical bars show wavelengths discussed in the text associated with the acetylization of α-cellulose.

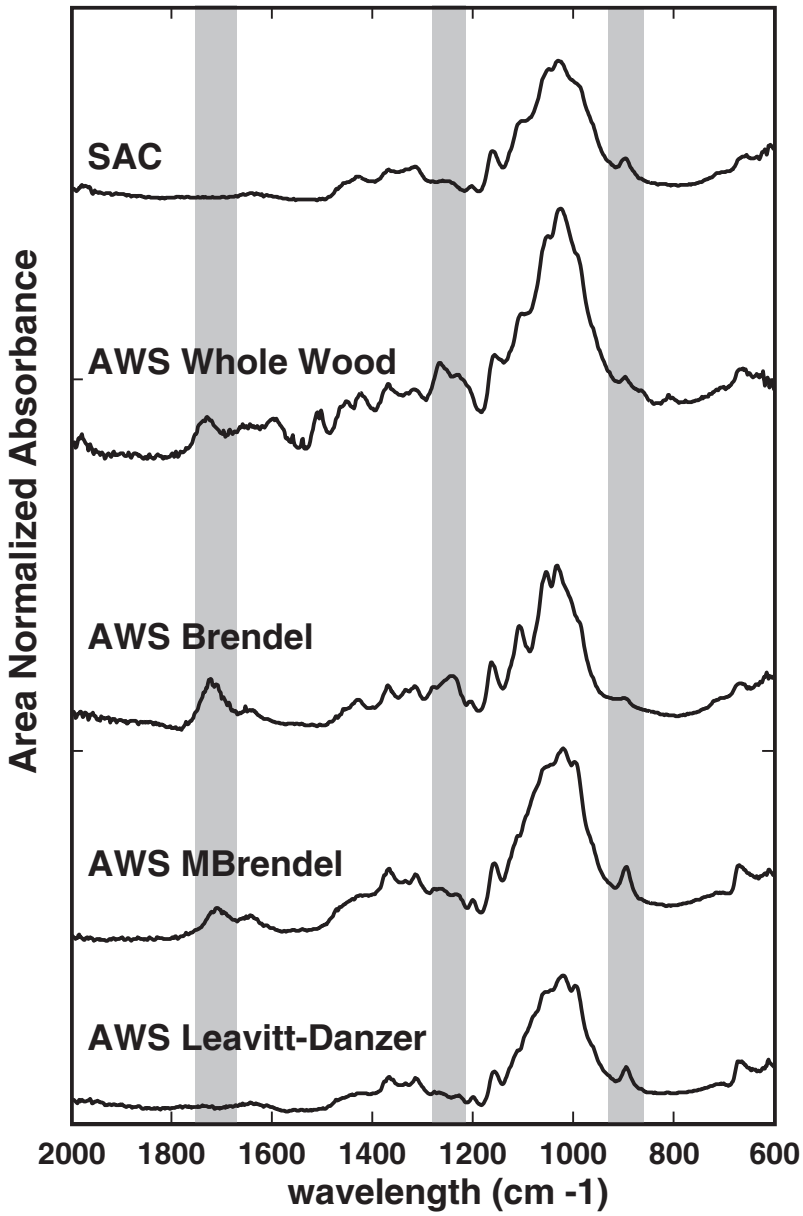

Figure A.5: Area normalized absorbance spectra derived from ATR FTIR analysis of Alaskan White Spruce (AWS) processed using SBrendel, Leavitt-Danzer and MBrendel. Spectra from untreated Sigma Alpha Cellulose (SAC) and Alaskan White Spruce (AWS) are shown for comparison. Shaded vertical bars show wavelengths discussed in the text associated with the acetylization of α-cellulose.

separately. Leaves and roots, in particular, may pose a particular challenge for cellulose extraction. In this respect, however, concerns raised by *Gaudinski et al.* [2005] apply equally for any methods used to extract α-cellulose from these tissues.

Peaks in the FTIR absorbance spectra for SBrendel samples at ~1720, 1245, and 1110 cm^{-1} are associated with carbonyl group C=O and C-O bond stretching, and are most likely related to the presence of cellulose acetate or triacetate esters [*Cherian et al.*, 1994; *Krasovskii et al.*, 1996; *Matsumura and Saka*, 1992; *Adebajo and Frost*, 2004a; *Sun and Tomkinson*, 2004; *Silverstein et al.*, 2005]. The appearance of FTIR peaks in the regions associated with cellulose acetate were originally interpreted by *Brendel et al.* [2000], using DRIFT spectroscopy, as arising from modified non-cellulosic polysaccharides (glucimannans) present in the wood of *Pinus sylvestris*. Our infrared analysis, however, indicates that it is a slight acetylation of cellulose that is causing the differences detected in the radiocarbon results and NMR spectroscopy in previous studies [*Gaudinski et al.*, 2005]. If it were instead acetic acid residue, as has been alternatively suggested [*Gaudinski et al.*, 2005], we would expect the diagnostic peaks in the carbonyl band (C=O) near 1700 cm^{-1} and the C-O band near 1250 cm^{-1} [*Sun and Tomkinson*, 2004; *Silverstein et al.*, 2005].

Furthermore, it is highly unlikely that acetic acid residue would persist following treatments in strong NaOH and subsequent repeated solvent washes. Differences in SAC processed with SBrendel and MBrendel (Figure 3b) might be partially related to acetic acid residue or perhaps to removal of acetylized acid-insoluble hemicelluloses, but the diagnostic peak near ~1720 cm^{-1} is almost certainly indicative of cellulose acetate formation. The shift of this carbonyl peak toward a maximum at ~1710 might indicate partial hydrolysis of the acetylized α-cellulose [*Sun et al.*, 2005b], but it is clear that saponification is incomplete and a portion of the cellulose acetate or triacetate ester

remains insoluble [*Matsumura and Saka*, 1992]. We believe that the acetylation found here is similar in nature to that reported previously for stable isotope analyses of pollen grains [*Amundson et al.*, 1997; *Loader and Hemming*, 2000], where it occurs occurs during standard acetolysis procedures for pollen extraction and preparation [*Charman*, 1992], and in industrial chlorine-free pulping applications [*Sun and Tomkinson*, 2004].

The SBrendel method does successfully delignify and remove most hemicelluloses from our whole wood samples. The method, however, slightly acetylates some of the non-extracted cellulose fraction. A similar conclusion about the efficacy of the cellulose extraction and the concomitant acetylation has been reached for industrial applications of the nitric/acetic acid delignification approach [*Sun and Tomkinson*, 2004; *Sun et al.*, 2004a, b, c, 2005a, b; *Xu et al.*, 2005]. One hypothesis concerning the shape of the peak near 900 cm^{-1} and the presence of additional bands near 1240 and 1110 cm^{-1} could be that they are related to incomplete removal of some residual (alkali-soluble) hemicellulose; however, since the SAC processed with the SBrendel method also has these features (Figure A.3b), it must instead be predominantly related to the creation and presence of acetylized cellulose. The additional of an NaOH step [*Brendel et al.*, 2002], or use of the MBrendel technique [*Gaudinski et al.*, 2005] may indeed remove some remaining acid-insoluble hemicelluloses and any partially acetylized hemicelloses [*Liu and Hsieh*, 2002; *Son et al.*, 2004], but still incompletely removes the acetylized α-cellulose. That the diagnostic peak near 1720 cm^{-1} largely remains even after the alkaline hydrolysis suggests perhaps that either a portion of the cellulose acetate cannot be deacetylized by saponification in NaOH, possibly because the C=O bonds cannot be readily hydrolyzed, or that partial hydrolysis of the cellulose acetate does occur, but an additional solvent treatment is necessary to subsequently dissolve and remove the remaining acetate.

Gaudinski et al. [2005] conclude that the SBrendel potentially leaves behind hemicelluloses, lipid and/or waxes, as well as acetic acid contamination which can potentially bias stable isotope measurements. As we have indicated here, however, the primary contaminating residue is most likely a small amount of insoluble cellulose acetate which persists even after the application of a strong alkali treatment and additional water washes in the MBrendel [*Gaudinski et al.*, 2005] protocols. The NMR spectra which *Gaudinski et al.* [2005] identified as diagnostic of lipids and waxes is also diagnostic for the presence of cellulose acetate [*Torii et al.*, 1994; *Ohkoshi et al.*, 1997; *Kono et al.*, 2002; *Czimczik et al.*, 2002; *Bootten et al.*, 2004], which would also explain the apparent inconsistency between the higher δ^{18}O values they observed for Brendel samples in contrast to the expected lighter values that would result from incomplete removal of these compounds. Because the dominant contamination is from acetyl groups, with one oxygen atom and two carbon, there is no biochemical reason to conclude that ^{18}O analyses utilizing wood processed with SBrendel techniques is any more problematic than for ^{13}C isotope ratios. That there is no difference in δ^{13}C rations between SBrendel and traditional α-cellulose preparation methods despite this contamination suggests that the carbon isotope signature of the contaminating acetyl groups is similar to that of the cellulose of C3 plants. This could be tested by using a C4 standard like maize or sugar cane, as opposed to wood from C3 trees as has been previously done [*Brendel et al.*, 2000; *Gaudinski et al.*, 2005].

A.5.2 Approaches to deacetylation

Our experiments with a variety of pre- and post-treatments have failed to completely remove the small amount of acetylized cellulose as indicated by the 1710-1720 cm^{-1} peak. Our experimental goal was to either prevent acetylation during the delignification

step, or to remove it *post hoc* following acid digestion. Approaches to solubilizing the refractory cellulose acetate using extended, hot alkali saponification with NaOH (0.05 to 4N) in various combination of water and in ethanol [*Liu and Hsieh*, 2002; *Son et al.*, 2004] failed to further reduce or shift the diagnostic FTIR peak near 1710 cm^{-1}. There was no detectable difference as a function of temperature, time, solvent, or alkali normality. Adding extended vortex mixing between NaOH washes likewise has no discernible effect. We also attempted to prevent acetylation using sulfolane as an additional solvent during delignification [*Zaleski et al.*, 2002], but FTIR spectra indicated that acetyl group substitution still occurred. The addition of other solvents during the acid delignification step could in theory help reduce the eventual acetylation, but it may be impossible to prevent the conversion of some number of the hydroxyl groups to acetyl groups [*Ramsden and Blake*, 1997; *Saka et al.*, 1998]. The overall inefficacy of these experimental methods may be a consequence of the low-order, heterogeneous or random nature of the minor acetylization of the cellulose structure, which could render the acetate fraction largely insoluble [*Sassi and Chanzy*, 1995; *Klemm et al.*, 1998].

A.5.3 Radiocarbon analysis

Radiocarbon assays demonstrate significant differences between samples processed using SBrendel and those prepared with conventional pretreatments. Furthermore, these differences are not resolved using the MBrendel procedure [*Gaudinski et al.*, 2005], indicating that both SBrendel and MBrendel protocols introduce contamination from radiocarbon-dead sources, and should be used with considerable caution. It remains unclear whether the MBrendel [*Gaudinski et al.*, 2005] technique should be used for either radiocarbon or stable isotope analysis, though, since it appears to inconsistently remove acetylized cellulose components (Figure A.2), at least across the wood and cellulose types

examined in our study. The use of a weak NaOH wash by *Brendel et al.* [2002], without additional solvent washes, has a similar effect on the extracted cellulose as the MBrendel technique, but also leaves a considerable alkali residue which can be readily detected in the FTIR spectra (results not shown).

Using our radiocarbon measurements (Figure A.2, Table A.2), a simple mass balance equation comparing samples processed using Leavitt-Danzer and SBrendel suggests that approximately 6% of the carbon (and therefore, approximately 3% of the oxygen) in the SBrendel samples comes from the contaminating acetyl groups. This assumes that petroleum-derived acetic acid possesses no detectable ^{14}C. This percentage is also consistent with preliminary tests of the Brendel method conducted by *Poussart* [2004].

Ultimately, however, the choice of α-cellulose extraction protocols for environmental and paleoenvironmental studies will depend rather specifically on the particular application. The Brendel technique, even without the additional of an NaOH wash, is acceptable for stable oxygen isotope analysis, but not for many radiocarbon applications. Other, non-dendroclimatological uses, especially those employing plant tissues besides wood, need to be closely examined [*Gaudinski et al.*, 2005], although this issue is generalizable to all cellulose extraction procedures, and not limited to the Brendel procedure. Wood types with considerable resin content, particularly pines and other conifers, often require additional treatments even using standard Leavitt-Danzer type protocols [*Miller et al.*, 2006]. We continue to investigate changes to the SBrendel procedure which preserve its advantages in terms of speed, sample size, and safety for removing the insoluble fraction of the acetylized cellulose, to allow this technique to be used in the future for radiocarbon analyses.

A.5.4 A statistical radiocarbon correction

Radiocarbon measurements on a range of wood types and ages consistently shows that the contamination with ^{14}C dead carbon due to the SBrendel method is approximately 6±0.8% (Table A.2). The similarly between the mass balance calculations of the percent of radiocarbon-dead contamination suggests that, for the delignification duration, temperature, and acid molarity used in the Brendel protocols described by *Evans and Schrag* [2004], the degree of acetyl group substitution is similar between samples. This finding leads us to believe that, in the temporary absence of a procedural chemical solution to the acetylation bias, a statistical correction can be applied to develop a corrected radiocarbon date.

An example of this correction is shown in Figure A.6. Accounting for the observed 6±0.8% contribution from a carbon source with FMC = 0,

$$FMC_{corrected} = FMC_{measured}/(1 - 0.06) \quad \text{(A.1)}$$

results in calibrated calendar ages [*Bronk Ramsey*, 1995] with a difference of less than 1 year during the post-1955 atmospheric ^{14}C peak that resulted from aboveground atomic weapons testing [*Hua et al.*, 1999; *Reimer et al.*, 2004a; *Hua and Barbetti*, 2004], compared to radiocarbon dates on wood processed using the traditional Leavitt-Danzer technique (Figure A.6). Errors could be somewhat larger for portions of the radiocarbon curve between 1700 and 1950, during which time large oscillations in atmospheric ^{14}C production make precise calibration difficult [*Reimer et al.*, 2004b]; however, the calibration errors associated with the wide range of probability density functions for single radiocarbon determinations during that time period are substantially larger than those arising from the uncertainty in the SBrendel correction. Whenever possible, replicate radiocarbon assays on samples processed using both SBrendel and

Sample Identification	FMC_m	FMC_a	*% contamination*	reference
AA64893	1.114 (0.0088)	1.1908 (0.0058)	5.9±0.6%	this study
AA64894	1.0693 (0.0047)	1.1558 (0.0056)	7.4±0.4%	this study
AA64895	1.0889 (0.0054)	1.1573 (0.0062)	6.5±0.5%	this study
Brendel-A02	1.5247 (0.0061)	1.6453 (0.0108)	5.0±1.0%	*Poussart*, 2004; *Poussart et al.*, 2004
PG1-1	1.0941 (0.0043)	1.174 (0.0045)	6.8±0.4%	*Poussart*, 2004; *Poussart et al.*, 2004
AA74380	1.0143 (0.0083)	1.0842 (0.0088)	6.4±1.0%	*Anchukaitis et al.*, 2007
Mean (σ)			6.0 ±0.8%	

Table A.2: Radiocarbon offsets associated with the Brendel technique with no NaOH step. FMC_m is the measured fraction modern carbon, FMC_a is the 'actual' fraction modern carbon measured on traditionally extracted α-cellulose [*Leavitt and Danzer*, 1993; *Westbrook et al.*, 2006]. Percent contamination is the calculation of the contribution from a radiocarbon dead source (FMC = 0).

Leavitt-Danzer or ABA can help verify the correction factor proposed here. Alterations to the SBrendel procedure, such as a change in the time or temperature of the acid delignification step, or a change in the strength of the acetic acid, would be expected to change the degree of acetylation and therefore the magnitude of the contamination and the necessary correction factor.

A.6 Conclusions

Wood and cellulose samples prepared using the standard Brendel methodology [*Evans and Schrag*, 2004] have δ^{18}O values statistically indistinguishable than those processed using traditional Leavitt-Danzer type protocols. More importantly, there is no indication that the Brendel method biases the range of δ^{18}O variability between samples. α-cellulose prepared using this technique can therefore be securely used for paleoclimate and other time series applications, and absolute mean values can be compared between samples processed with either method. The Brendel method does result in a slight acetylation of the α-cellulose that is sufficient to bias radiocarbon measurements by approximately 6%, but which can be corrected statistically if necessary. MBrendel does appear to remove some of the acetyl group contamination, but results in an inconsistent shift in the offset between measured radiocarbon ages on samples extracted with different methods. The SBrendel technique accomplishes the goal of rapidly extracting very small whole wood samples to stable α-cellulose, which is important for the application of high-resolution isotope dendroclimatology in the tropics [*Evans and Schrag*, 2004].

A.7 Acknowledgements

We thank Greg Eischeid, Jonathan Buchanan, Chris Jones, Brianna Muhlenkamp, Jim Burns, Li Cheng, and Sonya Issaeva for valuable laboratory support. We also benefitted

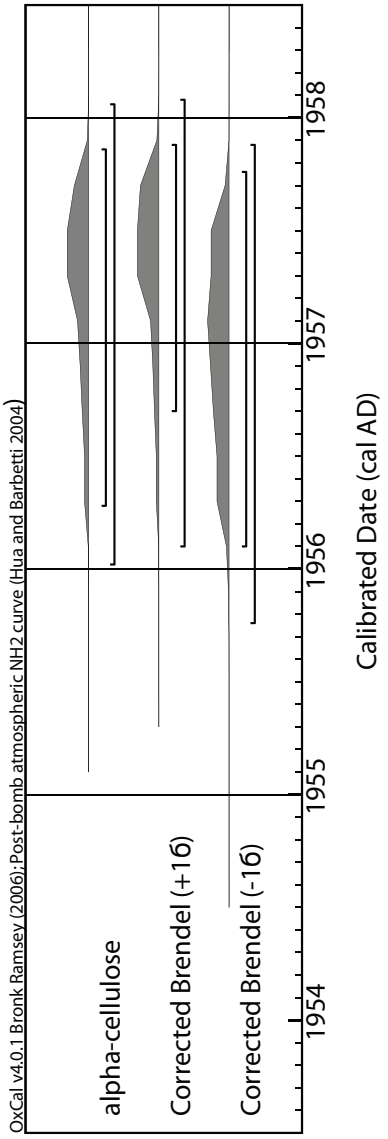

Figure A.6: Example of potential error associated with the statistical correction of the SBrendel radiocarbon bias. Within the post-1950 bomb radiocarbon curve, the influence of the uncertainty in the correction factor applied to the calibrated calendar age is < 1 year.

from helpful discussions with and advice from with Pascale Poussart, Iain Robertson, Mary Gagen, Julia Gaudinski, and Todd Dawson. KJA was supported by a graduate training fellowship from the NSF IGERT Program (DGE-0221594) and a Graduate Research Environmental Fellowship from the US Department of Energy. The research was supported by a grant from NSF-ESH (NSF/ATM0349356).

A.8 References

Adebajo, M. O., and R. L. Frost (2004a), Acetylation of raw cotton for oil spill cleanup application: an FTIR and ^{13}C-MAS-NMR spectroscopic investigation, *Spectrochimica Acta Part A-molecular Biomolecular Spectr.*, *60*, 2315–2321.

Adebajo, M. O., and R. L. Frost (2004b), Infrared and ^{13}C-MAS nuclear magnetic resonance spectroscopic study of acetylation of cotton, *Spectrochimica Acta Part A - Molecular Biomolecular Spectr.*, *60*, 449–453.

Amundson, R., R. R. Evett, A. H. Jahren, and J. Bartolome (1997), Stable carbon isotope composition of Poaceae pollen and its potential in paleovegetational reconstructions, *Rev. Palaeobotany Palynology*, *99*, 17–24.

Anchukaitis, K. J., M. N. Evans, and T. Lange (2007), Dry season climate variability in a tropical montane cloud forest reconstructed from trees without rings, *in preparation*.

Barbour, M. M., T. J. Andrews, and G. D. Farquhar (2001), Correlations between oxygen isotope ratios of wood constituents of *Quercus* and *Pinus* samples from around the world, *Australian Journal of Plant Physiology*, *28*(5), 335–348.

Bootten, T., P. Harris, L. Melton, and R. Newman (2004), Solid-state ^{13}C-NMR spectroscopy shows that the xyloglucans in the primary cell walls of mung bean

(*Vigna radiata* L.) occur in different domains: a new model for xyloglucan-cellulose interactions in the cell wall, *Journal of Experimental Botany*, *55*(397), 571.

Borella, S., M. Leuenberger, M. Saurer, and R. Siegwolf (1998), Reducing uncertainties in δ^{13}C analysis of tree rings: Pooling, milling, and cellulose extraction, *J. Geophys. Res.*, *103*(D16), 19,519–19,526.

Borella, S., M. Leuenberger, and M. Saurer (1999), Analysis of δ^{18}O in tree rings: Wood-cellulose comparison and method dependent sensitivity, *J. Geophys. Res.*, *104*(D16), 19,267–19,273.

Brendel, O., P. P. M. Iannetta, and D. Stewart (2000), A rapid and simple method to isolate pure α-cellulose, *Phytochemical Analysis*, *11*, 7–10.

Brendel, O., L. Handley, and H. Griffiths (2002), Differences in δ^{13}C and diameter growth among remnant Scots pine populations in Scotland, *Tree Physiology*, *22*, 983–992.

Bronk Ramsey, C. (1995), Radiocarbon calibration and analysis of stratigraphy: the OxCal program, *Radiocarbon*, *37*(2), 425–430.

Charman, D. J. (1992), The effects of acetylation on fossil *Pinus* pollen and sphagnum spores discovered during routine pollen analysis, *Rev. Palaeobotany Palynology*, *72*, 159–164.

Cherian, X. M., P. Satyamoorthy, J. J. Andrew, and S. K. Bhattacharya (1994), Application of FTIR photoacoustic-spectroscopy in the determination of the level of chemical modification of jute fibers, *J. Macromolecular Science-pure Appl. Chem.*, *A31*, 261–270.

Czimczik, C., C. Preston, M. Schmidt, R. Werner, and E. Schulze (2002), Effects of

charring on mass, organic carbon, and stable carbon isotope composition of wood, *Org. Geochem*, *33*, 1207–1223.

de Water, P. K. V., S. W. Leavitt, and J. L. Betancourt (1994), Trends in stomatal density and $^{13}C/^{12}C$ ratios of *Pinus flexilis* needles during last glacial-interglacial cycle, *Science*, *264*, 239–243.

DeVries, H., and G. Barendsen (1954), Measurements of age by the carbon-14 technique, *Nature*, *174*, 1138 – 1141.

Donahue, D. J., A. J. T. Jull, and L. J. Toolin (1990), Radiocarbon measurements at the University of Arizona AMS facility, *Nuclear Instruments and Methods B*, *52*, 224–228.

Evans, M. N. (2007), Forward modeling for paleoclimatic proxy signal calibration: a case study with oxygen isotopic composition of tropical woods, *Geochemistry, Geophysics, Geosystems*,, in press.

Evans, M. N., and D. P. Schrag (2004), A stable isotope-based approach to tropical dendroclimatology, *Geochim. Cosmochim. Acta*, doi:10.1016/j.gca.2004.01.006.

Gaudinski, J. B., T. E. Dawson, S. Quideau, E. A. G. Schuur, J. S. Roden, S. E. Trumbore, D. R. Sandquist, S.-W. Oh, and R. E. Wasylishen (2005), A comparative analysis of cellulose preparation techniques for use with ^{13}C, ^{14}C and ^{18}O isotopic measurements, *Analytical Chemistry*, *77*, 7212–7224, doi:10.1021/ac050548u.

Gray, J., and P. Thompson (1977), Climatic information from $^{18}O/^{16}O$ analysis of cellulose, lignin and wholewood from tree-rings, *Nature*, *270*.

Green, J. W. (1963), Wood cellulose, in *Methods of Carbohydrate Chemistry*, edited by R. L. Whistler, pp. 9–21, Academic Press, New York.

Hoper, S. T., F. G. McCormac, A. G. Hogg, T. F. G. Higham, and M. J. Head (1998), Evaluation of wood pretreatments on oak and cedar, *Radiocarbon*, *40*, 45–50.

Hua, Q., and M. Barbetti (2004), Review of tropospheric bomb ^{14}C data for carbon cycle modeling and age calibration purposes, *Radiocarbon*, *46*(3), 1273–1298.

Hua, Q., M. Barbetti, M. Worbes, J. Head, and V. Levchenko (1999), Review of radiocarbon data from atmospheric and tree ring samples for the period 1945-1997 ad, *IAWA Journal*, *20*, 261–283.

Klemm, D., B. Philipp, T. Heinze, U. Heinze, and W. Wagenknecht (1998), *Comprehensive Cellulose Chemistry*, vol. 2, 389 pp., Wiley-VCH, Weinheim, Germany.

Kono, H., T. Erata, and M. Takai (2002), CP/MAS ^{13}C-NMR study of cellulose and cellulose derivatives. 2. Complete assignment of the ^{13}C resonance for the ring carbons of cellulose triacetate polymorphs, *J. Am. Chem. Soc.*, *124*, 7512–7518.

Krasovskii, A. N., A. B. Plodistyi, and D. N. Polyakov (1996), IR study of distribution of primary and secondary functional groups in highly substituted cellulose acetates, acetomaleates, and acetophthalates, *Russian J. Appl. Chem.*, *69*, 1048–1054.

Leavitt, S. W., and S. R. Danzer (1993), Method for batch processing small wood samples to holocellulose for stable carbon isotope analysis, *Analytical Chemistry*, *65*, 87–89.

Liu, H. Q., and Y. L. Hsieh (2002), Ultrafine fibrous cellulose membranes from electrospinning of cellulose acetate, *J. Polymer Science Part B-Polymer Phys.*, *40*, 2119–2129.

Loader, N. J., and D. L. Hemming (2000), Preparation of pollen for stable carbon isotope analyses, *Chem. Geology*, *165*, 339–344.

Loader, N. J., I. Robertson, A. C. Barker, V. R. Switsur, and J. S. Waterhouse (1997), An improved technique for the batch processing of small wholewood samples to alpha-cellulose, *Chem. Geology*, *136*, 313–317.

Loader, N. J., I. Robertson, and D. McCarroll (2003), Comparison of stable carbon isotope ratios in the whole wood, cellulose and lignin of oak tree-rings, *Palaeogeogr. Palaeoclim. Palaeoecol.*, *196*(3-4), 395–407.

Matsumura, H., and S. Saka (1992), Cellulose triacetate prepared from low-grade wood pulp, 1: insoluble residue in acetylation solution, *Mokuzai Gakkaishi*, *38*, 270–276.

Miller, D., C. Mora, H. Grissino-Mayer, C. Mock, M. Uhle, and Z. Sharp (2006), Tree-ring isotope records of tropical cyclone activity, *Proc. U. S. Natl. Acad. Sci.*, *103*(39), 14,294.

Moore, A., and N. Owen (2001), Infrared spectroscopic studies of solid wood, *Applied Spectroscopy Reviews*, *36*(1), 65–86.

Ohkoshi, M., A. Kato, and N. Hayashi (1997), ^{13}C-NMR analysis of acetyl groups in acetylated wood, Part 1: Acetyl groups in cellulose and hemicellulose, *Mokuzai Gakkaishi*, *43*, 327–336.

Pandey, K. (1999), A study of chemical structure of soft and hardwood and wood polymers by FTIR spectroscopy, *Journal of Applied Polymer Science*, *71*(12), 1969–1975.

Poole, I., P. F. van Bergen, J. Kool, S. Schouten, and D. J. Cantrill (2004), Molecular isotopic heterogeneity of fossil organic matter: implications for δ^{13}C biomass and δ^{13}C palaeoatmosphere proxies, *Organic Geochemistry*, *35*, 1261–1274.

Poussart, P. F. (2004), Isotopic investigations of tropical trees, Ph.D. thesis, Harvard University.

Poussart, P. F., M. N. Evans, and D. P. Schrag (2004), Resolving seasonality in tropical trees: multi-decade, high-resolution oxygen and carbon isotope records from Indonesia and Thailand, *Earth Planet. Sci. Lett.*, *218*(3-4), 301–316.

Putzig, C., M. Leugers, M. McKelvy, G. Mitchell, R. Nyquist, R. Papenfuss, and L. Yurga (1994), Infrared Spectroscopy, *Analytical Chemistry*, *66*(12), 26–66.

Ramsden, M. J., and F. S. R. Blake (1997), A kinetic study of the acetylation of cellulose, hemicellulose and lignin components in wood, *Wood Science Technology*, *31*, 45–50.

Reimer, P., T. Brown, and R. Reimer (2004a), Discussion: reporting and calibration of post-bomb 14 C data, *Radiocarbon*, *46*(3), 1299–1304.

Reimer, P., et al. (2004b), IntCal04 terrestrial radiocarbon age calibration, 0-26 Cal Kyr BP., *Radiocarbon*, *46*(3), 1029–1058.

Rinne, K. T., T. Boettger, N. J. Loader, I. Robertson, V. R. Switsur, and J. S. Waterhouse (2005), On the purification of α-cellulose from resinous wood for stable isotope (H,C, and O) analysis, *Chem. Geol.*, *222*(1-2), 75–82.

Roden, J. S., G. Lin, and J. R. Ehleringer (2000), A mechanistic model for interpretation of hydrogen and oxygen ratios in tree-ring cellulose, *Geochim. Cosmochim. Acta*, *64*, 21–35.

Saka, S., K. Takanashi, and H. Matsumura (1998), Effects of solvent addition to acetylation medium on cellulose triacetate prepared from low-grade hardwood dissolving pulp, *J. Appl. Polymer Science*, *69*, 1445–1449.

Sassi, J. F., and H. Chanzy (1995), Ultrastructural aspects of the acetylation of cellulose, *Cellulose*, *2*, 111–127.

Saurer, M., P. Cherubini, and R. Siegwolf (2000), Oxygen isotopes in tree rings of *Abies alba*: The climatic significance of interdecadal variations, *J. Geophys. Res.*, *105*(D10), 12,461–12,470.

Saurer, M., F. Schweingruber, E. A. Vaganov, S. G. Shiyatov, and R. Siegwolf (2002), Spatial and temporal oxygen isotope trends at the northern tree-line in Eurasia, *Geophys. Res. Lett.*, *29*(9).

Schleser, G. H., J. Frielingsdorf, and A. Blair (1999), Carbon isotope behaviour in wood and cellulose during artificial aging, *Chem. Geology*, *158*, 121–130.

Sheu, D. D., and C. H. Chiu (1995), Evaluation of cellulose extraction procedures for stable carbon-isotope measurement in tree-ring research, *Int. J. Environmental Analytical Chem.*, *59*, 59–67.

Silverstein, R. M., F. X. Webster, and D. J. Kiemle (2005), *Spectrometric identification of organic compounds*, 7 ed., 512 pp., John Wiley and Sons, Hoboken, NJ.

Son, W. K., J. H. Youk, T. S. Lee, and W. H. Park (2004), Electrospinning of ultrafine cellulose acetate fibers: Studies of a new solvent system and deacetylation of ultrafine cellulose acetate fibers, *J. Polymer Science Part B-polymer Phys.*, *42*, 5–11.

Stewart, D., H. Wilson, P. Hendra, and I. Morrison (1995), Fourier-Transform Infrared and Raman Spectroscopic Study of Biochemical and Chemical Treatments of Oak Wood (*Quercus rubra*) and Barley (*Hordeum vulgare*) Straw, *Journal of Agricultural and Food Chemistry*, *43*(8), 2219–2225.

Sun, J. X., X. F. Sun, H. Zhao, and R. C. Sun (2004a), Isolation and characterization of cellulose from sugarcane bagasse, *Polymer Degradation Stability*, *84*, 331–339.

Sun, J. X., F. Xu, Z. C. Geng, X. F. Sun, and R. C. Sun (2005a), Comparative study of cellulose isolated by totally chlorine-free method from wood and cereal straw, *J. Appl. Polymer Science*, *97*, 322–335.

Sun, J. X., F. Xu, X. F. Sun, B. Xiao, and R. C. Sun (2005b), Physico-chemical and thermal characterization of cellulose from barley straw, *Polymer Degradation Stability*, *88*, 521–531.

Sun, R. C., and J. Tomkinson (2004), Separation and characterization of cellulose from wheat straw, *Separation Science Technology*, *39*, 391–411.

Sun, X. F., R. C. Sun, Y. Q. Su, and J. X. Sun (2004b), Comparative study of crude and purified cellulose from wheat straw, *J. Agr. Food Chem.*, *52*, 839–847.

Sun, X. F., R. C. Sun, J. Tomkinson, and M. S. Baird (2004c), Degradation of wheat straw lignin and hemicellulosic polymers by a totally chlorine-free method, *Polymer Degradation Stability*, *83*, 47–57.

Torii, T., M. Takatani, R. Hamada, and T. Okamoto (1994), ^{13}C-NMR studies on acetylated wood - distribution of acetyl substituents in the course of acid-hydrolysis, *Mokuzai Gakkaishi*, *40*, 27–35.

Tukey, J. W. (1977), *Exploratory Data Analysis*, Addison-Wesley, Reading, MA, USA.

Vazquez, G., G. Antorrena, J. Gonzalez, and S. Freire (1997), FTIR, ^{1}H and ^{13}C-NMR characterization of acetosolv-solubilized pine and eucalyptus lignins, *Holzforschung*, *51*, 158–166.

Verheyden, A., M. Roggeman, S. Bouillon, M. Elskens, H. Beeckman, and N. Koedam (2005), Comparison between δ^{13}C of alpha-cellulose and bulkwood in the mangrove tree *Rhizophora mucronata*: Implications for dendrochemistry, *Chem. Geology*, *219*, 275–282.

Westbrook, J. A., T. P. Guilderson, and P. A. Colinvaux (2006), Annual growth rings in a sample of *Hymenaea courbaril*, *IAWA Journal*, *27*(2), 193–197.

Xu, F., J. X. Sun, and R. C. Sun (2005), Characteristics of cellulose isolated by a totally chlorine-free method from fast-growing poplar wood, oil palm frond fibre and cereal straws, *Cellulose Chem. Technology*, *39*, 3–23.

Zaleski, J., Z. Daszkiewicz, and J. Kyziol (2002), Structure of N, 4-dinitroaniline and its complex with sulfolane at 85 K; on the proton donor-acceptor affinity of the primary nitramine (HNNO 2) group, *Acta Cryst.*, *58*(Part 1), 109–115.

APPENDIX B

STABLE ISOTOPE CHRONOLOGY AND CLIMATE SIGNAL CALIBRATION IN NEOTROPICAL MONTANE CLOUD FOREST TREES

Manuscript for submission to *Journal of Geophysical Research – Biogeosciences*

Stable isotope chronology and climate signal calibration in neotropical montane cloud forest trees

Kevin J. Anchukaitis[1,2], Michael N. Evans[1,2], Nathaniel T. Wheelwright[3], and Daniel P. Schrag[4]

1. Laboratory of Tree-Ring Research, The University of Arizona, Tucson, AZ
2. Department of Geosciences, The University of Arizona, Tucson, AZ
3. Department of Biology, Bowdoin College, Brunswick, ME
4. Department of Earth and Planetary Sciences, Harvard University, Cambridge, MA

B.1 Abstract

Tropical montane cloud forests are ecosystems intrinsically linked to a narrow range of geographic and meteorological conditions, making them potentially sensitive to small changes in precipitation or temperature. We investigate the potential application of stable isotope analysis to cloud forest dendroclimatology at Monteverde in Costa Rica, in order to be able to extract both chronological and paleoclimate information from trees without annual growth rings. High-resolution δ^{18}O measurements are used to identify regular cycles in wood of up to 9‰, which are associated with seasonal changes in precipitation and moisture sources. The calculated annual growth rates derived from the isotope time series match those observed from long-term basal growth measurements. Interannual variability in the oxygen isotope ratio of lower forest trees is primarily related to interannual changes in summer precipitation. Forward modeling independently supports our detection of both annual chronology and a climate signal. Trees from elevations

above the orographic cloud bank show larger interannual variability, but less consistently show coherent annual cycles. The confirmation of annual chronology and sensitivity to interannual climate anomalies suggests that tropical cloud forest dendroclimatology can be used to investigate local and regional hydroclimatic variability and change.

B.2 Introduction

In the absence of long instrumental records, scientists investigating the causes and consequences of climate variability and change depend on proxy records, which can be used to reconstruct past ocean-atmosphere conditions. In temperate latitudes, extensive networks of tree-ring width and density time series ('chronologies') provide a high-resolution proxy record of past climate state and variability. Relatively few such chronologies, however, have been developed in tropical regions. Despite some notable exceptions [c.f. *Worbes*, 2002; *Fichtler et al.*, 2004; *Brienen and Zuidema*, 2005; *D'Arrigo et al.*, 2006; *Therrell et al.*, 2006], tropical trees seldom develop reliable annual rings whose variability reflects the influence of climate variability and can be used to reconstruct past climate. Even when they appear to form annual increment bands, patterns of ring width variability may be incoherent between individual trees, making both chronology development and climate signal detection difficult [*Worbes and Junk*, 1989; *February and Stock*, 1998; *Dünisch et al.*, 2002; *Speer et al.*, 2004; *Robertson et al.*, 2004; *Bauch et al.*, 2006]. As a consequence, high-resolution, long terrestrial proxy climate records from the tropics remain sparse compared to temperate regions.

Tropical montane cloud forests cover as much as 50 million hectares worldwide [*Stadtmüller*, 1987; *Hamilton et al.*, 1995], about half of which is found in Latin America [*Brown and Kappelle*, 2001]. These forests have high rates of endemism and are important in regional hydrology, because they intercept and capture cloud moisture and

nutrients, increasing available water and influencing biogeochemistry within catchments and in areas downstream [*Bruijnzeel*, 1991; *van Dijk and Bruijnzeel*, 2001; *Bruijnzeel*, 2004]. Tropical cloud forests are ecosystems found within a relatively narrow set of both geographic and meteorological conditions, and as a consequence, they are particularly sensitive to climate change [*Loope and Giambelluca*, 1998; *Foster*, 2001; *Bush*, 2002].

Rising tropical surface and sea surface temperature associated with anthropogenic global climate change may be fundamentally altering the suite of environmental conditions that create and maintain unique cloud forest ecosystems. At Monteverde, in the mountains of Costa Rica, the extinction of the endemic Golden Toad in 1987 and subsequent species disappearances have been linked to apparent decreases in cloud cover and moisture availability and related to rising temperatures [*Pounds et al.*, 1999]. Indeed, higher temperatures in montane regions throughout the tropics have been linked to widespread species extinction and alterations to cloud forest biogeography [*Pounds et al.*, 2006]. A rise in tropical air temperatures above 1000 meters has been observed since 1970 [*Diaz and Graham*, 1996]. Climate change appears to be exposing plant and animal communities to increased environmental stress, which may exacerbate other proximal threats, including disease and habitat destruction [*Root et al.*, 2003; *Pounds et al.*, 2006].

Limited long-term instrumental climate records from the tropics, and in particular tropical montane regions [*Bradley et al.*, 2006], impede efforts to better understand both global climate variability and its influence on local hydroclimatology and ecology. Without a historical baseline and the context provided by long-term climate records, it is difficult to attribute the observed changes in climate and ecological systems at Monteverde and other tropical mountain forests to (1) anthropogenic climate forcing [*Still et al.*, 1999; *Pounds et al.*, 2006], (2) mesoscale influences including land clearance [*Lawton et al.*, 2001; *Nair et al.*, 2003], or (3) natural variability in tropical and extratropical climate.

Limited observational data and the lack of high resolution proxies from these ecosystems also restrict any opportunity to validate GCM predictions for future change [*Foster*, 2001]. Both observed and potential future changes, and their hypothesized ecological consequences, need to be placed in the context of low-frequency (decadal to centennial) climate variability and trends over the recent past.

We hypothesize that the unique hydroclimatic conditions associated with cloud forests creates an annual climate signal to the δ^{18}O in tree stems that can be used to develop a proxy record of climate variability from tropical montane regions. High-resolution oxygen isotope measurements can be used for both chronological control and climatic interpretation and reconstruction. Our study focuses on the Monteverde Cloud Forest in Costa Rica where environmental and meteorological data available over the last 20 years provides the data necessary to validate this hypothesis. We seek to develop the basis for proxy reconstructions of interannual climate variability using stable oxygen isotope series from cloud forest trees without annual rings.

B.3 Hypothesis and Approach

Tropical montane cloud forests are ecosystems characterized by frequent or persistent orographic cloud immersion [*Bruijnzeel and Veneklaas*, 1998]. During the dry season, water stripped from the cloud bank by vegetation provides sufficient soil moisture such that trees may experience no effective water deficit [*Bruijnzeel and Proctor*, 1995; *Kapos and Tanner*, 1985; *Holder*, 2004]. Precipitation, which provides the bulk of available water during the rainy season, and cloud water, which is the primary moisture source during the dry season, are isotopically distinct [*Ingraham*, 1998]. Phase transitions between liquid and vapor result in fractionation effects, which create isotopic differences between these two water sources. Condensation of clouds by orographic uplift results in

liquid water which has relatively heavy δ^{18}O values as compared to rainfall, which has a lower δ^{18}O value due to progressive Rayleigh distillation [*Ingraham*, 1998]. Similarly, the limited amount of rainfall received during the dry season has a relatively heavy δ^{18}O signature. This is related primarily to the 'amount effect', where the δ^{18}O of precipitation is negatively correlated to the quantity, and is one of the primary causes of intra-annual patterns in the isotopic composition of rainfall throughout the tropics [*Gat*, 1996]. The amount effect is evident in the stable isotopic composition of Costa Rican surface waters [*Lachniet and Patterson*, 2002].

Data from both Monteverde [*Feild and Dawson*, 1998] and other fog-dependent environments [*Ingraham and Matthews*, 1990, 1995; *Dawson*, 1998] indicate that differences of 4‰ to 6‰ δ^{18}O exist between cloud water and rainfall. *Rhodes et al.* [2006] also report differences between dry (winter) and wet (summer) season volume-weighted precipitation δ^{18}O as great as 8.2 ‰. The waters available to plants in cloud forest ecosystems are therefore distinctly different between seasons. *Feild and Dawson* [1998] confirmed that the xylem water of canopy trees at Monteverde had the isotopic signature of rainfall during the summer wet season. Cloud water should be the primary source water available to trees during the winter dry season [c.f. *Dawson*, 1998].

The seasonal changes in the isotopic composition of the primary water sources for trees in cloud forests should produce a seasonal cycle in the oxygen isotope ratio of cellulose in the secondary radial growth of these trees [*Evans and Schrag*, 2004]. Fine-scale analysis of isotope ratios of cellulose along the growth radius of a tree's main trunk will yield a time series of water use by the trees. The seasonal cycle can be used to identify the growth increment from an individual year (with 1 cycle = 1 calendar year), even in the absence of visible annual banding. Significant departures from the regular isotope cycle should result from local hydroclimatic alterations, including precipitation anomalies and

changes in cloudiness, moisture advection, relative humidity, and temperature (Figure B.1).

The relationship between the local hydroclimatology of tropical montane cloud forests and the resulting δ^{18}O value of cellulose in trees can be understood using the mechanistic model developed by *Roden et al.* [2000]:

$$\delta^{18}O_{cellulose} = f_o \cdot (\delta^{18}O_{wx} + \epsilon_o) + (1 - f_o) \cdot (\delta^{18}O_{wl} + \epsilon_o) \quad \text{(B.1)}$$

Where $\delta^{18}O_{cellulose}$ is the oxygen isotope ratio of tree-ring cellulose, $\delta^{18}O_{wx}$ is that of the portion of xylem water that does not experience evaporative enrichment in the leaves, $\delta^{18}O_{wl}$ is the oxygen isotope ratio of leaf water at the sites of photosynthesis, f_o is the fraction of oxygen in stem water that does not exchange with the enriched sucrose that results from transpiration in the leaf, and ϵ_o is the fractionation that results from the synthesis of cellulose. The model shows that α-cellulose δ^{18}O is influenced primarily by the δ^{18}O of the source water taken up by the plant, and by the amount of isotopic enrichment of that water that subsequently occurs in the leaf, and whose signature is inherited by the sucrose used in the eventual biosynthesis of cellulose. As detailed above, source water differences in cloud forests will be a function of the seasonal regimes of rainfall and cloud water. Lower relative humidity levels during the peak of the dry season should result in higher evapotranspiration rates and enrichment of the δ^{18}O value of leaf water and the resultant cellulose.

Barbour et al. [2004] modified the model of *Roden et al.* [2000] to include the potential influence of the Peclet effect, a diffusion of isotopically-enriched water away from the sites of transpiration in the leaves back into the unenriched source water, which results in lower δ^{18}O value for bulk leaf water than would be predicted from a simple calculation based on evapotranspiration in the leaf [*Barbour et al.*, 2000]:

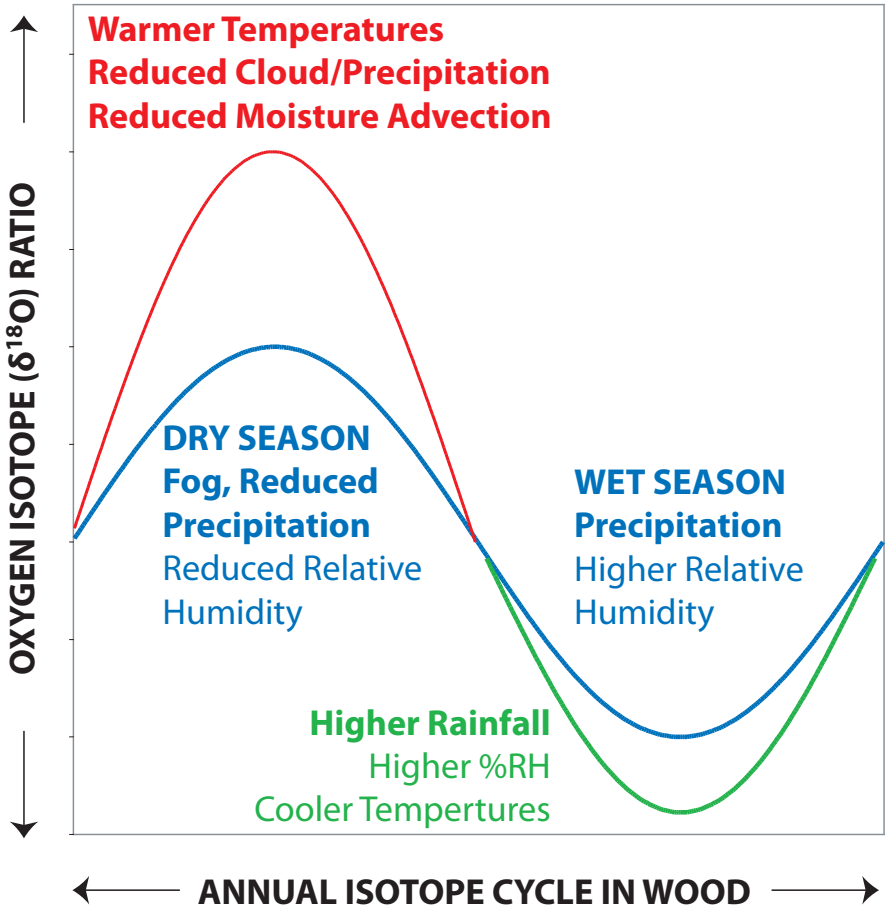

Figure B.1: Conceptual model of climatic controls on the annual and interannual patterns of stable oxygen isotope ratios in the α-cellulose of cloud forest tree radial growth. The annual cycle is generated primarily by the seasonal change in the δ^{18}O of rainfall, the use of cloud water by trees in the dry season, and the isotopic enrichment of source water by evapotranspiration during the dry season. Interannual variability in annual maximum values is expected to be related to temperature, relative humidity, cloudiness, and moisture advection during the dry season. Anomalies in the annual minima are likely related primarily to wet season precipitation amounts.

$$\Delta_c = \Delta_l(1 - p_x p_{ex}) \tag{B.2}$$

For our purposes, Δ_c is the enrichment of the cellulose δ^{18}O above that of the original source water, Δ_l reflects the enrichment of the source water signal in the leaf at the sites of photosynthesis, as a function of the vapor pressure difference within the leaf, the δ^{18}O of atmospheric water vapor, the fractionation from the liquid-vapor phase change, and the Peclet Effect. p_{ex} is the proportion of oxygen atoms exchanged during the formation of cellulose from sucrose, equivalent to f_0 from Equation (1). p_x is the proportion of unenriched water at the site of cellulose formation. For large trees and for cellulose formation in the xylem, it is believed that p_x approaches 1, as the site of cellulose synthesis is sufficiently distal from the diffusion of enriched leaf water into unaltered source water that it is primarily those waters that provide the exchangeable oxygen during cellulose biosynthesis [*Barbour et al.*, 2002]. In this case, $p_x p_{ex}$ is equivalent to f_0 from Equation (1) and represents the mixing between enriched δ^{18}O signatures from the leaf and δ^{18}O from the original source water.

We hypothesize (Figure B.1) that the isotopic difference between wet season precipitation and dry season rainfall and cloud water is sufficient to generate annual isotope cycles in the xylem of cloud forest trees. We rely on the seasonal shift in primary water source to drive concomitant changes in cellulose, enabling identification of annual cycles and chronology development. Interannual variability should be manifested as enhancement or suppression of the amplitude of the mean annual isotope cycle through changes in precipitation, temperature, and relative humidity. Year-to-year differences in annual maximum values are expected to be related to temperature, relative humidity, cloudiness, and moisture advection during the dry season. Anomalies in the annual minima are likely related primarily to wet season precipitation amounts.

B.4 Methods and Materials

We test our hypotheses using samples and data collected from the Monteverde Cloud Forest Reserve in Costa Rica. Long-term vegetation monitoring and daily climate records from the Reserve can be used to calibrate, model, and interpret the δ^{18}O content of tree cellulose, making the site an ideal location in which to establish if the necessary chronological control and climate signal exist. Establishing both of these is a necessary prerequisite for the development of robust climate reconstructions.

B.4.1 Site description

The Monteverde Cloud Forest (10.2^{o}N, 85.35^{o}W, 1500m) is draped over the Cordillera de Tilarán in northwestern Costa Rica. The cloud forest extends from ∼1500 m on the Pacific slope upward to the continental divide, and down the windward Atlantic slope as low as 1300 m [*Haber*, 2000]. Below the cloud forest and downslope to 700m elevation on the leeward Pacific slope the vegetation is predominantly evergreen tropical premontane wet forests with a distinct dry season. Between 1400 and 1500m, the premontane forest transitions to lower montane wet forests with greater orographic cloud influence [*Haber*, 2000]. The cloud forest above 1500m receives an average of 2500mm of precipitation in a year and has a mean annual temperature of 18.5^{o}C [Figure B.2; *Pounds et al.*, 1999; *Clark et al.*, 2000]. These forests are characterized by the presence of tradewind-driven orographic clouds in the transitional (November through January) and dry (February through April) seasons. During the summer (May through October), the precipitation regime is dominated by the position of the Intertropical Convergence Zone (ITCZ) and characterized by strong convective rainfall and thunderstorms [*Clark et al.*, 2000; *Rhodes et al.*, 2006]. A midsummer drought, common to the Pacific Coast of tropical Central America [*Magaña et al.*, 1999], is present in July and August (Figure B.2). The cloud

forest receives the majority of its rainfall during the summer wet season, but the annual moisture regime has substantial and seasonally important inputs from orographic cloud water between November and April. Whereas the Atlantic slope is perpetually wet, the leeward slope depends on the northeasterly trade wind-driven moisture over the continental divide as a critical dry season water source. *Clark et al.* [1998] found that at Monteverde these moisture inputs accounted for perhaps 22% of the annual hydrological budget. However, estimates of the contribution from cloud water at different tropical montane cloud forest sites vary from 6 up to 154% of precipitation [*Bruijnzeel and Proctor*, 1995; *Bruijnzeel*, 2001]. Cloud water inputs are consistently more important during the dry season, accounting for up to 75% of total moisture inputs in some forests [*Bruijnzeel*, 2001].

Samples for our calibration study of cloud forest isotope dendroclimatology come from two locations. We first take advantage of two stands of planted and monitored *Ocotea tenera* (Lauraceae) from forest plots in the transitional zone between lower montane and cloud forest [*Wheelwright and Logan*, 2004] in order to calibrate and confirm our hypothesized age model and precisely evaluate potential climate signals. We also analyze a set of pilot samples from mature cloud forest canopy trees above 1500m to allow us to identify potential candidate species and sites for future long-term climate reconstructions. Together, the combination of different sites and different species allows us to investigate spatiotemporal variability in cloud forest hydroclimatology as reflected in the δ^{18}O of cloud forest trees.

B.4.2 Field and laboratory sampling

Increment cores from *O. tenera* were collected in February 2004 from the Trostles (NWT) and Hoges (NWH) plantation sites [*Wheelwright and Logan*, 2004] (1410 and 1430m).

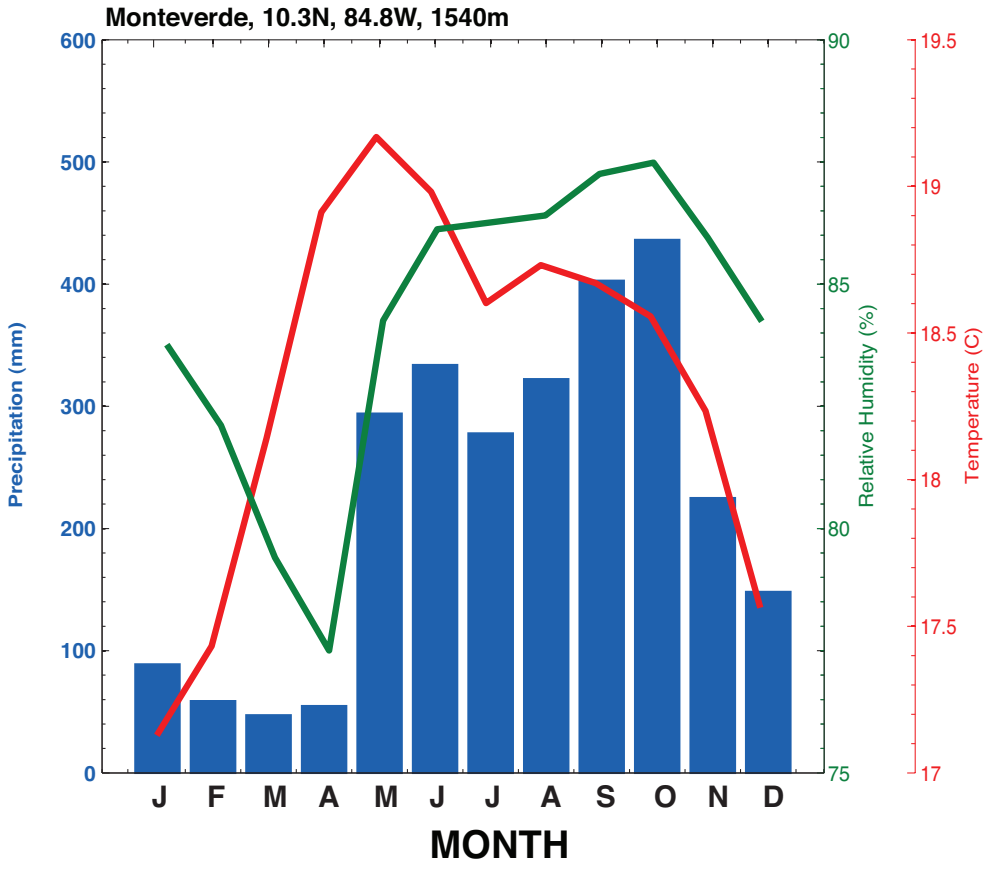

Figure B.2: Patterns of mean annual temperature and precipitation for Monteverde from the Campbell weather station and derived relative humidity (1979-2000,10.2 ^{o}N, 85.35 ^{o}W, 1540m, *Pounds et al.* [1999].

Three cores were obtained from the Trostles plantation, with two collected from a single tree (NWT02A/B), and one from a separate individual (NWT01A). A fourth core was collected from the Hoges plantation (NWH03A). This sampling approach was designed to evaluate the fidelity and consistency of the chronological and climatic signal both within and between trees, and amongst sites.

Seven additional cores or entire cross-sectional discs were also opportunistically collected in and around the Monteverde Cloud Forest Reserve (1500-1660m), largely from mature canopy trees killed or damaged in a December 2003 windstorm. This group included individuals from the genus *Quercus* (tropical oaks) as well as from the cosmopolitan Sapotaceae and Lauraceae families (Table B.1). The forest trees were sampled along a rudimentary transect up the Pacific slope toward the continental divide. This strategy was intended to accomplish two complementary goals. First, to permit discovery of sites or species that have maximum sensitivity to both annual and interannual changes in climate. Second, the comparison of δ^{18}O values from both below and within the cloud bank should allow us to estimate the relative importance across the landscape of changes in precipitation, temperature, and relative humidity to the α-cellulose δ^{18}O of cloud forest trees.

B.4.3 Sample preparation

The cores were subsampled in the laboratory on a rotary microtome at 20 μm increments. Ten slices were then aggregated into a single sample for a sampling depth resolution of 200 μm. Radial subsections approximating the diameter of the cores (5mm) were cut from the large full stem discs using a bandsaw prior to microtoming. Our subsampling interval resulted in approximately 700 to 1500 μg of wood per sample, depending on wood density, structure, and moisture content.

Raw wood was then extracted to α-cellulose using the standard Brendel technique [*Brendel et al.*, 2000; *Gaudinski et al.*, 2005; *Anchukaitis et al.*, 2007b] as modified for small samples [*Evans and Schrag*, 2004]. The Brendel procedure uses a hot 10:1 acetic:nitric acid delignification extraction that also removes most hemicelluloses and mobile resins, followed by progressive solvent washes and sample drying in distilled water, ethanol, and acetone [*Evans and Schrag*, 2004; *Anchukaitis et al.*, 2007b]. Following α-cellulose extraction, samples were dried in a warm oven, and then overnight under vacuum. Use of the Brendel technique allows for single-day chemical preprocessing of samples and, most critically, permits the use of very small ($<$ 1 mg) samples with a sufficient final sample yield [*Evans and Schrag*, 2004] for replicate isotopic measurements. The Brendel technique results in α-cellulose which is not significantly biased in its isotopic composition compared to traditional methods [*Evans and Schrag*, 2004; *Anchukaitis et al.*, 2007b].

B.4.4 Isotopic analysis

100 to 150 μg of α-cellulose of each sample from the plantation *O. tenera* core were wrapped in silver capsules and converted to CO in a ThermoFinnigan Thermal Conversion/Elemental Analyzer (TC/EA) at 1450 ^{o}C. The oxygen isotope composition of the CO gas was analyzed on a ThermoFinnigan Delta XL continuous flow mass spectrometer at Harvard University. Measurement precision for several hundred Baker α-cellulose standards was 0.45‰ Long-term precision on the instrument is better than 0.1‰ on internal reference gas standards.

For the analysis of pilot samples from canopy trees in the Monteverde Cloud Forest Preserve, 300 to 350 μg of α-cellulose were loaded in silver capsules and converted online to CO in a Costech High Temperature Generator/Elemental Combustion System

(HTG/ECS) system with a quartz outer reactor and molybdenum crucible packed with graphite [*Evans et al.*, 2007]. Our HTG pyrolysis system at The University of Arizona is a 1MHz radio frequency induction heater which quickly brings the molybdenum susceptor inside the reactor assembly to $>1500^{o}$C, at which time the sample is introduced to the crucible and pyrolysed. Use of the HTG peripheral reduces laboratory consumables, simplifies reactor maintenance and replacement, and results in an efficient high-temperature conversion of the sample to CO [*Evans et al.*, 2007]. This study is the first application of this technology to paleoenvironmental research using oxygen isotopes. The isotopic ratio of the CO gas was measured on a ThermoFinnigan Delta+XP. Precision on our Sigma Alpha Cellulose (SAC) solid standard material was 0.34‰, and internal precision consistently 0.08‰ or better. All δ^{18}O results from both instruments are reported with respect to the international Vienna Standard Mean Ocean Water (VSMOW).

B.4.5 Forward modeling

We use the *Barbour et al.* [2004] model of the environmental controls on the stable isotope composition of wood, as modified and adapted for time series prediction in tropical environments by *Evans* [2007], to simulate a theoretical stable oxygen isotope time series based on local meteorological data. Synthetic isotope time series are then compared with our actual measured δ^{18}O chronology from *O. tenera* to independently test the age model and climate signal detection. The model takes as input monthly temperature, precipitation, and relative humidity data. There are 6 parameters in the model, many of which are only weakly constrained by observations, particularly for tropical species and environments. Following *Evans* [2007], we parameterized leaf temperature as a function of air temperature [*Linacre*, 1964] and atmospheric water vapor as a function of condensation temperature and the fractionation related to the vapor-

liquid phase change. *Evans* [2007] derived stomatal conductance as a function of vapor pressure deficit calculated from leaf and air temperature and relative humidity. This allows stomatal conductance, and therefore transpiration, to vary temporally in response to environmental conditions. Two additional parameters provide the coefficients for the model relating precipitation to δ^{18}O of meteoric waters (see below).

Precipitation and temperature data are available from the Campbell (1540m) weather station [*Pounds et al.,* 1999] for the period 1977 to 2005, and from the Monteverde Institute [*Rhodes et al.,* 2006] from 2004 through 2006 (1420m). We calculated monthly source water δ^{18}O as a function of the observed relationship between rainfall amount and the δ^{18}O composition of rainfall (the amount effect) from *Rhodes et al.* [2006]. We regressed the δ^{18}O on rainfall amounts for those data with aggregate collection periods of two weeks to two months. Single-storm events and shorter collection periods showed a higher variability which likely reflected the time of sampling and the trajectory and history of individual weather systems, while longer periods excessively smoothed monthly differences related to the timing and onset of precipitation seasonality. Three samples which were observed by *Rhodes et al.* [2006] to have algae growing on the collection container were excluded from the regression model. Source water δ^{18}O values were then calculated based on monthly total precipitation values from the Campbell data set:

$$\delta^{18}O_{sw}‰ = -0.0155 \times P(mm/month) - 1.2614 \qquad \text{(B.3)}$$

The regression model accounts for 56% of the variance in the observed dataset and is significant at $p < 0.01$ with 14 effective degrees of freedom.

The *Rhodes et al.* [2006] data also includes relative humidity for July 2005 through the end of 2006. In order to develop modeled synthetic chronologies which spanned the full

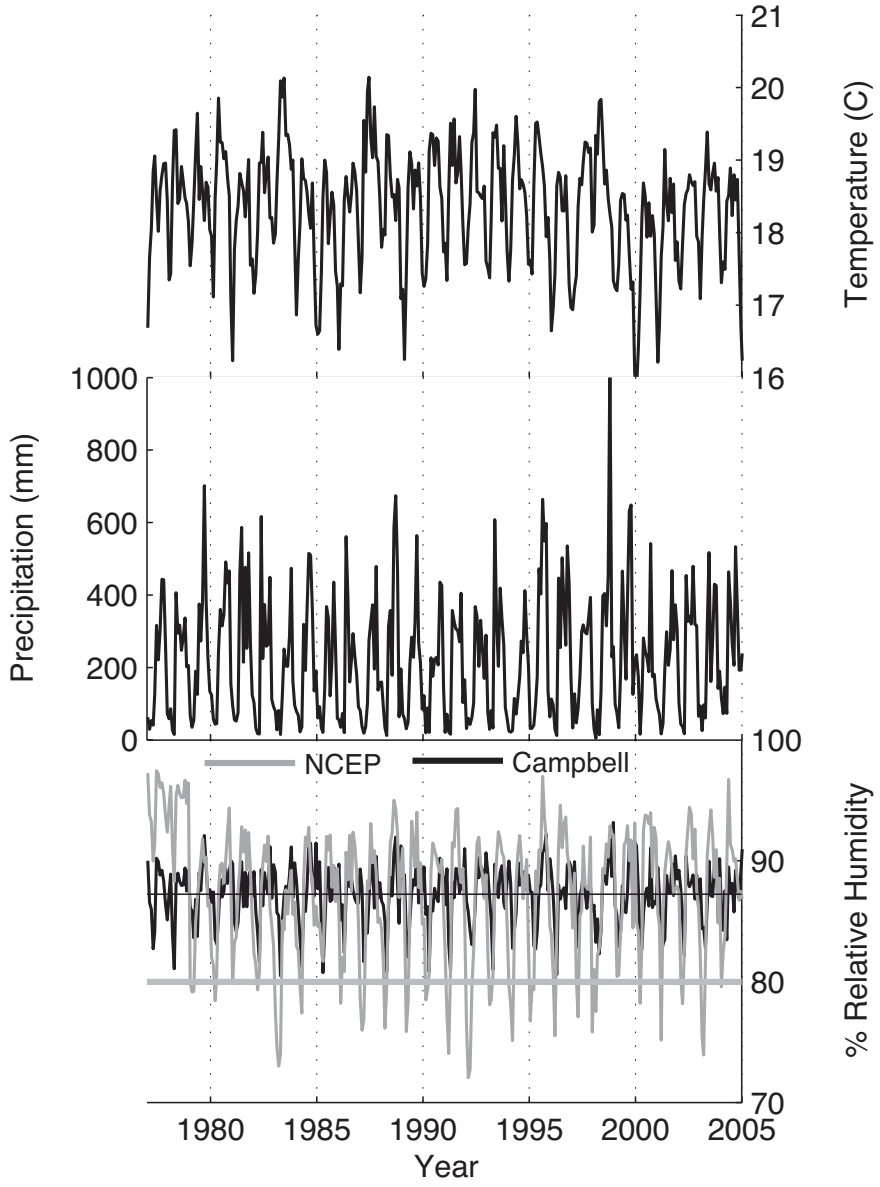

Figure B.3: Meteorological data from Monteverde used as input for the forward model of tree α-cellulose δ^{18}O. (a) Temperature (^{o}C) and (b) Precipitation from the Campbell meteorological station [*Pounds et al.*, 1999], and (c) relative humidity derived from the Campbell data and from the NCEP Reanalysis 2 [*Kanamitsu et al.*, 2002]. The NCEP relative humidity has been scaled to give it the same mean as that observed in *Rhodes et al.* [2006], but allowed to retain its variance. The horizonal lines of the same color show the original overall mean value. Sensitivity to the choice of relative humidity data is 0.20‰ per month per percent mean relative humidity.

timescale of our oxygen isotope chronologies from the *O. tenera* plantations, we derived a relative humidity time series to use with the model by regressing the daily relative humidity measurement from *Rhodes et al.* [2006] on the maximum daily temperature and daily precipitation values for the same station. This model was then applied to create a daily relative humidity time series spanning the full length of the Campbell [*Pounds et al.*, 1999] daily temperature and precipitation record:

$$RH\% = (-1.0191 \times Tmax(C)) + (0.2459 \times P(mm)) - 105.1180 \qquad \text{(B.4)}$$

The regression model accounted for 43% of the variance, and was significant at $p < 0.01$. Relative humidity values were then adjusted so that the long-term seasonal mean and variance matched those from the observations by *Rhodes et al.* [2006]. Daily values from all three variables were then combined to form monthly means and total precipitation for model input. We also extracted a time series of monthly relative humidity from the NCEP Reanalysis II gridded data [*Kanamitsu et al.*, 2002] for the latitude, longitude, and atmospheric pressure level (850mb) which most closely corresponds to the Monteverde Cloud Forest, in order to test the sensitivity of our results to the choice of available relative humidity data.

Evans [2007] used the forward model to reconstruct the patterns of interannual variability in δ^{18}O cycles in a tropical trees from La Selva Biological Station in Costa Rica. In those simulations, the mean and variance of the simulation were adjusted to that of the observed δ^{18}O time series. Here, we use a simple single-component soil mixing model in place of the variance adjustment to capture the influence of the temporal smoothing of individual monthly water δ^{18}O as a result of soil water residence times. Following *Evans* [2007], we use a Monte Carlo procedure (1000 simulations) and

randomized adjustments (up to 20%) of the 6 model and 2 source water coefficients to estimate the sensitivity of the interannual patterns of variability to the selection of the parameter values.

B.5 Results

B.5.1 Plantation trees (NWT, NWH)

δ^{18}O from all four plantation cores show regular isotope cycles as large as 9‰ (Figure B.4). Based on our conceptual model (Figure B.1, we assigned the local maxima of each peak to the month of April of each year. Age models were developed individually for each tree (Figure B.5), and confirmed based on the sampling date and incremental growth measurements over the last two decades [*Wheelwright and Logan*, 2004]. We were able to detect missing years primarily using these growth observations, and secondarily through identification of apparently truncated cycles in the raw δ^{18}O record, a rudimentary crossdating [*Fritts*, 1976] between the four cores, and the results of the forward model simulations. These missing years are not obviously associated with any climatic cause, however, nor are they common amongst the four cores from the plantations.

Annual radial growth increments calculated from the age modeled δ^{18}O chronologies match those from the basal diameter measurements [*Wheelwright and Logan*, 2004]. The mean of the radial growth rate from sample NWT01A is 4.5mm year^{-1}, while the estimate from basal diameter measurements is 5.4mm year^{-1}. The overall mean growth rate from tree NWT02 is 4.3mm year^{-1} from the age modeled isotope time series, and approximately 4.4mm year^{-1} from the repeated diameter measurements. Tree NWH03A from the Hoges plantation has a δ^{18}O derived mean growth rate of 4.6mm year^{-1} and 4.4mm year^{-1} from observations. The mean interseries correlation [c.f. *Fritts*, 1976] between the monthly δ^{18}O series for the three trees is 0.75, and 0.68 when the amplitudes

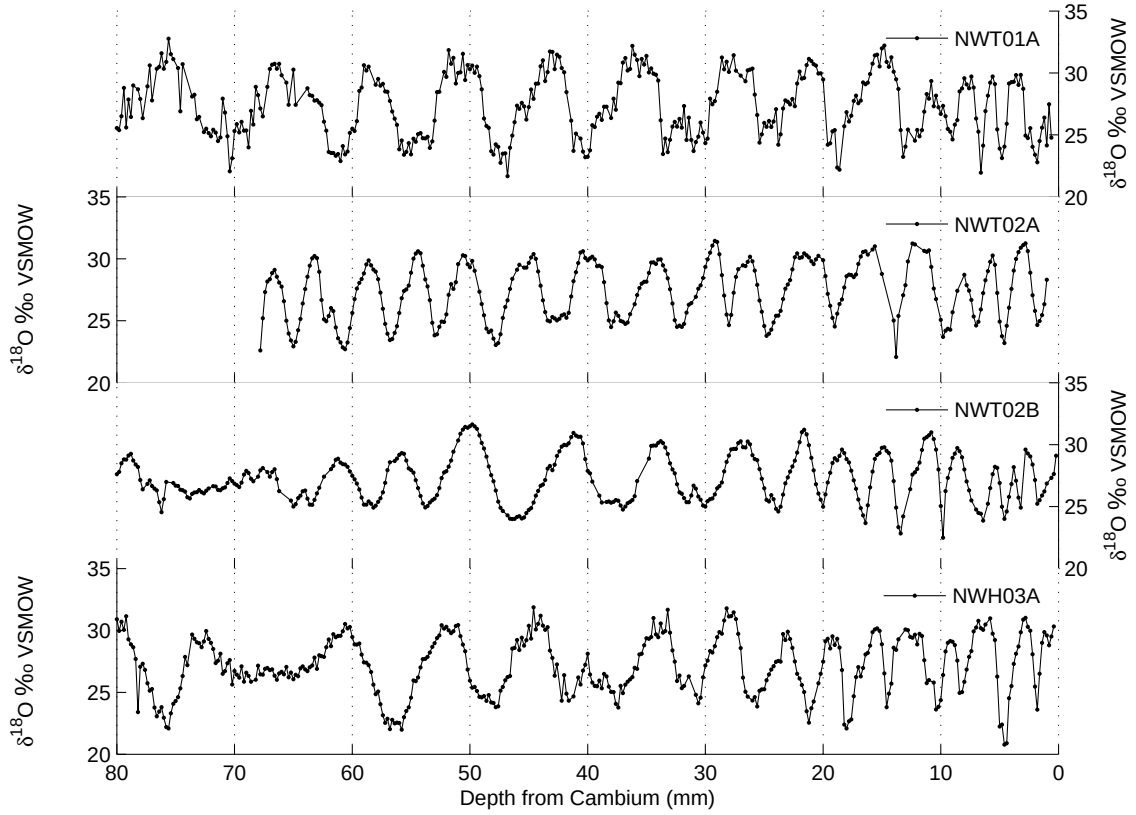

Figure B.4: Isotope ratios as a function of sampling depth for the four plantation *Ocotea tenera* from the Trostles and Hoges sites. Individual samples are indicated by dots. In NWT02B and NWH03A, samples across or close to the pith can be seen in the δ^{18}O plateau near the center of the tree.

of the annual cycles are compared. The samples from the Trostles plantation are better correlated with one another than with the single core from the Hoges plantation, almost entirely because NWH03A does not show the reduction in growth rate and δ^{18}O amplitude after 1999 observed in the older trees from the Trostles plantation (see below).

There are some notable features in the δ^{18}O series as a function of depth. Cores NWT02A and NWT02B, although from the same trees, show different mean growth rates, although in combination their average growth rate is similar to observations. At least two cores show evidence of a reduced cycle amplitude near the center of the tree, with NWH03A showing a clear plateau in δ^{18}O and a subsequent resumption of regular cycles. Both the variance reduction and plateau are likely related to either passing through the pith of the tree, or as a result of sampling tangential to the growth radius near the center of the tree. At least three out of the four cores (NWT01, NWT02A, and NWT02B) also show growth reductions in the outermost 10mm of growth. This is also consistent with the basal growth observations from *Wheelwright and Logan* [2004], which show a clearly reduced growth rate (as small as 2.2mm year^{-1} in NWT01A) after 1997. A suppression of the amplitude of the annual δ^{18}O cycle is also observed in the most recent xylem growth.

The mean annual δ^{18}O cycle from each of the individual trees has the same amplitude within the instrumental precision of measurements (Figure B.6a). The seasonal maximum is set by the age model to April, while the annual mean minimum is in September for NWT01A and NWH03A, and in October for NWT02. These correspond to the peak of the climatological dry and wet seasons, respectively. The composite mean time series formed from the overlapping portions (1990 to 2001) of the time series of each core shows an average annual cycle of 5.72‰. The δ^{18}O chronology shows patterns of interannual variability as anomalous amplitude in the annual cycles, ranging from 2.40‰ to 7.55‰ and a standard deviation of = 1.45‰ (Figure B.6b).

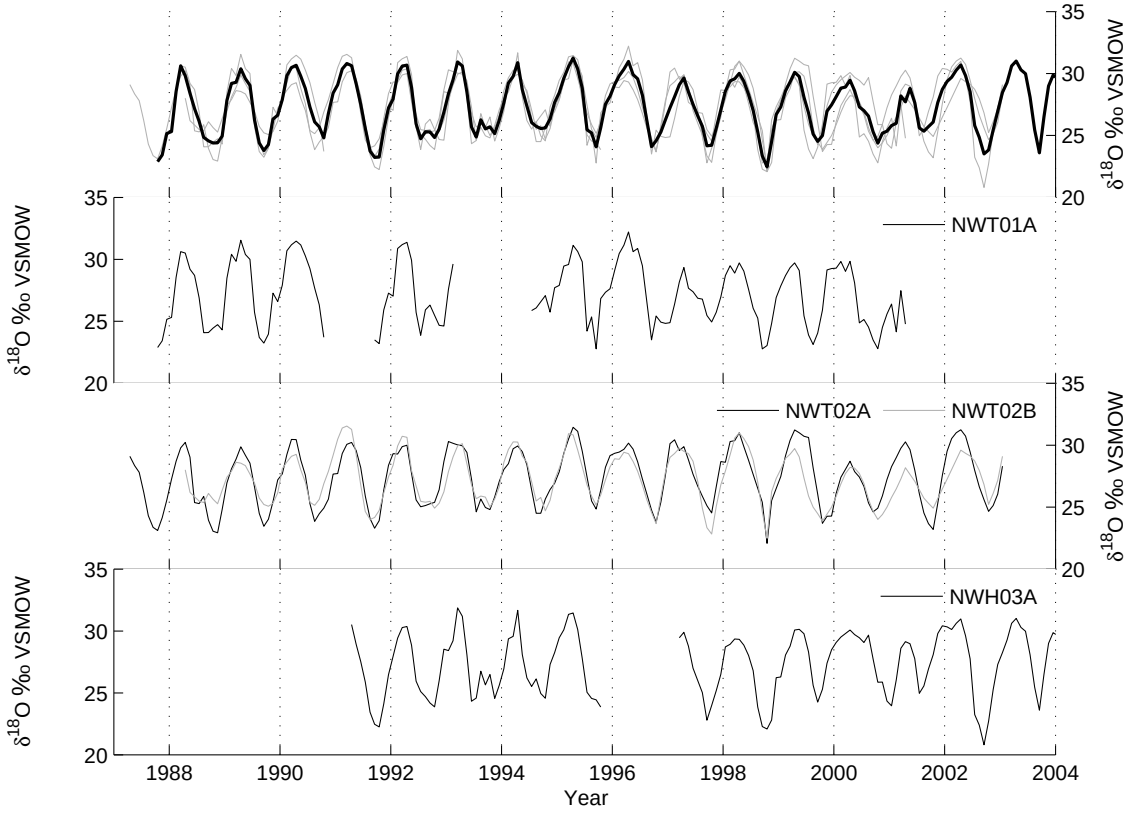

Figure B.5: Isotope ratios as a function of time for the four plantation *Ocotea tenera* from the Trostles and Hoges sites. 'Missing' years in the age model chronologies reflect both known growth hiatuses from the annual diameter measurements [*Wheelwright and Logan*, 2004] and their confirmation with rudimentary crossdating between cores, and is supported by the results of forward modeling

The interannual variability in annual cycle amplitude is driven primarily by a combination of year-to-year changes in the annual minimum value ($\sigma = 0.95‰$) and a declining trend in the value of the annual cycle maximum, most clearly influenced by a decrease after 1996 (Figure B.6c), which accounts for the majority of the variance in the annual maxima. Interannual variability in δ^{18}O is most clearly linked to precipitation (Figure B.6d), with wet season precipitation anomalies showing a clear association with detrended amplitude anomalies and a significant relationship that explains more than 50% of the variance, despite the small degrees of freedom ($r = 0.74$, $R^2 = 0.56$, $p < 0.01$). The declining trend in maximum annual δ^{18}O values mirrors somewhat the declining trends in Monteverde maximum temperature [*Pounds et al.*, 2006] and dry season relative humidity over the same period. The decline in maximum δ^{18}O after 1996 (Figure B.6c) in the composite plantation time series is also seen in the relative humidity corresponding to the location of Monteverde from the NCEP II reanalysis. However, the individual δ^{18}O series maxima at the calibration site do not in turn mirror the large summer anomalies seen in both the temperature and relative humidity data in, for example, 1992 and 1998 (Figure B.3).

B.5.2 Forest canopy trees (MV)

Whereas all four plantation samples showed distinct, large magnitude changes in δ^{18}O associated with annual changes in precipitation, pilot samples from forest trees showed a range of temporal stable oxygen isotope patterns, most without consistent annual isotope cycles (Figure B.7a-f, Table B.1). Of the seven pilot forest trees examined here, only three (MV03, MV05, and MV14B) show periodic indications of annual cyclicity in δ^{18}O than could be used for chronology. Because of this limited sample set, we include here in subsequent analyses data from two additional trees (MV12A and MV15C)

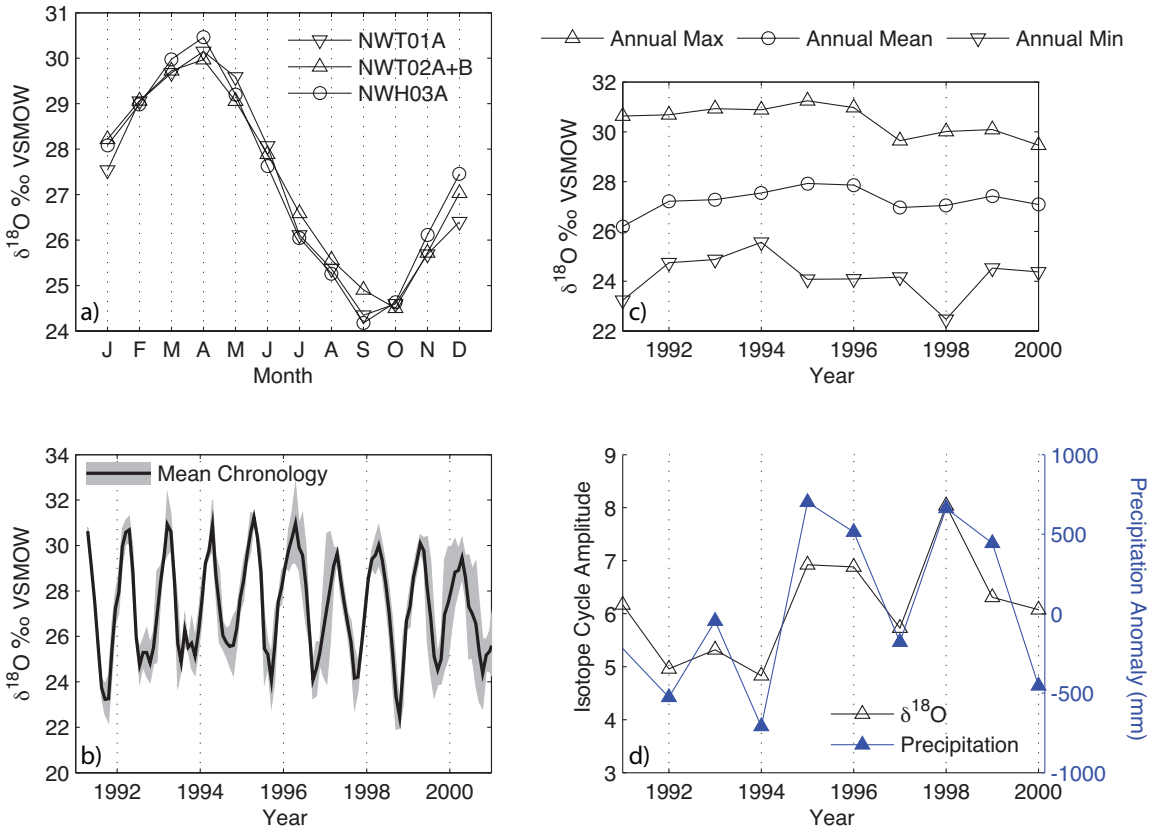

Figure B.6: Composite isotope timeseries for the Trostles/Hoges calibration set. (a) Mean δ^{18}O annual cycle ('climatology') for the three trees and the mean of all trees. The amplitude and seasonal patterns are indistinguishable within measurement precision, with temporal age model differences of approximately 1 month. (b) Composite timeseries mean of the three trees (four cores), showing variability (1σ) around the overall mean. (c) Annual maxima, minima, and mean values from the composite mean site chronology. Most of the interannual variability (is related to the minima, while the trend in the mean is a result of patterns observed in the annual maxima. (d) The amplitude of the mean annual δ^{18}O cycle, which shows a clear relationship to interannual patterns in the wet season rainfall ($R^2 = 0.56$, $p < 0.01$, $d.f. = 10$)

with confirmed coherent annual cycles over their full length, which we have analyzed elsewhere [*Anchukaitis et al.*, 2007a].

Quercus could be an excellent candidate genus for tropical isotope dendroclimatology, because it is relatively common, is straightforward to identify in the field, and is a long-lived mature canopy tree. However, neither of our two samples from *Quercus,* one at 1540m and the other higher in the cloud forest at 1660 meters shows consistent cycles in δ^{18}O that could be used for chronological control. The lower forest sample (MV05) shows periods of identifiable cyclicity, but much longer periods with no coherent temporal pattern for chronology. The upper cloud forest oak (MV11) shows no detectable δ^{18}O cycles at all. Similarly, our pilot sample (MV14B) from *Podocarpus* shows short periods of coherent large magnitude changes comparable to those from the plantation calibration set, but sustained periods with no detectable cycles in δ^{18}O. Samples from *Sideroxylon* (MV23A, Sapotaceae) from ∼1500m and *Pouteria* (MV15A, Sapotaceae) at 1580m likewise showed no apparent coherent δ^{18}O cycles in pilot isotopic measurements. The most promising evidence of cycles outside of the plantation trees came from a Lauraceae (MV03) in which they could be detected for approximately 12 years. However, the tree appears to have experienced extremely suppressed growth in the most recent period (0 to 18mm depth), making it impossible to tie the chronology to the meteorological record and develop an absolute chronology. Moreover, an individual of the same species growing at the same location (MV02) showed no obvious signs of annual δ^{18}O cycles.

There is an increasing but statistically insignificant trend in total mean δ^{18}O value with increasing altitude in the Monteverde Cloud Forest (Figure B.7g). The two oak trees both show lower average δ^{18}O with respect to elevation, and overall, than any of the plantation or forest trees. There is a distinct and statistically significant pattern ($R^2 = 0.99$, $p < 0.01$, $n = 5$) associated with elevation in the mean amplitude of the

Sample	Taxon	Elevation(m)	Mean (‰)	Annual Cycle (‰)			Reference
				Amplitude (*n*)	σ Amplitude	σ Max/Min	
NWT/NWH	*Ocotea tenera*	1410	27.27	5.72 (11)	1.45	0.89/0.95	This study
MV02	Lauraceae	1530	28.06	-	-	-	This study
MV03	Lauraceae	1530	27.71	3.23 (13)	1.34	1.00/1.05	This study
MV05	*Quercus*	1540	25.16	1.72 (13)	0.84	0.81/0.6	This study
MV11	*Quercus*	1660	26.23	-	-	-	This study
MV12	Sapotaceae (*Pouteria*)	1560	27.73	2.59 (55)	1.08	0.99/0.64	*Anchukaitis et al.* [2007a]
MV14B	Podocarpus	1580	28.88	2.19	1.42 (8)	0.71/0.97	This study
MV15A	Sapotaceae (*Pouteria*)	1580	27.28	-	-	-	This study
MV15C	Sapotaceae (*Pouteria*)	1580	26.97	1.79 (70)	1.08	0.83/0.72	*Anchukaitis et al.* [2007a]
MV23A	Sapotaceae (*Sideroxylon*)	1480	26.95	-	-	-	This study

Table B.1: Site elevation, mean δ^{18}O value, and characteristics of annual oxygen isotope cycles from plantation composite mean and cloud forest trees from Monteverde. Elevations are estimated from altimeter readings and topographic maps. Overall mean δ^{18}O is based on all measured values, irrespective of the presence or absence of annual cycles. The characteristics of the annual cycle are calculated from the portion of the age modeled series where they could be detected, with *n* equal to the number of identified annual cycles.

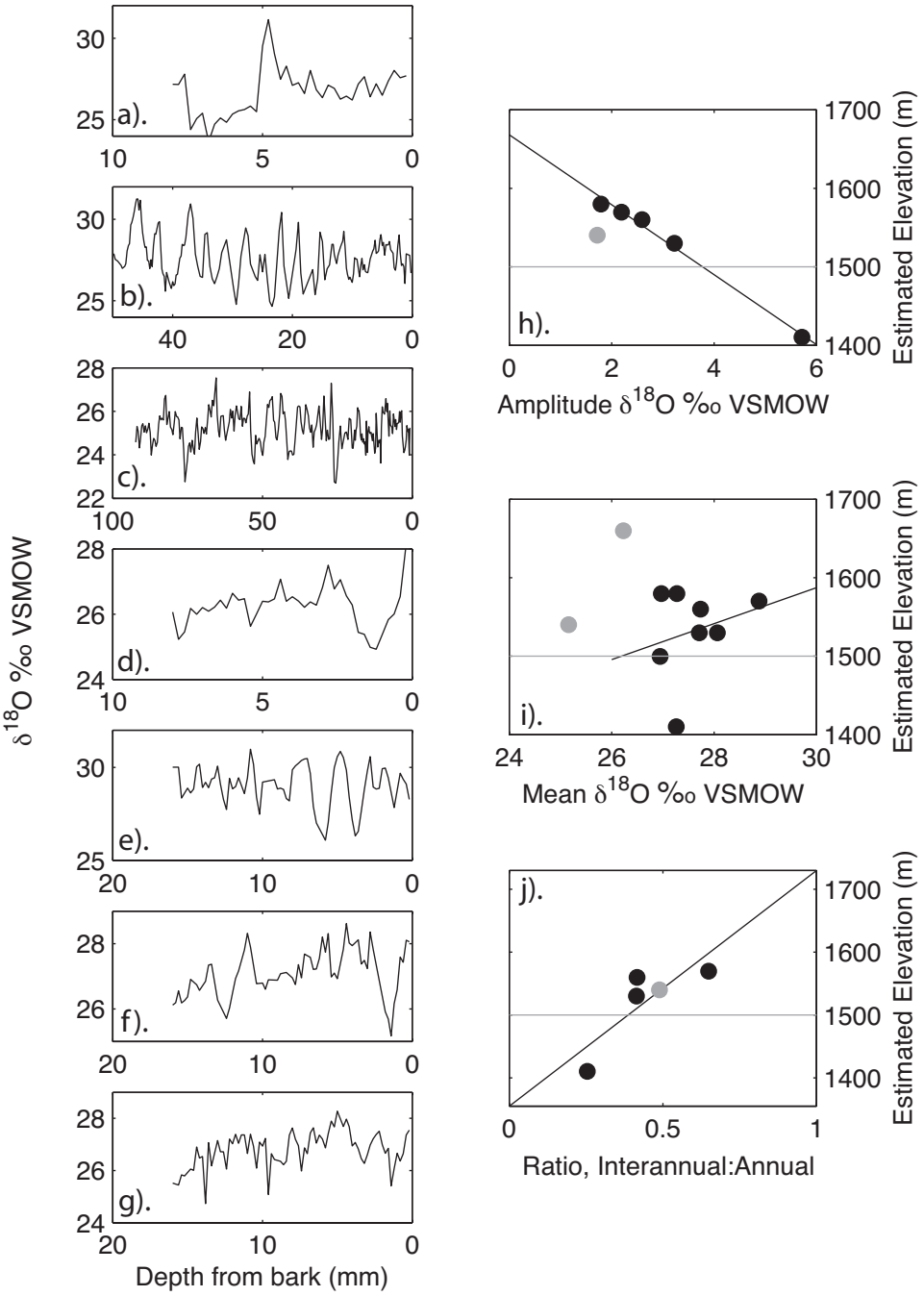

Figure B.7: Isotope timeseries for the canopy tree calibration set and the observed relationships between elevation, δ^{18}O mean, and the amplitude of the annual δ^{18}O cycle. δ^{18}O by depth from (a) MV02, (b)MV03, (c) MV05, (d) MV11, (e) MV14B, (f) MV15A, and (g) MV23A (see Table B.1 for details). (h) Amplitude of the annual cycle (including data from (b,c,e), see text for details), and (i) overall mean δ^{18}O versus elevation. (j) The ratio of the interannual amplitude variance to the mean isotope climatology increases with elevation, showing greater year-to-year climate variability above the orographic cloud bank (indicated by the gray line in (h-j).

annual cycle in trees (MV05, MV14B, MV03, MV12A, and MV15C) in those instances where it could be detected (Figure B.7h). Annual mean δ^{18}O amplitude ranges from 5.72‰ for the plantation species at approximately 1410m to 1.79‰ for sample MV15C at approximately 1580 meters. The lower forest oak (MV05) appears to have cycles of, on average, 1.72‰. Both of the oak samples (MV05 and MV11) show lower overall mean δ^{18}O values and MV05 has a suppressed annual cycle amplitude compared to those at similar elevations. The ratio of the mean annual δ^{18}O cycle to the standard deviation of the annual amplitude decreases with elevation, indicating that as the annual cycle is reduced with increasing elevation, the magnitude of the year-to-year variability (anomalies) with respect to the annual cycle increases and a greater proportion of the total variability is in the interannual or longer time scales.

B.5.3 Forward δ^{18}O modeling

Simulations using our forward model produce annual cycles similar to those seen in the measured δ^{18}O from the plantation trees (Figure B.8a-b). The best match between overall variance in the simulated and actual isotope chronologies for the plantation trees is achieved using a soil water mixing ratio of approximately 30:70 (30% new precipitation mixing with 70% of the previous month's soil water). Using the Campbell meteorological data, including the derived relative humidity series, the observed and modeled chronologies are significantly correlated ($r = 0.73, R^2 = 0.52, p < 0.01$), taking into account the high degree of serial autocorrelation ($ar(1,2)_{obs} = [0.83, 0.45]$, $ar(1,2)_{model} = [0.77, 0.46]$) in both series [*Ebisuzaki*, 1997]. Simulations using the NCEP Reanalysis II relative humidity (Figure B.8) for the grid cell associated with Monteverde are similarly correlated ($r = 0.74$, $R^2 = 0.55$, $p < 0.01$), but are not significantly different. This is largely because the correlation between the simulations

and the observed δ^{18}O time series reflects the large proportion of the total variance in the annual cycle, which is predominantly controlled by the seasonal amount effect reflected in all plantation trees. Overall, there is no statistically significant (two-tailed t- and F-test, $\alpha = 0.05$) difference in the means or variances of the residuals ($observed - modeled$) using either NCEP or Campbell-derived relative humidity.

The observed and modeled annual amplitude show similar patterns, but are weakly correlated at this scale (NCEP %RH: $r_{[model,obs]} = 0.55$, $p = 0.08$; Campbell %RH: $r_{[model,obs]} = 0.51$, $p = 0.11$), largely influenced by the mismatch between the measured and simulated values for 1991 (Figure B.8c). The modeled amplitude is significantly correlated over the same period with the wet season precipitation anomalies (NCEP %RH: $r_{[model,precip]} = 0.71$, $p < 0.01$; Campbell %RH: $r_{[model,precip]} = 0.91$, $p < 0.01$), with a substantially stronger correlation between precipitation anomalies and the simulation using the lower amplitude Campbell derived RH record. A downward trend in the annual maximum δ^{18}O values is seen for model simulations, irrespective of the relative humidity input used, although the NCEP data results in a slightly better match to the actual, observed isotope time series, particularly the annual maxima δ^{18}O values (Figure B.8d). The simulated chronology that results from using this dataset, however, has larger positive excursions in maximum annual δ^{18}O that are not seen in the actual chronology (1992,1994), and results in a overall mean δ^{18}O value approximately 1.35‰ enriched above that of the simulation using the Campbell derived relative humidity when the simulations are not adjusted to the observed mean. These differences indicate a model sensitivity of approximately 0.20‰ for every percent relative humidity.

When compared over the limited period for which both climate data and volume-weighted seasonal δ^{18}O of meteoric waters at Monteverde are available, simulations using calculated and observed source water isotope ratios show similar seasonal patterns and

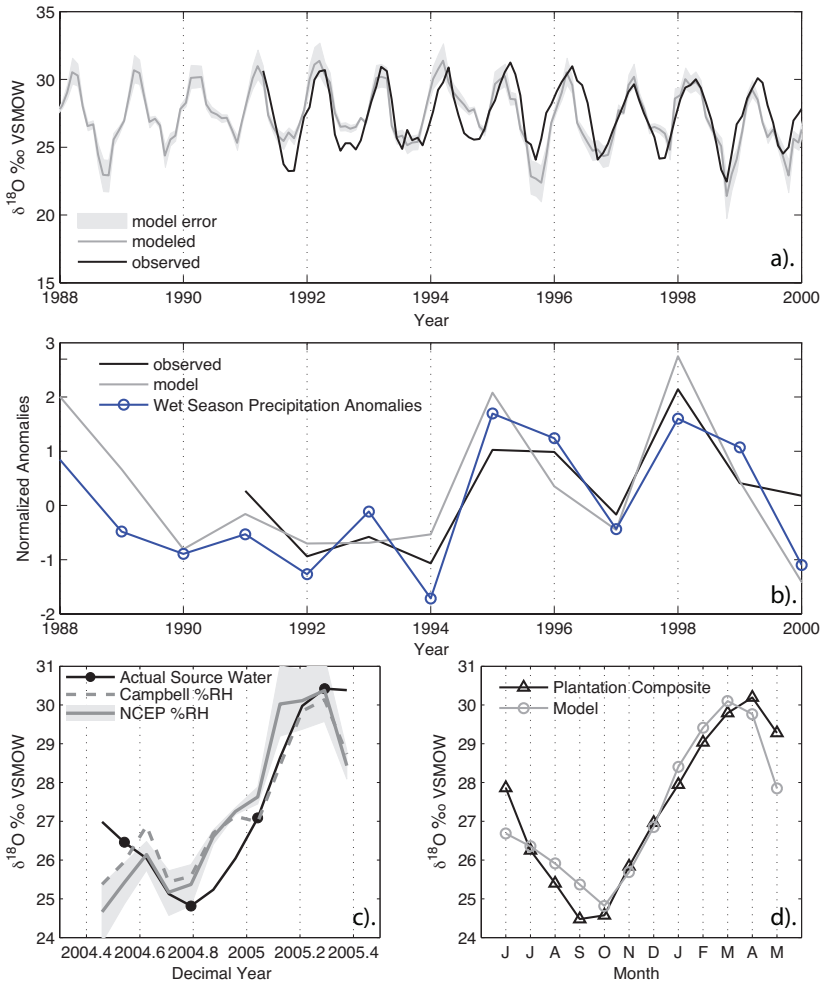

Figure B.8: Comparison between observed composite mean plantation isotope timeseries and forward model simulation [*Barbour et al.*, 2004; *Evans*, 2007] (see text for details). Input to the model was observed precipitation and temperature from Monteverde [*Pounds et al.*, 1999], and the mean monthly relative humidity from the NCEP/NCAR Reanalysis [*Kanamitsu et al.*, 2002]. (a) The simulated isotope time series is significantly correlated with the observed δ^{18}O from the plantation trees ($r = 0.74$, $R^2 = 0.55$, $p < 0.01$). (b) Observed and modeled chronologies are correlated with wet season precipitation anomalies ($r_{obs} = 0.75$, $p < 0.01$; $r_{model} = 0.71$, $p < 0.01$). (c) The source water model and actual source water produce annual cycle of similar magnitude, and the magnitude of the modeled annual cycle is similar irrespective of the relative humidity data set. (d) The seasonal patterns and isotope climatology of the mean adjusted oxygen isotope climatology are also similar, with an estimated age model error of 1 month.

amplitudes (Figure B.8c). The amount effect model (Equation 3) reproduces the seasonal pattern of observed meteoric water $\delta^{18}O$ on which it was based, with a slight loss of variance at the annual maxima and minima (Figure B.8c). The modeled α-cellulose $\delta^{18}O$ cycle amplitude is also similar whether observed or modeled source water is used, and irrespective of the relative humidity dataset. However, uncertainties in model parameters result in a confidence interval up to 1.5‰ wide, particularly at the local maxima and minima of the simulated annual $\delta^{18}O$ cycles.

B.6 Discussion

B.6.1 Annual oxygen isotope cycles

Annual $\delta^{18}O$ cycles are clearly present in our set of plantation trees, and are sufficiently large and well-defined that they are easily distinguished from the occasional smaller positive excursions at the time of the annual minima, which are probably the result of the existence and magnitude of the Central American mid-summer drought, which can be seen in some years (i.e. 1993) in both the observed and modeled α-cellulose $\delta^{18}O$ time series. The similarity between the measured radial growth rates from long-term monitoring and those derived from the age modeled isotope time series, and supported by the forward model simulations, demonstrates conclusively that the proxy $\delta^{18}O$ chronology can be securely established using these cycles. Given the potential uncertainties associated with both individual repeated basal growth measurements [*Sheil*, 2003; *McLaughlin et al.*, 2003] and the increment estimates from age modeled $\delta^{18}O$, the consistency between the two datasets indicates the age model (1 cycle = 1 year) is particularly robust. There is no indication from the isotope time series that the *Ocotea tenera* have a significant growth hiatus during the year, which is supported by comparison to our forward modeling results.

Unlike traditional dendroclimatological approaches using tree-ring widths or density, where massive sample replication and robust crossdating result in an overall composite age model error which is effectively negligible [*Fritts*, 1976], the smaller sample depth and limited opportunity for crossdating in our plantation site δ^{18}O chronology leaves open the possibility of error in assigning the isotope time series to calendar years. This is exacerbated here by the short length of the chronologies developed from our calibration set. Even in our *O. tenera* calibration samples, development of the age model is complicated by years where individual trees did not have appreciable basal growth, the reduced growth rates since 1997, and gaps in the annual observational data. This latter factor is particularly important between 1997 and 2002, because sometime between 2001 and 2004 all basal growth in several trees in Trostles plantation had ceased or slowed to imperceptible increments. For our *O. tenera* chronology, we estimate an age model error no larger than $\pm$ 2 years, based on the basal growth measurements and comparison with the forward model simulations, for our plantation calibration tree set. In non-plantation trees and particularly in trees growing at average rates less than 2mm year^{-1}, age model error can be determined by the range of possible realistic age models, and may be complemented by high-resolution radiocarbon assays on the period since A.D. 1955 [*Worbes and Junk*, 1989; *Anchukaitis et al.*, 2007a]. Unfortunately, while the plantation *O. tenera* allow us to test and calibrate our proposed age model and detect the imprint of climate variability on the δ^{18}O cycles, this early successional species is unlikely to provide the material for long isotope chronologies.

There are several factors which could potentially complicate identification of annual isotope cycles. Long residence times for meteoric waters in the soil would result in temporal mixing of different seasonal water sources, which would both smooth and dampen the amplitude of the annual signal we seek for chronological control.

Likewise, trees which access primarily deeper sources of ground water would be relatively insensitive to the intra-annual change in the δ^{18}O of available moisture [c.f. *Evans and Schrag*, 2004]. However, shallow rooting depths for cloud forest trees [*Matelson et al.*, 1995] in response to soil nutrient availability should mean that shallow soil water is their primary moisture source and they do not have access, or need to access, deeper groundwaters. One hypothesis for the lack of annual cycles in some of the forest trees analyzed here is that they are able to access deeper groundwater or well-mixed stream water, and are relatively insensitive to the seasonal δ^{18}O cycle of meteoric waters.

At our current sampling resolution and given requirements for α-cellulose yield, growth rates must be sufficiently rapid, $\sim$2mm per year, to allow for enough samples per year in order to sufficiently resolve the annual cycle and its amplitude, but not so rapid as to limit the ultimate length of the reconstruction. Slower growth rates would currently make it difficult to resolve the full amplitude of the annual cycle given current analytical constraints. This can be partially addressed by using larger-diameter increment borers, whole cross-sections, or improved analytical procedures that require less cellulose for a precise measurement.

B.6.2 Climate analysis

Interannual anomalies in the amplitude of the plantation *O. tenera* δ^{18}O cycles are dominated by variability in the annual minima value, which in agreement with our conceptual model (Figure B.1) is primarily controlled by the amount of rainfall received during the wet season (Figure B.6d). There is little year-to-year variance in the annual maxima in the composite mean δ^{18}O series from the plantation sites, with only a slight downward trend related primarily to a slight step change between 1996 and 1997. This downward trend might be related to decreases in relative humidity or maximum

temperatures [*Pounds et al.*, 2006] over the common period, but missing from the δ^{18}O maxima are distinct large positive anomalies which could be related to interannual temperature or relative humidity anomalies associated with El Niño events.

The most likely reason for the lack of a clear dry season δ^{18}O anomaly signal in the *O. tenera* series is the elevational position of our pilot calibration site at ∼1410m in the transitional region between premontane wet and cloud forest. At this lower elevation, the persistent cloud immersion that characterizes forests along the continental divide above 1500m is considerably reduced, although mist can still be an important moisture source for vegetation. Trees in the premontane wet forest and below the mean lifting condensation level would be relatively insensitive to changes in orographic clouds and relative humidity since the magnitude of the local hydroclimatic alterations to fluctuations would therefore be relatively small. At higher elevations above the mean lifting condensation level, where forests are on average consistently within or at the margin of the prevailing orographic cloud bank, fluctuations between cloud and cloud-free conditions would be accompanied by rather large local changes in temperature, relative humidity, water vapor, and solar irradiance. Support for this interpretation comes from analysis of the canopy trees in which annual cycles were detected. In 3 out of the 5 forest trees with annual cycles, variance in annual maxima is greater than the annual minima (Table B.1). Additional data supporting the importance of elevation in determining controls on interannual δ^{18}O variability in cloud forest trees has been developed by *Anchukaitis et al.* [2007a], who identify cycles in two Sapotaceae (MV12 and MV15C) where, contrary to our premontane wet forest calibration set, the interannual δ^{18}O amplitude anomalies are most strongly controlled by the annual maxima and associated with dry season climate variability.

Two robust features characterize the annual cycles in the forest trees considered here.

The amplitude of the annual cycle decreases with elevation, as does the ratio of the mean annual cycle amplitude to the variability in the interannual amplitude. The reduction in the amplitude of the annual cycle is likely related to longer soil water residence times and increased mixing of seasonal water sources, which in turn is probably a result of lower temperatures, increased cloud cover, and reduced solar irradiance at higher elevations within the orographic cloud bank. The decrease in the ratio of the mean and anomalous annual cycle amplitude indicates that the higher elevation trees may be more sensitive to year-to-year variability than trees from the lower premontane forest. There are indications that this is related in some trees to larger interannual variations in the annual cycle maxima.

There is an upward trend in the mean oxygen isotope ratio with elevation for all the trees, when *Quercus* is excluded. While the trend is not statistically significant, it suggests that higher elevation trees may on average use more ^{18}O-enriched cloud water, which would be consistent with their position progressively closer to the continental divide and within the region of persistent cloud. *Quercus* appears to be a special case, with overall mean δ^{18}O values substantially lower than other species, and a smaller average amplitude in MV05. Collectively, these data suggest that our *Quercus* samples preferentially sample soil water with a more negative δ^{18}O. This could arise if the trees did not add basal growth during part of the transition or dry season, when δ^{18}O values are higher. If *Quercus* ceased growth during part of the dry season, both the mean isotopic value and the annual cycle, where present, would preferentially reflect the more negative δ^{18}O during the rainy season. Alternatively, this species may have access to some deeper soil water sources, which would also explain the suppressed amplitude of the mean annual cycle. Finally, if transpiration were more restricted in *Quercus*, potentially through particular characteristics or structure of the leaves, enrichment of the source water in the leaves

would be limited and the resultant cellulose would have a more negative δ^{18}O value. In general, though, there are several reasons some of the cloud forest trees sampled do not display annual rings, with the most likely cause, however, being that our sampling interval of 200 μm failed to adequately resolve the annual cycle in very slow growing trees.

B.6.3 Forward modeling

The six environmental parameters from the model of *Barbour et al.* [2004] are assumed to be temporally stable [*Evans,* 2007], and therefore changes in the parameter set are predominantly reflected in changes in the overall mean of the series, and only secondarily in the annual maximum and minimum value and in the overall amplitude of the seasonal cycle. The results from Figure B.8c demonstrate that the interannual difference in the annual amplitude of the δ^{18}O cycle imparted by uncertainties in the model parameter set may be as large as 1.5‰. In agreement with the findings of *Evans* [2007], however, we find that the overall structure and mean amplitude of the annual cycle is driven predominantly by the seasonal change in the δ^{18}O related to changes in water sources as driven primarily by the amount effect and, in this case, the contribution of cloud water during the dry season. It is clear, however, from interannual differences observed between model simulations using the two difference relative humidity data sets, that difference in the input data can have an important influence on interannual patterns of variability. In general, neither relative humidity dataset produces a substantially improved overall match to the observed plantation δ^{18}O time series, although the simulation using the higher variance NCEP data has a slightly improved correlation between observed and simulated interannual amplitude patterns.

More interesting is the disparity between the correlations with each simulation and wet season anomalies. Modeled δ^{18}O values using the NCEP relative humidity dataset show

a weaker correlation with precipitation anomalies than the δ^{18}O time series simulated from the calculated Campbell relative humidity, although the coefficient is more similar to the relationship between the observed plantation δ^{18}O and summer precipitation. This indicates that increased variability in relative humidity can have a substantial influence on the controls on the interannual patterns of variability. This, and the observations of increasing interannual variability relative to the mean annual δ^{18}O with increases in elevation, suggest that samples within or at the boundary of the orographic cloud bank are likely to show great sensitivity to, and control by, changes in relative humidity and moisture advection than those below it. This finding can be used to guide future sampling strategies for the development of long chronologies.

In *Evans* [2007], the *Barbour et al.* [2004] model was used to construct the interannual variability in the amplitude of the seasonal cycle, while the mean and variance were scaled to that of the observed δ^{18}O time series. Here, using the default parameterization from *Evans* [2007], even without mean adjustment, and using the relative humidity derived from the Campbell meteorological data [*Pounds et al.*, 1999], the model actually reproduces the mean of the series within the precision of the instruments ($\bar{x}_{model} = 26.52‰$, $\bar{x}_{obs} = 26.27‰$), although this may simply be fortuitous, since large shifts in the overall mean can be the result of changing the model and source water parameters (see below). The use of the soil water model in the place of variance adjustment also produced a simulated isotope series with similar mean amplitude and variance as the δ^{18}O from *O. tenera*, and generally reproduced the visually coherent cyclicity of the actual time series. Most encouragingly, applying the soil water model reproduces the leading autocorrelation structure of the observed δ^{18}O chronologies, as well as the pattern of interannual variability and the relationship between the annual amplitude anomalies and wet season precipitation amount (Figure B.8c).

The monthly mixing ratio of 30:70 (precipitation to prior soil water) implies a mean water residence time somewhat longer than would be calculated from the turnover rate reported from lowland tropical rainforest soils derived from tritium measurements by *McGinnis et al.* [1969] in Panama. However, *McGinnis et al.* [1969] estimated soil water flux for only the top 30cm. Somewhat deeper soil water available to plants would presumably have a longer residence time. Additionally, reduced evapotranspiration due to persistent cloud cover, cooler temperatures, and higher relative humidity would likely increase water residence times in soils in tropical montane cloud forests.

The most obvious discrepancy between the *O. tenera* composite mean time series, the simulated model, and local climate variability is the wet season minimum of 1991. There are several possible reasons for this difference. One hypothesis is that the age model is incorrect, and that the cycle currently dated to 1991 corresponds to an anomalously wet summer such as occurred in 1988. However, the 1991 negative anomaly is apparent in the δ^{18}O from the most securely dated cores, those from tree NWT02, and there is no evidence from basal growth analysis to suggest an age adjustment of several years is warranted or realistic in this case. An additional, albeit entirely speculative, possibility is that the eruption of Mount Pinatubo in the summer of 1991 influenced cloud formation at that time. However, there is no obvious signal of the consequences of the Pinatubo eruption in the Campbell temperature record for either 1991 or 1992. Zonal winds across the Costa Rican cordillera were strongly anomalous, however, during the summer wet season in 1991 [*Kanamitsu et al.*, 2002], but it is not clear whether the local effect at our lower moist forest calibration site would be to increase cellulose δ^{18}O (by increasing the availability of isotopically-heavier source waters) or decrease it (through increased cloud cover and reduced evapotranspiration).

B.6.4 Spatial patterns and future work

There are clear patterns in both annual mean δ^{18}O cycle amplitudes and their interannual variability related to elevation. Annual variability, as measured by the standard deviation of the annual amplitudes, is lower with increasing elevation. However, particularly when expressed as a ratio with respect to the mean annual cycle amplitude, there are indications that higher elevation trees show a greater sensitivity to year-to-year variability, particularly to dry season climate likely related to the influence of orographic clouds. This suggests that optimal sampling locations for reconstructing both cloudiness and the regional-scale forcing associated with changes in cloud coverage and moisture advection will be at those elevations where the annual cycle is coherent and of a sufficient magnitude to be differentiated from short term fluctuations, but where high-frequency variance suggests sensitivity to these changes [*Anchukaitis et al.*, 2007a]. Additional complicating factors may arise from the heterogeneous nature of cloud cover [*Clark et al.*, 2000; *Haber*, 2000]. Gaps in the cordillera can allow orographic clouds to pass to lower elevations on the leeward side, often along stream courses. Likewise, topography may dictate the extent to which individual trees are exposed to direct tradewind moisture advection, and soil type and depth may influence the amount of source water buffering and soil water mixing that determines the baseline amplitude for the formation of annual δ^{18}O cycles.

Our selection of tropical cloud forests as a site for tropical paleoclimate reconstruction parallels, in a somewhat paradoxical manner, the approach of classical dendroclimatology in seeking out sampling locations where trees are likely to be sensitive to relatively small changes in annual climate. In temperate regions and for trees with regular annual changes in morphology or wood density, these are typically dry or cold sites at the limits of a species range. For tropical isotope dendroclimatology, however, we seek sites which are wet enough to allow trees to grow throughout the year, yet are subjected to

seasonal changes in the stable oxygen isotope composition of available moisture which provides the means of establishing annual chronology. In cloud forest environments, the largest interannual changes of interest are likely to be wet season rainfall and dry season cloudiness. As such, site selection for tropical isotope dendroclimatology is very different from that of classical field approaches in dendrochronology in terms of climate regimes, but the guiding principle is the same.

Our approach to tropical isotope dendroclimatology [*Evans and Schrag*, 2004] has a closer methodological and procedural affinity to paleoclimate analysis using speleothems or corals than to classical dendrochronology. Despite rapid advances [*Kornexl et al.*, 1999; *Brendel et al.*, 2000], the analytical requirements for sample preparation and mass spectrometry still limit the number of samples and measurement replication that can be realistically achieved. The result is relatively large uncertainties (several years) in the age modeled chronologies. However, as demonstrated by *McCarroll and Pawellek* [1998] and *Gagen et al.* [2004], stable isotope ratios in tree-ring chronologies often have a higher signal-to-noise ratio that rings width data. As a consequence, fewer chronologies are required to achieve a robust common signal. For the Monteverde *O. tenera* chronology, 4 cores over the common period of overlap are sufficient to exceed an Expressed Population Signal threshold [EPS; *Wigley T. M. L.*, 1984] of 0.85. Furthermore, the protocols allow for the development of high-resolution terrestrial proxy records that bypasses some of the extant challenges to developing ring width chronologies in tropics, and can be applied even when appropriate species for traditional dendrochronology cannot be identified. Continued application of these techniques will necessarily be guided by the specific research question and the ability of complementary proxies to provide the information necessary to address them. Cloud forests, given their biogeographical and hydrological importance at the regional scale, and their sensitivity to broad-scale mode of climate at

the global-scale [*Loope and Giambelluca*, 1998; *Still et al.*, 1999; *Pounds et al.*, 1999; *Foster*, 2001; *Bush*, 2002; *Pounds et al.*, 2006] represent a particular ecosystem where the application of tropical isotope dendroclimatology can support an improved understanding of critical environmental processes across a range of spatiotemporal scales.

B.7 Summary and Conclusions

The results from our plantation study clearly identify an annual isotope cycle in trees growing at lower cloud forest elevations that can be used to develop an annual chronology. Interannual variability in the amplitude of the annual cycle is most closely related to wet season precipitation anomalies at our premontane wet forest calibration site. Our forward model simulations successfully reproduce the annual pattern of δ^{18}O observed in our plantation trees, and using the soil water mixing model demonstrate a similar leading autocorrelation structure in both synthetic and actual isotope time series. The model also reproduces quite well the dependence of the interannual patterns of δ^{18}O amplitude on the amount of summer wet season rainfall, although there is at least one notable discrepancy observed in 1991. Using two different relative humidity datasets does result in a change in the mean and interannual variance, indicating that the forward model is partially sensitive to the selection of input data in reproducing year-to-year variability.

Analysis of canopy trees presents a more complicated picture, however. Five out of nine mature canopy trees considered here from sites ranging from 1500 to 1660m show an annual isotope cycle, although only two of these have δ^{18}O cycles that can be detected over their entire length [*Anchukaitis et al.*, 2007a]. Four trees showed no annual cycles at all. These pilot results demonstrate the potential importance of species, site, and sampling resolution, but can help guide the future development of long climate reconstructions from older cloud forest trees. Collectively, the results of our calibration study at Monteverde

demonstrate that annual stable oxygen isotope cycles in tropical cloud forest trees can be used for both chronology development and the detection of climate variability that can then be applied to the development of climate reconstructions and the interpretation of recent trends in tropical montane forest hydroclimatology.

B.8 Acknowledgments

We are grateful for comments and suggestions from Julio Betancourt, Malcolm Hughes, Mary Gagen, Alan Pounds, Julie Cole, Jonathan Overpeck, and Tim Shanahan. Greg Eischeid, John Buchanan, Mau-Chuang Foo, Brianna Muhlenkamp, Frank Joyce, Rex Adams, Arturo Cruz, Eladio Cruz, Koky Porras, and Lisa Wade provided excellent laboratory and field assistance and support. We appreciate technical instrumentation support and advice from Bruno Lavettre. Our thanks to the Organization for Tropical Studies (OTS) for assistance with permits and to the Tropical Science Center (CCT) for access to the Monteverde Cloud Forest Reserve (Rafael Bolanos and Carlos Hernandez). The Trostles and Hoges families generously allowed us access to the *Ocotea* plantations on their property at Monteverde. This research was supported by a graduate training fellowship from the NSF IGERT Program (DGE-0221594) (to KJA), a Graduate Research Environmental Fellowship (to KJA) from the US Department of Energy, grants from the National Science Foundation: NSF/ATM-0349356 (CAREER to MNE) and NSF/ATM-0321348 (MRI), and a pilot grant from the Biogeography Specialty Group of the Association of American Geographers (AAG) to KJA.

B.9 References

Anchukaitis, K. J., M. N. Evans, and T. Lange (2007a), Dry season climate variability in a tropical montane cloud forest reconstructed from trees without rings, *in preparation*.

Anchukaitis, K. J., M. N. Evans, T. Lange, D. R. Smith, D. P. Schrag, and S. W. Leavitt (2007b), Purity and isotopic results from a rapid cellulose extraction method for high-resolution isotope dendroclimatology, *Analytical Chemistry*, in preparation.

Barbour, M. M., U. Schurr, B. K. Henry, S. C. Wong, and G. D. Farquhar (2000), Variation in the oxygen isotope ratio of phloem sap sucrose from Castor Bean. evidence in support of the Peclet Effect, *Plant Physiol.*, *123*(2), 671–680, doi:10.1104/pp.123.2.671.

Barbour, M. M., A. S. Walcroft, and G. D. Farquhar (2002), Seasonal variation in δ^{13}C and δ^{18}O of cellulose from growth rings of *Pinus radiata*, *Plant Cell and Environment*, *25*(11), 1483–1499.

Barbour, M. M., J. S. Roden, G. D. Farquhar, and J. R. Ehleringer (2004), Expressing leaf water and cellulose oxygen isotope ratios as enrichment above source water reveals evidence of a Peclet effect, *Oecologia*, *138*(3), 426–435.

Bauch, J., L. Quiros, G. Noldt, and P. Schmidt (2006), Study on the wood anatomy, annual wood increment and intra-annual growth dynamics of *Podocarpus oleifolius* var. *macrostachyus* from Costa Rica, *Journal of Applied Botany and Food Quality*, *80*(1), 19–24.

Bradley, R., M. Vuille, H. Diaz, and W. Vergara (2006), Threats to water supplies in the tropical Andes, *Science*, *312*(5781), 1755 – 1756, doi:10.1126/science.1128087.

Brendel, O., P. P. M. Iannetta, and D. Stewart (2000), A rapid and simple method to isolate pure α-cellulose, *Phytochemical Analysis*, *11*, 7–10.

Brienen, R., and P. Zuidema (2005), Relating tree growth to rainfall in Bolivian rain forests: a test for six species using tree ring analysis, *Oecologia*, *146*(1), 1–12.

Brown, A. D., and M. Kappelle (2001), Introducción a los bosques nublados del neotrópico: una síntesis regional, in *Bosques nublados del neotrópico*, edited by M. Kappelle and A. D. Brown, pp. 25–40.

Bruijnzeel, L. (1991), Hydrological impacts of tropical forest conversion, *Nature & Resources, 27*, 36–46.

Bruijnzeel, L. A. (2001), Hydrology of tropical montane cloud forests: a reassessment, *Land Use and Water Resources Research, 1*, 1–18.

Bruijnzeel, L. A. (2004), Hydrological functions of tropical forests: not seeing hydrological functions of tropical forests: not seeing the soil for the trees?, *Agriculture, Ecosystems and Environment, 104*, 185–228.

Bruijnzeel, L. A., and J. Proctor (1995), Hydrology and biochemistry of tropical montane cloud forests: what do we really know?, in *Tropical montane cloud forests*, edited by L. Hamilton, J. O. Juvik, and F. N. Scatena, Springer-Verlag, New York.

Bruijnzeel, L. A., and E. J. Veneklaas (1998), Climatic conditions and tropical, montane forest productivity: The fog has not lifted yet, *Ecology, 79*, 3–9.

Bush, M. B. (2002), Distributional change and conservation on the Andean flank: a palaeoecological perspective, *Global Ecology And Biogeography, 11*, 463–473.

Clark, K. L., N. M. Nadkarni, D. Schaefer, and H. L. Gholz (1998), Cloud water and precipitation chemistry in a tropical montane forest, Monteverde, Costa Rica, *Atmospheric Environment, 32*, 1595–1603.

Clark, K. L., R. O. Lawton, and P. R. Butler (2000), The physical environment, in *Monteverde: Ecology and Conservation of a Tropical Cloud Forest*, edited by N. M.

Nadkarni and N. T. Wheelwright, pp. 15–38, Oxford University Press, Oxford, United Kingdom.

D'Arrigo, R., R. Wilson, J. Palmer, P. Krusic, A. Curtis, J. Sakulich, S. Bijaksana, S. Zulaikah, and L. O. Ngkoimani (2006), Monsoon drought over Java, Indonesia, during the past two centuries, *Geophys. Res. Lett.*, *33*, 4709, doi:10.1029/2005GL025465.

Dawson, T. E. (1998), Fog in the California redwood forest: ecosystem inputs and use by plants, *Oecologia*, *117*, 476–485.

Diaz, H. F., and N. E. Graham (1996), Recent changes in tropical freezing heights and the role of sea surface temperature, *Nature*, *383*, 152–5.

Dünisch, O., J. Bauch, and L. Gasparotto (2002), Formation of increment zones and intraannual growth dynamics in the xylem of Swietenia macrophylla, Carapa guianensis, and Cedrela odorata (Meliaceae), *IAWA Journal*, *23*, 101–119.

Ebisuzaki, W. (1997), A method to estimate the statistical significance of a correlation when the data are serially correlated, *J. Climate*, *10*(9), 2147–2153.

Evans, M. N. (2007), Forward modeling for paleoclimatic proxy signal calibration: a case study with oxygen isotopic composition of tropical woods, *Geochemistry, Geophysics, Geosystems*, in press.

Evans, M. N., and D. P. Schrag (2004), A stable isotope-based approach to tropical dendroclimatology, *Geochim. Cosmochim. Acta*, doi:10.1016/j.gca.2004.01.006.

Evans, M. N., B. Lavettre, and K. J. Anchukaitis (2007), Online δ^{18}O analyses using high temperature pyrolysis by radio-frequency induction heating, *Rapid Comm. in Mass Spectr.*, in preparation.

February, E. C., and W. D. Stock (1998), An assessment of the dendrochronological potential of two *Podocarpus* species, *The Holocene*, *8*(6), 747.

Feild, T. S., and T. E. Dawson (1998), Water sources used by *Didymopanax pittieri* at different life stages in a tropical cloud forest, *Ecology*, *79*, 1448–1452.

Fichtler, E., V. Trouet, H. Beeckman, P. Coppin, and M. Worbes (2004), Climatic signals in tree rings of *Burkea africana* and *Pterocarpus angolensis* from semiarid forests in Namibia, *Trees - Structure and Function*, *18*(4), 442–451.

Foster, P. (2001), The potential negative impacts of global climate change on tropical montane cloud forests, *Earth Science Reviews*, *55*, 73–106.

Fritts, H. C. (1976), *Tree Rings and Climate*, Academic Press, New York.

Gagen, M., D. McCarroll, and J. L. Edouard (2004), Latewood width, maximum density, and stable carbon isotope ratios of pine as climate indicators in a dry subalpine environment, French Alps, *Arctic Antarctic Alpine Research*, *36*, 166–171.

Gat, J. R. (1996), Oxygen and hydrogen isotopes in the hydrologic cycle, *Ann. Rev. Earth Planet. Sci.*, *24*, 225–262.

Gaudinski, J. B., T. E. Dawson, S. Quideau, E. A. G. Schuur, J. S. Roden, S. E. Trumbore, D. R. Sandquist, S.-W. Oh, and R. E. Wasylishen (2005), A comparative analysis of cellulose preparation techniques for use with ^{13}C, ^{14}C and ^{18}O isotopic measurements, *Analytical Chemistry*, *77*, 7212–7224, doi:10.1021/ac050548u.

Haber, W. A. (2000), Plants and vegetation, in *Monteverde: Ecology and Conservation of a Tropical Cloud Forest*, edited by N. M. Nadkarni and N. T. Wheelwright, pp. 39–70, Oxford University Press, Oxford, United Kingdom.

Hamilton, L. S., J. O. Juvik, and F. N. Scatena (Eds.) (1995), *Tropical Montane Cloud Forests*, Springer-Verlag.

Holder, C. D. (2004), Rainfall interception and fog precipitation in a tropical montane cloud forest of Guatemala, *Forest Ecology and Management*, *190*, 373–384.

Ingraham, N. (1998), Isotopic variations in precipitation, in *Isotope tracers in catchment hydrology*, edited by C. K. J. McDonnell, Elsevier Press, Amsterdam, The Netherlands.

Ingraham, N., and R. Matthews (1990), A stable isotopic study of fog - The Point Reyes Peninsula, California, USA, *Chemical Geology*, *80*, 281–290.

Ingraham, N. L., and R. Matthews (1995), The importance of fog-drip water to vegetation - Point Reyes Peninsula, California, *Journal of Hydrology*, *164*(1-4), 269–285.

Kanamitsu, M., W. Ebisuzaki, J. Woollen, S. Yang, J. Hnilo, M. Fiorino, and G. Potter (2002), NCEP-DOE AMIP-II Reanalysis (R-2), *Bull. Amer. Meteor. Soc*, *83*(11), 1631–1643.

Kapos, V., and E. V. J. Tanner (1985), Water relations of Jamaican upper montane rain forest trees, *Ecology*, *66*(1), 241 – 250.

Kornexl, B. E., M. Gehre, R. Höfling, and R. A. Werner (1999), On-line δ^{18}O measurement of organic and inorganic substances, *Rapid Comm. in Mass Spectr.*, *13*, 1685–1693.

Lachniet, M. S., and W. P. Patterson (2002), Stable isotope values of Costa Rican surface waters, *Journal of Hydrology*, *260*, 135–150.

Lawton, R. O., U. S. Nair, R. A. Pielke, and R. M. Welch (2001), Climatic impact of

tropical lowland deforestation on nearby montane cloud forests, *Science, 294*, 584–587.

Linacre, E. (1964), A note on a feature of leaf and air temperatures, *Agricultural Meteorology, 1*(1), 66–72.

Loope, L. L., and T. W. Giambelluca (1998), Vulnerability of island tropical montane cloud forests to climate change, with special reference to East Maui, Hawaii, *Clim. Change*, *39*, 503–517.

Magaña, V., J. A. Amador, and S. Medina (1999), The Midsummer Drought over Mexico and Central America, *J. Climate*, *12*(6), 1577–1588.

Matelson, T. J., N. M. Nadkarni, and R. Solano (1995), Tree damage and annual mortality in a montane forest in Monteverde, Costa Rica, *Biotropica*, *27*, 441–447.

McCarroll, D., and F. Pawellek (1998), Stable carbon isotope ratios of latewood cellulose in *Pinus sylvestris* from northern Finland: variability and signal-strength, *The Holocene*, *8*(6), 675–684.

McGinnis, J. T., F. B. Golley, R. G. Clements, G. I. Child, and M. J. Duever (1969), Elemental and hydrologic budgets of the Panamanian tropical moist forest, *Bioscience*, *19*(8), 697–700.

McLaughlin, S. B., S. D. Wullschleger, and M. Nosal (2003), Diurnal and seasonal changes in stem increment and water use by yellow poplar trees in response to environmental stress, *Tree Physiology*, *23*, 1125–1136.

Nair, U. S., R. O. Lawton, R. M. Welch, and R. A. Pielke (2003), Impact of land use on Costa Rican tropical montane cloud forests: Sensitivity of cumulus cloud field characteristics to lowland deforestation, *J. Geophys. Res.*, *108*.

Pounds, J. A., M. Fogden, and J. H. Campbell (1999), Biological response to climate change on a tropical mountain, *Nature*, *398*, 611–615.

Pounds, J. A., et al. (2006), Widespread amphibian extinctions from epidemic disease driven by global warming, *Nature*, *439*(7073), 161–167.

Rhodes, A. L., A. J. Guswa, and S. E. Newell (2006), Seasonal variation in the stable isotopic composition of precipitation in the tropical montane forests of Monteverde, Costa Rica, *Water Resources Research*, *42*, W11,402, doi:10.1029/2005WR004535.

Robertson, I., C. A. Froyd, R. P. D. Walsh, D. M. Newbery, S. Woodborne, and R. C. Ong (2004), The dating of dipterocarp tree rings: establishing a record of carbon cycling and climatic change in the tropics, *J. Quaternary Science*, *19*, 657–664.

Roden, J. S., G. Lin, and J. R. Ehleringer (2000), A mechanistic model for interpretation of hydrogen and oxygen ratios in tree-ring cellulose, *Geochim. Cosmochim. Acta*, *64*, 21–35.

Root, T. L., J. T. Price, K. R. Hall, S. H. Schneider, C. Rosenzweig, and J. A. Pounds (2003), Fingerprints of global warming on wild animals and plants, *Nature*, *421*, 57–60.

Sheil, D. (2003), Growth assessment in tropical trees: large daily diameter fluctuations and their concealment by dendrometer bands, *Can. J. Forest. Res.*, *33*(10), 2027–2035.

Speer, J. H., K. H. Orvis, H. D. Grissino-Mayer, L. M. Kennedy, and S. P. Horn (2004), Assessing the dendrochronological potential of *Pinus occidentalis* Swartz in the Cordillera Central of the Dominican Republic, *The Holocene*, *14*(4), 563.

Stadtmüller, T. (1987), *Cloud forests in the humid tropics*, United Nations University.

Still, C., P. Foster, and S. Schneider (1999), Simulating the effects of climate change on tropical montane cloud forests, *Nature*, *398*, 608–610.

Therrell, M. D., D. W. Stahle, L. P. Ries, and H. H. Shugart (2006), Tree-ring reconstructed rainfall variability in Zimbabwe, *Climate Dynamics*, *26*(7), 677–685.

van Dijk, A., and L. Bruijnzeel (2001), Modelling rainfall interception by vegetation of variable density using an adapted analytical model. Part 2. Model validation for a tropical upland mixed cropping system, *Journal Of Hydrology*, *247*, 239–262.

Wheelwright, N. T., and B. A. Logan (2004), Previous-year reproduction reduces photosynthetic capacity and slows lifetime growth in females of a neotropical tree, *Proceedings of the National Academy of Sciences*, *101*(21), 8051–8055.

Wigley T. M. L., J. P. D., Briffa K. R. (1984), On the average value of correlated time series, with applications in dendroclimatology and hydrometeorology, *Journal of Climate and Applied Meteorology*, *23*, 201–213.

Worbes, M. (2002), One hundred years of tree-ring research in the tropics – a brief history and an outlook to future challenges, *Dendrochronologia*, *20*(1-2), 217–231.

Worbes, M., and W. Junk (1989), Dating tropical trees by means of C14 from bomb tests, *Ecology*, *70*, 503–507.

APPENDIX C

DRY SEASON CLIMATE VARIABILITY IN A TROPICAL MONTANE CLOUD FOREST RECONSTRUCTED FROM TREES WITHOUT RINGS

Manuscript for submission to *Global Change Biology*

Dry season climate variability in a tropical montane cloud forest reconstructed from trees without rings

Kevin J. Anchukaitis[1,2], Michael N. Evans[1,2], and Todd Lange[3]

1. Laboratory of Tree-Ring Research, The University of Arizona, Tucson, AZ
2. Department of Geosciences, The University of Arizona, Tucson, AZ
3. Accelerator Mass Spectrometry Laboratory, The University of Arizona, Tucson, AZ

C.1 Abstract

We use stable oxygen isotopes to investigate the evidence for trends in anomalously dry winters at the Monteverde Cloud Forest as preserved in the wood of tropical trees. Reconstructions of past climate are necessary to the interpretation of these recent climatic changes in the context of interannual and multidecadal variability in the ocean-atmosphere system. High-resolution isotope measurements along the growth radius reveal coherent annual cycles in δ^{18}O that are used to establish annual chronological control in the absence of growth rings. The annual maxima and amplitude of these cycles reflects interannual variability in dry season orographic cloud cover, moisture advection, and temperature. The minima reflects summer precipitation anomalies. Positive dry season δ^{18}O anomalies are associated with El Niño events and weaker northeasterly trade winds. Lower frequency variability may be related to multidecadal climate trends in the tropical Atlantic. According to our oxygen isotope chronology, the extinction of the Monteverde Golden Toad after 1987 occurred during one of the driest periods in the last 50 years, and potentially in the last century.

C.2 Introduction

In Central America, northeasterly moisture-laden tropical trade winds blow across the isthmus, encountering and ascending mountain ranges and resulting in the formation of orographic cloud banks. Higher relative humidity, increased moisture, persistent cloud cover, and reduced temperatures support montane forests rich in endemic organisms and important for local hydrology [*Brown and Kappelle*, 2001; *Bruijnzeel*, 2001]. Tropical montane cloud forests are ecosystems intrinsically linked to a relatively narrow range of geographic and meteorological conditions, and are therefore particularly sensitive to relatively small changes in precipitation or temperature [*Loope and Giambelluca*, 1998; *Foster*, 2001].

The population crash and apparent extinction of the Monteverde Golden Toad (*Bufo periglenes*) in Costa Rica in 1987 as well as other observed changes in neotropical cloud forest ecology are believed to have been a consequence of global warming [*Pounds et al.*, 1999, 2006]. Indeed, general circulation model (GCM) simulations of climate under doubled CO2 conditions predict higher lifting condensation levels and reduced cloud contact for tropical montane cloud forests as a result of increasing tropospheric temperatures [*Still et al.*, 1999]. Increases in global surface and sea surface temperatures (SST) may therefore already be fundamentally altering the suite of climatic and biophysical conditions that maintain cloud forest environments in Central America [*Pounds et al.*, 2006]. Analysis of the limited available observational data since the late 1970s suggests that a trend toward decreasing cloud cover at Monteverde reflects the influence of increasing tropical air and sea surface temperatures [*Pounds et al.*, 1999, 2006]. However, imprinted on the long-term instrumental drying trend at Monteverde, El Niño events also cause local increases in temperature and reductions in cloud cover [*Pounds and Crump*, 1994]. The strong warm El Niño-Southern Oscillation

(ENSO) event in 1986-1987 immediately preceded the rapid disappearance of the Monteverde Golden Toad [*Crump*, 2000], suggesting that temperature anomalies may have contributed to the species' demise.

Limited long-term instrumental climate records from the tropics, and particularly montane regions, impede an improved understanding of past, present, and future climate variability and trends and their relationship with montane forest hydroclimatology and biogeography [*Bradley et al.*, 2006]. Without the context provided by long-term climate records, it is difficult to confidently conclude whether the observed changes in neotropical cloud forest ecology are the result of anthropogenic climate forcing [*Pounds et al.*, 2006], land-surface feedbacks [*Lawton et al.*, 2001; *Nair et al.*, 2003], or the interaction of an introduced pathogen and natural variability in tropical climate [*Pounds and Crump*, 1994; *Crump*, 2000]. The observed changes in climate in tropical montane cloud forests and their hypothesized biogeographic consequences need to be placed in the context of low-frequency climate variability.

Here, we seek to develop annually-resolved proxy records of interannual variability and trends in dry season climate from the tropical montane cloud forest at Montverde in Costa Rica using stable isotope dendroclimatology [*Evans and Schrag*, 2004]. The advantage of our approach to tropical dendrochronology is that it does not rely on the formation nor width variations of annual growth rings, which in tropical trees can be absent or may not reflect local climate variability. Annual oxygen isotope cycles have been previously identified in lowland rainforests [*Evans and Schrag*, 2004; *Poussart et al.*, 2004; *Verheyden et al.*, 2004]. At Monteverde, *Anchukaitis et al.* [2007b] have demonstrated that the seasonal cycle between the summer wet season and cloud-dominated winter dry season is sufficient to induce an annual δ^{18}O cycle along the radial xylem growth of cloud forest trees, and that the record from higher elevation cloud forest

trees is sensitive to interannual changes in dry season climate.

The goals of our current study are necessarily two-fold. First, we seek to establish the basis for interpreting the δ^{18}O ratio of the radial growth of long-lived tropical canopy trees as a high-resolution proxy of cloud forest hydroclimatology. The presence of annual δ^{18}O cycles has been established in plantations [*Anchukaitis et al.*, 2007b], but not in mature canopy trees, nor in this species. We can then apply this record toward an understanding of the broad-scale ocean-atmosphere phenomena associated with these local climatic conditions at Monteverde.

C.3 Methods and Materials

C.3.1 Site description

The Monteverde Cloud Forest (10.2 ^{o}N, 85.35 ^{o}W, 1500m) sits astride the continental divide in the Cordillera de Tilaran in northwestern Costa Rica. Above 1500m elevation, vegetation is classified montane wet cloud forest [*Haber*, 2000] and its unique hydroclimatology is characterized by persistent immersion in the orographic cloud bank formed as the northeasterly trade winds moving across the warm waters of the Caribbean are forced to rise over the cordillera. During boreal summer (May to October), cloud forests receive most of their rainfall as the northward movement of the Intertropical Convergence Zone (ITCZ) brings strong convective storms to the region. During the dry season (February through April), moisture advection and cloud water deposition are an important component of cloud forest hydrology [*Clark et al.*, 2000], particularly on the leeward Pacific slope which would otherwise experience the effects of a pronounced dry season.

C.3.2 Heuristic model

The origin of annual cycles in the stable oxygen isotope composition of the wood of tropical cloud forest trees is the differential δ^{18}O composition of dry and wet season moisture sources (Figure C.1) [*Evans and Schrag*, 2004; *Anchukaitis et al.*, 2007b]. This hypothesis is not specific to any particular species. Annual and interannual oxygen isotope ratios in tropical meteoric waters are primarily controlled by the 'amount effect', the inverse relationship between the amount of precipitation and its δ^{18}O value [*Gat*, 1996]. The amount effect is evident in surface waters from Costa Rica and Panama [*Lachniet and Patterson*, 2002] and in seasonal precipitation from Monteverde [*Rhodes et al.*, 2006; *Anchukaitis et al.*, 2007b]. In montane forests, moisture inputs from clouds are an additional source of water for trees, particularly in the dry season. Cloud water has an enriched isotopic signature similar to tropical dry season rainfall [*Feild and Dawson*, 1998; *Ingraham and Matthews*, 1990; *Ingraham*, 1998; *Rhodes et al.*, 2006]. Dry season sources of moisture provide trees with sufficient water to avoid water stress and potentially the need for a seasonal growth hiatus, but have a distinct isotopic signature.

The δ^{18}O of cellulose reflects the original oxygen isotope composition of the source water (precipitation or cloud water), the isotopic enrichment via transpiration in the leaves, and the fractionation associated with the synthesis of α-cellulose from sucrose [*Roden et al.*, 2000; *Barbour et al.*, 2004; *McCarroll and Loader*, 2004]. Assuming the latter is constant, cellulose in cloud forest trees should therefore reflect both the amount of rainfall received and climatic influences on the rate of evapotranspiration from the leaf. On annual time scales in our model (Figure C.1), cellulose δ^{18}O is controlled by the seasonal change in δ^{18}O of source water as determined by the amount effect and the trees' use of ^{18}O-enriched cloud water. On interannual time scales, departures from the mean annual cycle are likely to result from anomalous rainfall and changes in temperature,

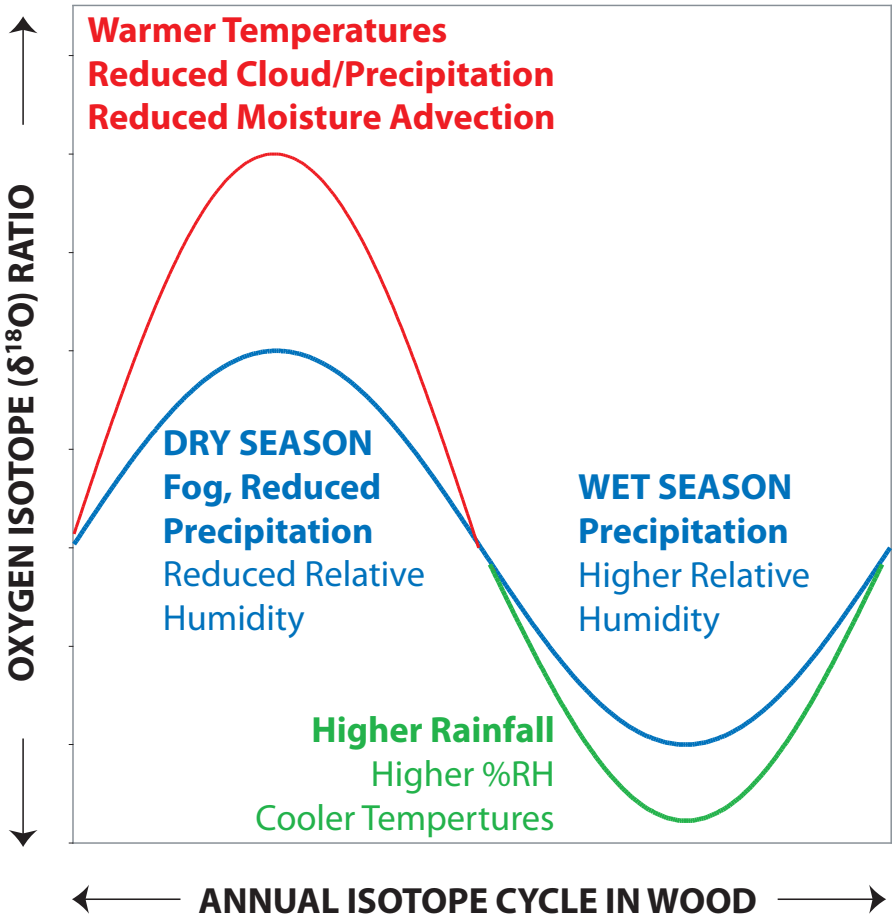

Figure C.1: Conceptual model of climatic controls on the annual and interannual patterns of stable oxygen isotope ratios in the α-cellulose of cloud forest tree radial growth. The annual cycle is generated primarily by the seasonal change in the δ^{18}O of rainfall, the use of cloud water by trees in the dry season, and the isotopic enrichment of source water during the dry season. Interannual variability in annual maximum values is related to temperature, relative humidity, cloudiness, and moisture advection. At Monteverde, temperature is strongly related to Pacific sea surface temperatures and tracks tropical surface air temperatures [*Pounds and Crump*, 1994; *Pounds et al.*, 2006]. Anomalies in the annual minima are likely related to wet season rainfall amounts and temperature.

relative humidity, and evapotranspiration. We expect that these will be related to changes in the intensity of moisture advection over the continental divide into the Pacific slope forests and to the amount of cloud cover. Interannual changes in the annual cycles can therefore be interpreted as changes in overall cloudiness and moisture inputs during the winter, and at Monteverde specifically during the February to April dry season.

In tropical cloud forests, cloud water inputs can vary from 6 to 154% of precipitation [*Bruijnzeel*, 2001]. *Clark et al.* [1998] estimated that moisture inputs from cloud and mist accounted for perhaps 22% of the annual hydrological budget of Monteverde. More recently, *Schmid* [2004] however, estimated that fog deposition was only 4% - 12% of rainfall during a dry period in the winter and spring of 2003, although for individual days cloud water could still account for 100% of short-term measured precipitation throughfall. Thus, while orographic clouds are critical determinants of tropical montane cloud forest ecosystems, large magnitude changes in cloud immersion can occur rapidly as well as for extended periods of time, even during the dry season when they are the critical element of cloud forest hydroclimatology.

C.3.3 Sampling and stable isotope analysis

Increment cores (5mm diameter) from two individual mature Sapotaceae (*Pouteria*) were collected in 2004 and 2006 at 1560m (MV12A) and 1580 (MV15C). MV12A was struck by lightning and subsequently felled in 2002. MV15C was living when cored, with a full canopy of leaves and abundant latex sap. The cores were subsampled in the laboratory at 200 μm increments using a rotary microtome. The raw wood samples were chemically processed to α-cellulose using the Brendel Method [*Brendel et al.*, 2000; *Anchukaitis et al.*, 2007a] as modified for high-resolution sampling [*Evans and Schrag*, 2004]. 300 to 350 μg of α-cellulose were wrapped in silver capsules and converted online to CO

in a Costech High Temperature Generator/Elemental Combustion System (HTG/ECS). The HTG uses a radio frequency induction heater with a thin molybdenum crucible susceptor packed with graphite for pyrolysis at $>1500^{o}$C. Measurement precision on a total of 320 Sigma Alpha Cellulose (SAC) solid standards was 0.28‰. Data was corrected based on the mean value of the solid standard material and monitoring gas values before and after each sample measurement. Data quality assurance was assessed based on sample peak voltages, peak shape, background stability, and repeated monitoring CO gas measurements between and during sample analysis.

C.3.4 Radiocarbon

In order to provide independent chronological control for our stable oxygen isotope series, three samples from each core were selected for radiocarbon analysis to support age model development (Table C.1). Samples were selected in order to provide high-resolution dates using the ^{14}C signature of atmospheric atomic weapons testing [*Hua et al.*, 1999]. A total of four samples were whole wood and were preprocessed using the acid-base-acid (ABA) method developed for tropical trees by *Westbrook et al.* [2006]. Two samples had been previously processed to α-cellulose using the Brendel Method [*Brendel et al.*, 2000]. A replicate sample of one of our ABA treated samples was intentionally selected and prepared using the Brendel technique, in order to provide a confirmation of the radiocarbon-bias correction for $\Delta^{14}C$ measurements on α-cellulose extracted using the Brendel Method [*Anchukaitis et al.*, 2007a]. Extracted wood and cellulose samples were combusted and the purified carbon dioxide reduced to an iron carbide powder over hot zinc for $\Delta^{14}C$ measurement by tandem accelerator mass spectrometer.

C.4 Results

C.4.1 Oxygen isotope chronology

δ^{18}O time series from both cores show coherent annual oxygen isotope cycles that can be used to construct the annual chronology. MV12A (Figure C.2) has distinct oxygen isotope cycles with a mean amplitude of 2.7‰. MV15C (Figure C.3) has cycles with a mean amplitude of 2.1‰. We developed an age model for both series by assigning the maxima of each discrete cycle to the month of April of the corresponding year and interpolating the δ^{18}O time series between these tie points to monthly resolution. Mean growth rates derived from these age models are 5.l6 mm year^{-1} for MV12A and 2.9 mm year^{-1} for MV15C, although growth rates vary considerably between the inner and outer portion of the latter core. These are within the range of median incremental basal diameter growth observed for tropical trees from La Selva Biological Station in Costa Rica [*Lieberman et al.*, 1985, 0.34 to 13.14 mm year^{-1}], and consistent with radial growth rates from long-term monitoring and isotopic analysis of of *Ocotea tenera* in the premontane wet forest near the Monteverde Cloud Forest reserve (0 to 10 mm/year; *Wheelwright and Logan* [2004]; *Anchukaitis et al.* [2007b]).

The δ^{18}O time series from MV15C shows an abrupt change in growth rates at approximately 121mm depth in the core. Accompanying this change is a substantial increase in the amplitude of the oxygen isotope cycles. The rapid growth rates which correspond with the inner portion of the core result in an increase in the number of individual samples per annual cycle. The higher sampling rate may translate into larger amplitude δ^{18}O cycles simply by virtue of more precisely resolving the monthly and seasonal changes in water use in the tree. Because this could potentially bias our climatic interpretation of the oxygen isotope time series, for the purpose of climate analysis we

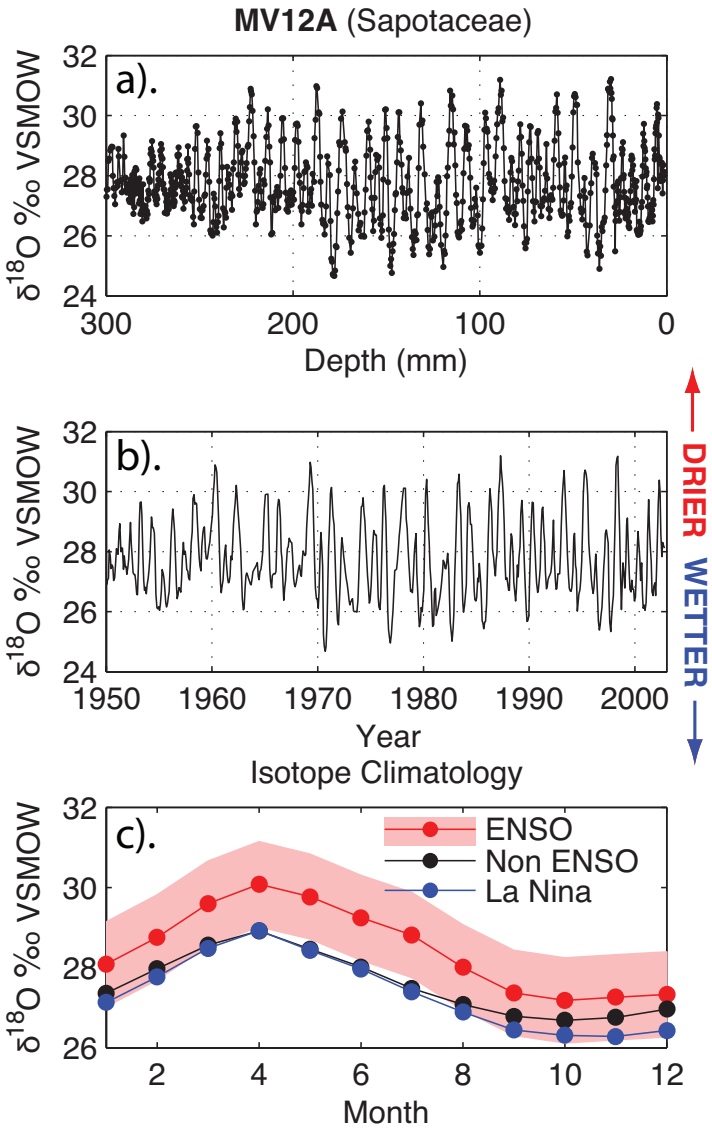

Figure C.2: Isotope chronology from MV12. (a) δ^{18}O as a function of depth from the bark showing the annual isotope cycle. (b) Age modeled δ^{18}O series. (c) Composite mean annual δ^{18}O isotope cycle for warm ENSO (El Niño; winter/dry season 1958; 1969; 1977; 1983; 1987; 1992; 1993; 1998), non-ENSO, and cold ENSO (La Niña) years. Warm ENSO events show a higher amplitude than neutral or La Niña years, slightly beyond the 1σ confidence range.

interpolated the sampling resolution to 6-10 samples per cycle to simulate that of the outer portion of the core (red line, Figure C.3a-b). Despite this correction, however, the inner part of MV15C has larger amplitude cycles than much of the outer core, and therefore we interpret these years cautiously, as they may still contain a growth rate sampling bias.

Radiocarbon measurements (Table C.1) on samples from MV12A confirmed our age modeled δ^{18}O time series, which spans the period 1949 to 2002. We estimate that age model error for this core is $\pm$ 2 years, based on the range of realistic age models as constrained by the 2 σ resolution of the post-1955 radiocarbon dates [*Hua et al.*, 1999; *Reimer et al.*, 2004a; *Hua and Barbetti*, 2004]. However, despite our assessment during field sampling, the radiocarbon measurements on three samples from MV15C revealed that the outer portion of the core does not correspond to its sampling date in 2006, suggesting that the tree experienced strongly suppressed basal growth in the recent decades, or the tree had ceased to add secondary xylem around part of its circumference. Because they occur during a period of large fluctuations in atmospheric radiocarbon, the $\Delta^{14}C$ measurements for MV15C calibrate to a large range of potential calendar dates between A. D. 1700 and A.D. 1950 [*Reimer et al.*, 2004b]. The magnitude of this uncertainty is also substantially larger than uncertainties associated with the correction applied to the Brendel-processed samples, and also exists for the sample from MV15C prepared with ABA.

The actual calendar dates that could be realistically associated with the radiocarbon assays on MV15C can be better constrained using Bayesian probability estimates and 'wigglematching' between the radiocarbon calibration curve and the sample measurements [*Bronk Ramsey and van der Plicht*, 2001; *Galimberti et al.*, 2004; *Robertson et al.*, 2004]. The likely dates are restricted foremost by the growth orientation of the tree – samples from near the bark must be more recently formed than those near

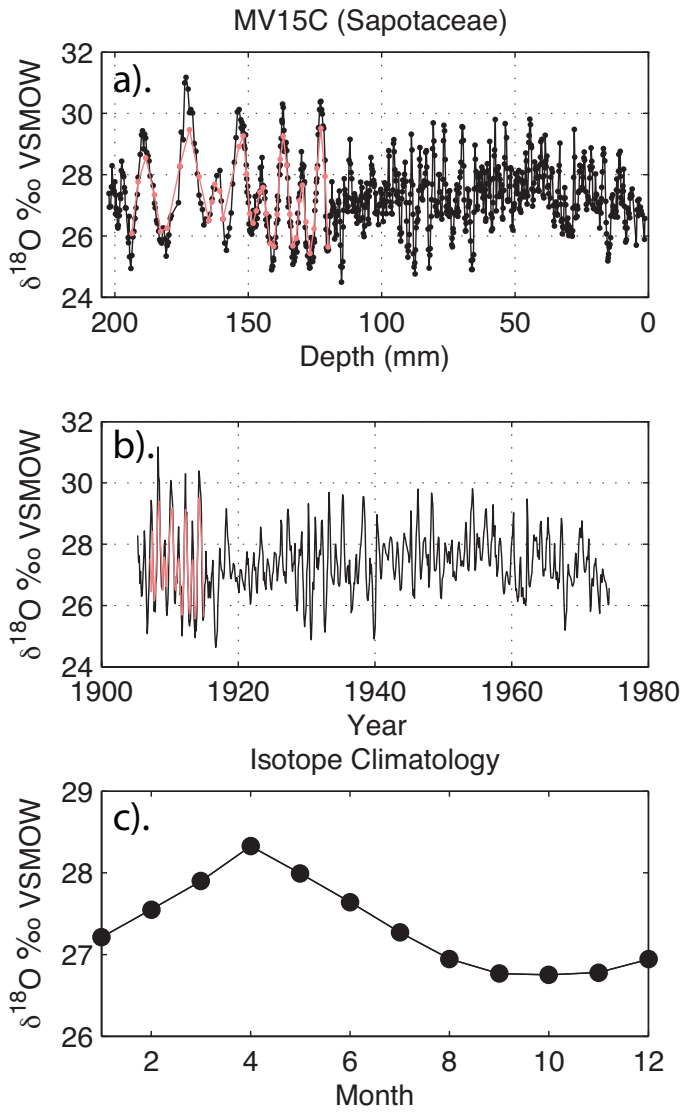

Figure C.3: Isotope chronology from MV15. (a) δ^{18}O as a function of depth from the bark showing the annual isotope cycle. (b) Age modeled δ^{18}O series. In these two panels, the red line shows the isotope chronology that results from statistically resampled the earlier period of rapid growth to better reflect a measurement resolution similar to the outer portion of the core . (c) Composite mean annual δ^{18}O isotope climatology.

Sample	AA74375	AA74376	AA74377	AA74381	AA74379	AA74378
Core	MV12A			MV15C		
Depth (mm)	167	230	242	57	69	121
Initial Data						
Fraction modern carbon (F14C)	1.5111	1.0842	0.992	0.9859	0.9882	0.9833
2 σ calibrated date (A.D.)	1969-1972	1955-1957	1951-1956	1526 (2.7) 1556 1632 (77.1) 1894 1905 (15.6) 1954	1646 (21.0) 1710 1716 (57.5) 1890 1909 (16.9) 1954	1669 (41.1) 1780 1798 (39.0) 1893 1906 (15.2) 1944
Bayesian Calibration						
Posteriori 2 σ range A.D. (% probability)				1724 (67.5) 1814 1834 (9.3) 1888 1926 (18.7) 1954	1716 (67.5) 1807 1828 (9.3) 1881 1918 (18.7) 1948	1694 (67.5) 1784 1804 (9.3) 1858 1896 (18.7) 1924
% Agreement				119.8	113.8	94.4
Sequence Model Agreement (threshold)						115.6 (40.8)

Table C.1: Radiocarbon analysis from MV12A and MV15C. Calibrated dates are shown with the percentage of the probability density function associated with each range of years. Post-bomb calibrated dates include any additional uncertainty associated with using from different atmospheric $\Delta^{14}C$ curves [*Reimer et al.*, 2004a; *Hua and Barbetti*, 2004].Bayesian analysis for development of *a posteriori* probability functions was performed using OxCal, applying the known temporal (stratigraphic) order of the dates and the estimated annual increment based on the δ^{18}O chronology [*Bronk Ramsey*, 1995; *Bronk Ramsey and van der Plicht*, 2001]. Agreement scores are uniformly above 60% for the individual dates and exceeds the lower minimum threshold ($\sim$ 40%) for the model as a whole [*Bronk Ramsey*, 1995]. F14C values have been corrected for those samples prepared with the Brendel method as described by *Anchukaitis et al.* [2007a] and discussed in the text.

the center of tree – and secondly using the number of identified annual cycles between each $\Delta^{14}C$ measurement in order to determine the most probable interval spanned by the core. Within these temporal, self-consistent constraints, the radiocarbon measurements and their individual probability density functions are then matched against the calibration curve and *a posteriori* probability functions calculated. Applying Bayesian analysis and these additional restrictions reveals that the core from MV15C most likely grew either during the middle of the 18th century, or during the early 20th century (Figure C.4). If we further assume that it is highly unlikely that the tree ceased growth for several hundred years along part of its intact and apparently healthy circumference, we can cautiously conclude that the MV15C sequence is anchored within the period 1886 to 1990, with a rather large residual uncertainty of at least ± 30 years associated with the range of possible radiocarbon dates and age model uncertainty from annual δ^{18}O cycle identification.

In addition to this logical constraint, we can attempt to cross-correlate the floating MV15C sequence with the well-dated MV12A chronology. We used the computer program COFECHA [*Holmes*, 1983; *Grissino-Mayer*, 2001] and the constraints from the $2\,\sigma$ wiggle-matched $\Delta^{14}C$ calibration to statistically compare potential periods of overlap between the two cores. Two likely matches for MV15C were found using both annual maximum and annual amplitude δ^{18}O time series, which results in a tentative age model for the periods 1905–1972 and 1896–1962. The former of these age ranges has a larger cross-correlation for monthly ($r = 0.44$, $p < 0.01$), minimum ($r = 0.65$, $p < 0.01$), and maximum ($r = 0.25$, $p = 0.18$) δ^{18}O and is supported by the visual crossdating of the amplitude of the overlapping monthly and annual δ^{18}O segments (Figure C.5), but the uncertainties associated with the radiocarbon dates, the validity of our logical constraints, and the pattern matching are sufficiently large that the composite chronology should be considered tentative and its interpretation placed in the context of the substantial age

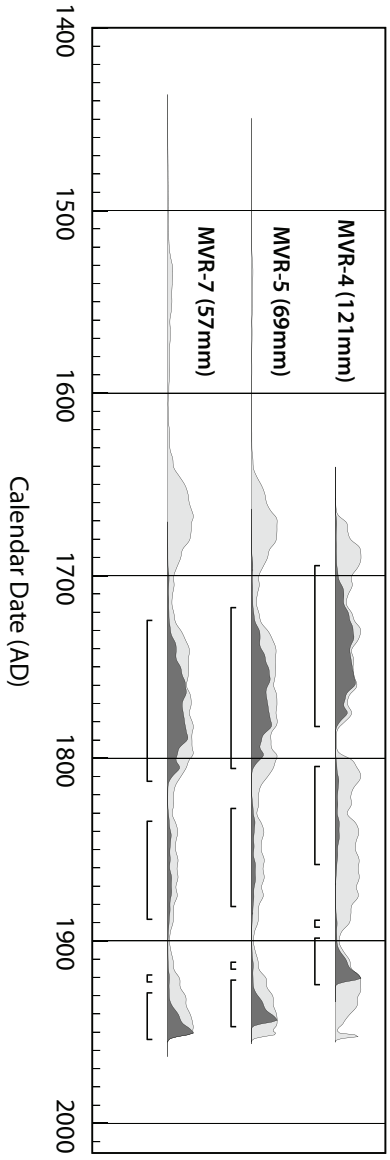

Figure C.4: Probability density functions from radiocarbon assays on wood and cellulose from MV15C. Markov Chain Monte Carlo wiggle-matching applied to the three dates, constrained constrained by stratigraphic sequence and spacing between samples. Assuming the logical constraints discussed in the text are correct, we estimate the absolute age model error at $\pm$ 6 years, but the full chronology is only weakly anchored to calendar years.

model uncertainties (Figure C.9, Table C.1).

In traditional dendrochronology, the proxy measurement of interest is a characteristic associated with the annual ring (width, maximum latewood density) and corresponding to a discrete year. Our isotopic approach to tropical dendroclimatology, however, requires that we first develop a continuous series of measurements in order to adequately resolve the annual cycle. From these cycles, we then need to extract information that can be statistically and mechanistically related to annual climate anomalies (Figure C.1). We do so by defining 5 characteristics of each annual cycle. The first 3 are the simple maximum, minimum, and mean value for each annual cycle, which correspond to the dry season, wet season, and average annual climate conditions, respectively (see Figure C.1). Our continuous δ^{18}O time series have a high degree of low order autocorrelation and therefore closely sampled prior values may influence the isotope ratio of the successive samples which follow it. For example, an anomalously dry wet season would result in a heavier δ^{18}O value, with the consequence that even if the dry season that followed was statistically average in terms of rainfall and temperature, we would expect the maximum value for that year to be elevated relative to others simply as a result of the autocorrelation between measurements and the already enriched δ^{18}O value which occurred in the prior increment. This persistence arises from the mixing of discrete precipitation events in the soil and as a result of short-term carbohydrate storage in the tree. The former phenomenon has been reproduced by forward modeling of monthly δ^{18}O values in tropical trees from Monteverde [*Anchukaitis et al.*, 2007b]. They show that the high degree of temporal autocorrelation observed in the actual isotope time series is best reproduced by including a simple soil water model that results in the mixing of precipitation events over several consecutive months. We apply two simple normalizations in order to compensate for the degree of autocorrelation in the continuous δ^{18}O series. We calculate a ‘dry season

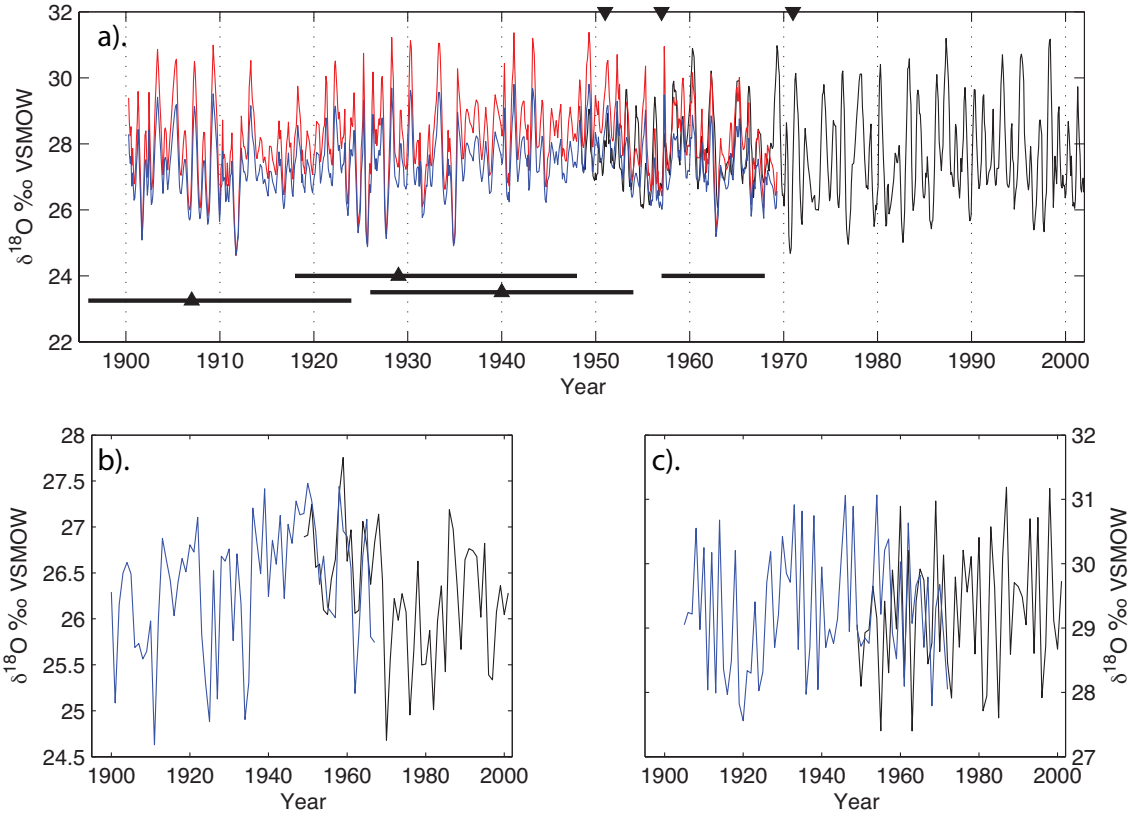

Figure C.5: Composite oxygen isotope chronology from MV12A (black line) and MV15C (blue line; red line is variance-adjusted), based on radiocarbon dates and cross-correlation analysis with the logical constraints discussed in the text. (a) Overlap the potential tie points for the two age modeled monthly chronologies. Triangles show radiocarbon dates and 2 sigma ranges for MV15C (bottom) and MV12A (top). The horizontal bar below the period 1962 to 1972 shows the potential range of overlap from cross-correlation analysis with COFECHA. (b) Overlap and pattern matching for composite δ^{18}O annual chronology and (c) annual maximum chronologies. Correlation for period of overlap is $r_{monthly} = 0.44$ ($p < 0.01$) for monthly δ^{18}O, $r_{minimum} = 0.65$ ($p < 0.01$), and $r_{maximum} = 0.25$ ($p < 0.18$). See text for details.

amplitude', which normalizes the maxima value of a given year with the value of the preceding wet season, and an 'annual amplitude', which is the difference between the maximum and minimum value of a given annual cycle and has the effect of normalizing the wet season δ^{18}O value. In nearly all cases, however, climate signal detection is not sensitive to the chosen annual metric (see below).

C.4.2 Climate analysis

Both MV12A and MV15A have interannual difference between wet-to-dry season δ^{18}O variability (σ) of 1.08‰, which is approximately 50% of their mean annual cycle amplitude. Most of the interannual variability in the chronologies come from variance in the annual maxima (MV12A = 0.99‰, MV15C = 0.83‰), suggesting that dry season variations largely determines the interannual anomalies recorded in these trees. MV12A shows a distinct change in the amplitude of the annual cycle after 1970, which is related to a change in both the wet season minimum and the dry season amplitude, suggesting a reduction in summer rainfall and an increase in dry season moisture prior to the early 1970s, if the cause was climatic.

Wet season δ^{18}O anomalies in MV12A are negatively associated with anomalous summer precipitation (δ^{18}O annual mean: $r = 0.46$, $R^2 = 0.22$, $p < 0.01$, $d.f = 22$; 1977 to 2000; δ^{18}O annual amplitude: $r = 0.536$, $R^2 = 0.29$, $p < 0.01$, $d.f = 22$), consistent with our heuristic model (Figure C.1) and with earlier findings [*Anchukaitis et al.*, 2007b]. Dry season amplitude anomalies in MV12A show a clear relationship to interannual climate variability in sea surface temperature anomalies (SSTA). ENSO years in the δ^{18}O chronology show a dry season isotopic enrichment (mean amplitude = 3.8‰) above the mean of both neutral and La Niña years (1σ; Figure C.2c). The local meteorological expression at Monteverde of strong ENSO events is a prolonged

period of elevated temperatures, particularly in 1982-1983, 1986-1988, and 1997-1998. These years correspond to discernable positive anomalies in the monthly δ^{18}O chronology (Figure C.2a), further consistent with our heuristic model (Figure C.1). In addition to dry season anomalies associated with strong El Niño events in 1983, 1987, and 1998, positive δ^{18}O anomalies are seen in $\sim$1960, 1969, 1993, and 1995. These anomalous peaks in dry season δ^{18}O correspond within age model error to years of significant positive ENSO and Western Hemisphere Warm Pool (WHWP; *Wang and Enfield* [2001]) temperature anomalies and spatial extent [*Wang and Enfield*, 2003]. 1993 and 1995 are also winters associated with a high index value of the North Atlantic Oscillation (NAO) [*Wang*, 2002].

In addition to evidence of the influence of local temperature and regional SSTA, NCEP/NCAR Reanalysis II data from the grid cell and geopotential height corresponding to the Monteverde Cloud Forest [*Kanamitsu et al.*, 2002] reveal that a weakening of the northeast trade winds consistently accompanies the δ^{18}O anomalies. Years with increased annual oxygen isotope cycle amplitude and anomalous maximum δ^{18}O values are related to dry season (February to April, 1979 to 2002) westerly zonal wind anomalies (Figure C.6). Because the slackening of the northeasterly tradewinds at Monteverde occur during both ENSO and WHWP warm events, the relationship between the dry season amplitude and zonal wind anomalies accounts for the largest portion of the total variance in δ^{18}O amplitude of any single local climate variable (δ^{18}O dry season amplitude/maximum: $r = 0.47$, $R^2 = 0.23$, $p = 0.01$, $d.f. = 22$; δ^{18}O annual mean $r = 0.53$, $R^2 = 0.29$, $p = 0.01$, $d.f. = 18$) (Figure C.6b). Winter (December through February) winds have a slightly stronger relationship with the δ^{18}O peak anomalies for El Niño events in 1983, 1987, and 1998, while winter-spring dry season (February through April) wind anomalies better account for peaks in 1993 and 1995. The regression statistics with δ^{18}O dry season amplitude improve somewhat ($r = 0.53$, $R^2 = 0.29$, $p = 0.01$, $d.f. = 18$) for boreal

winter (DJF) winds, but the increased skill is artificial and is leveraged by the anomalies associated with the three strong ENSO events of the period from 1979 to 2002.

Annual δ^{18}O cycle amplitude variability is related to sea surface temperature anomalies (SSTA) in both the eastern Pacific and the western Atlantic (Figure C.7). From the early 1970s to the end of the chronology in 2002, the amplitude of the δ^{18}O cycle is positively correlated ($r = 0.55$, $R^2 = 0.30$, $p < 0.01$, $d.f. = 28$) with an index of SSTA in the region of the WHWP (50 to 110^{o}W, 7 to 27^{o}N; *Wang and Enfield* 2001; *Kaplan et al.* 1998), which includes portions of the eastern equatorial Pacific, Caribbean, and tropical Atlantic (Figure C.7). Prior to that period (1949-1970), and concurrent with a period of reduced amplitude in the δ^{18}O annual isotope cycles, there is a weaker relationship with equatorial Pacific SSTA, and an enhanced association with tropical Atlantic SSTA (Figure C.7). A lagged cross-correlation analysis failed to find an improved match between either an index of the WHWP or NINO3.4 [*Kaplan et al.*, 1998], however, even when the MV12A chronology is incrementally adjusted up to 10 years backward or forward, a shift which is more than twice the age model error. The annual wet-dry amplitude time series from MV12 shows statistically significant spectral peaks [*Mann and Lees*, 1996] in the high frequency ENSO band ($\sim$ 3 years) as well as a trend component ($>$40 years). The MTM spectrum from MV15C alone shows no significant peaks.

Correlation between the annual δ^{18}O chronology from Monteverde and the dry season 850mb ($\sim$1500m) zonal wind field from NCEP Reanalysis [*Kanamitsu et al.*, 2002] shows coherent regions of positive correlation (increases in δ^{18}O are therefore associated with weaker tradewinds) over the WHWP and the central and eastern Pacific (Figure C.8). Correlations of the opposite sign exist through the tropical equatorial Atlantic stretching from Brazil to west Africa. Unlike the SST field, the pattern of correlations between

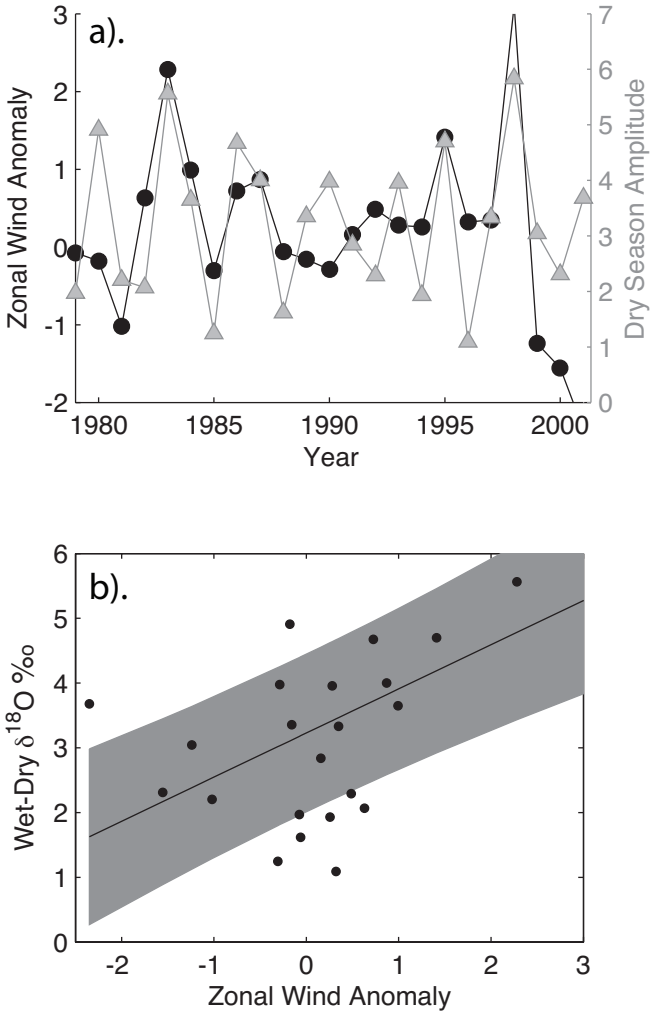

Figure C.6: Zonal wind anomalies and annual wet-dry season $\delta^{18}O$ amplitude from MV12A. (a) Temporal covariability of NCEP Reanalysis 850mb zonal wind anomaly [*Kanamitsu et al.*, 2002] corresponding to the Monteverde Cloud Forest and the annual oxygen isotope anomaly. Positive wind anomalies (weaker tradewinds) are associated with enriched $\delta^{18}O$ values and drier conditions. Several peaks (1983, 1987, and 1998) correspond to ENSO events, whereas other (1993, 1995) are not. El Niño tradewind anomalies occur primarily during winter (December-February) while non-ENSO anomalies occur in spring (February-May). The 1993 wind anomaly occurs in the dry season to wet season transition in May, and is therefore obscured by the winter dry season mean shown here. (b) Spring wind anomalies account for 23% of the variance in the $\delta^{18}O$ series ($p = 0.03$). Because they strongly covary, largely with the occurrence of warm ENSO events, temperature and relative humidity display similar correlation patterns.

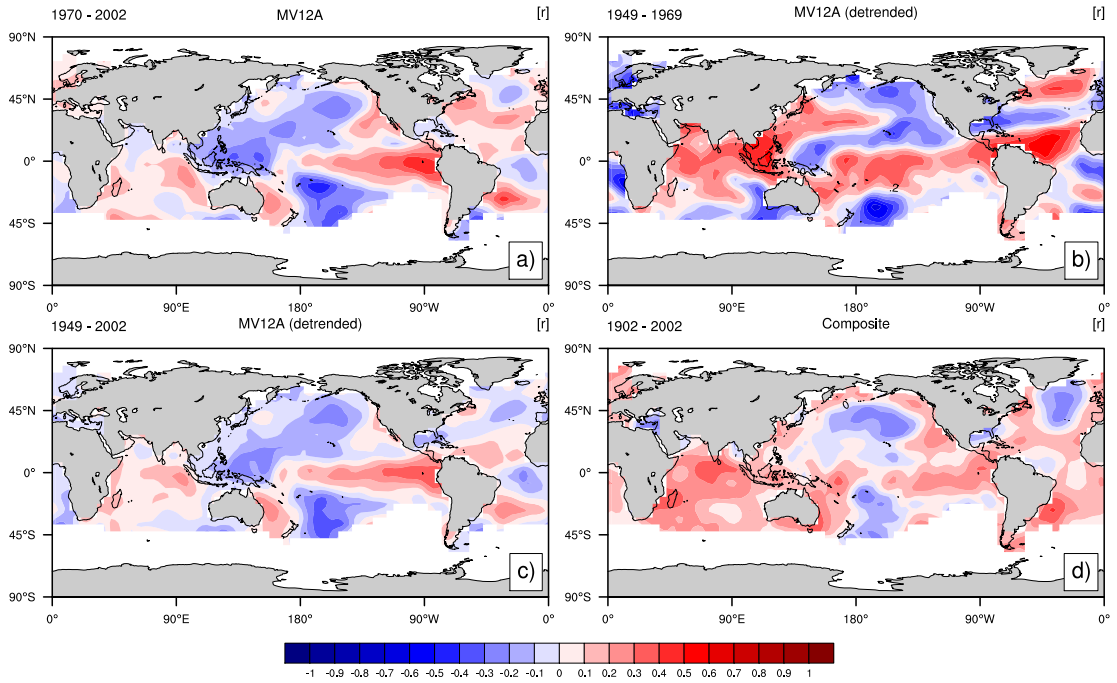

Figure C.7: Field correlations between Monteverde dry season δ^{18}O amplitude and dry season (February to April) sea surface temperature anomalies from *Kaplan et al.* [1998]. Correlations with mean and maximum δ^{18}O show similar patterns. (a) Correlation field for 1970 to 2002, a period of high amplitude the δ^{18}O chronology from MV12A, related to eastern equatorial Pacific and tropical Atlantic SSTA. (b) The structure of the early period (1949 to 1969) δ^{18}O-SSTA correlations are associated with the Atlantic SST-zonal wind tripole pattern [*Seager et al.*, 2000]. (c) Detrended full chronology from MV12A shows the combined influence of Pacific and Atlantic SSTA. Correlations between the MV12A δ^{18}O chronology and the SST field without detrending have a stronger expression in the Indian Ocean, similar to (d), the correlation of SSTA with the full composite (MV12A+MV15C) dry season δ^{18}O chronology. Significance levels for 1970 to 2002 are 0.34 ($p < 0.05$) and 0.27 ($p < 0.05$) for 1949 to 2002.

zonal winds and δ^{18}O appears to be stable over the period covered by the Reanalysis and Reanalysis II datasets and our isotope chronology (1979 to 2002; 1948 to 2002; *Kalnay et al.* [1996]; *Kanamitsu et al.* [2002]).

C.5 Discussion

C.5.1 Annual and interannual climate patterns

Annual δ^{18}O cycles can be successfully detected in both MV12 and MV15, although the age model for MV15 is less secure due to the reduced amplitude of the annual cycle, the slower growth rate of the tree, and the wide range of the calibrated radiocarbon dates on the cores. Annual maximum δ^{18}O and the annual oxygen isotope cycle amplitude show an upward trend over the period 1949 to 2002 in MV12A, which is caused almost entirely by the change in the variance of the annual cycle that occurs in the late 1960s. Local summer precipitation is a consistent influence on the annual amplitude and is similarly associated with the annual mean δ^{18}O value. Interannual variability in dry season amplitude is associated with positive SSTA in the WHWP and ENSO regions, and directly related to the strength of the trade winds. Trade wind strength in turn is related to moisture advection over the continental divide.

The trend in the number of days without rainfall (in runs $>$ 5 days) identified by *Pounds et al.* [1999] and *Pounds et al.* [2006] as being indicative of a reduction in cloud cover and an elevated orographic cloud base at Monteverde appears to be a result of (1) the rapid increase in the number of annual dry days which began with the strong 1983 El Niño and (2) the occurrence of long periods of drought during the 1998 dry season, also associated with ENSO. Obvious peaks in the number of consecutive dry days also occur during other El Niños, particularly in 1987 and concurrent with the subsequent extinction of the Monteverde Golden Toad. Over the period covered by both the instrumental

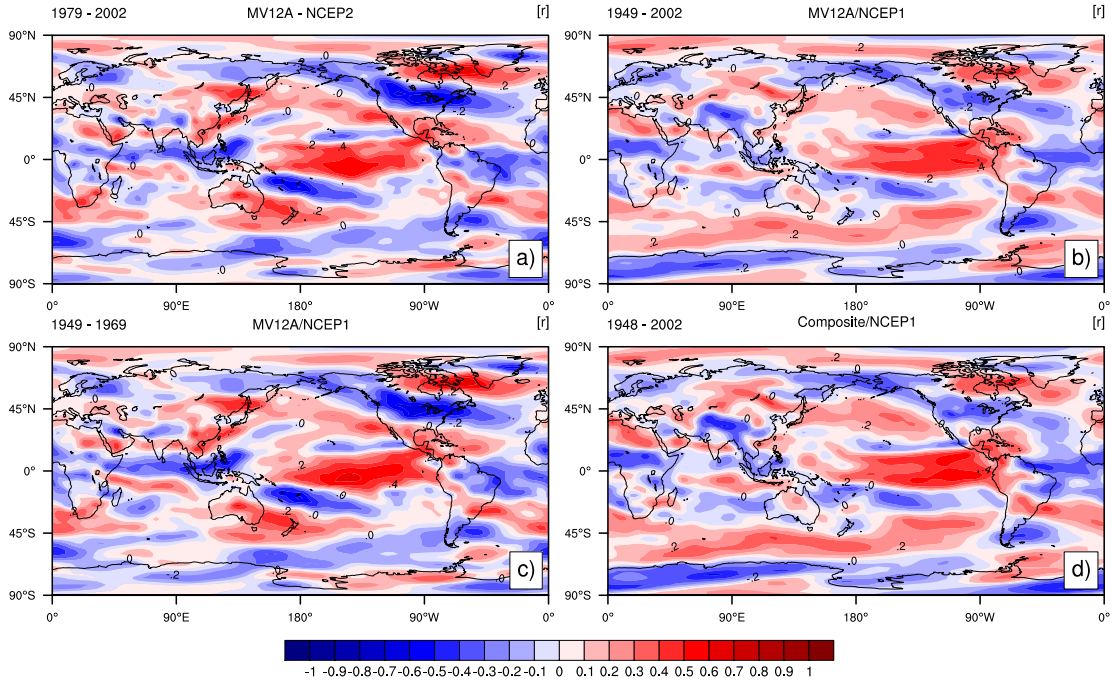

Figure C.8: Field correlations between Monteverde dry season δ^{18}O amplitude and dry season (February to April) zonal wind anomalies from *Kalnay et al.* [NCEP1: 1996] and *Kanamitsu et al.* [NCEP2: 2002]. The correlations are nearly identical if mean or maximum δ^{18}O is used. Patterns are broadly similar irrespective of the time period and the generation of NCEP data. (a) The period 1979 to 2002 covered by the chronology from MV12A and Reanalysis 2 [*Kanamitsu et al.*, 2002]. (b) The full period (1948 to 2002) over which MV12A and NCEP Reanalysis [*Kalnay et al.*, 1996] overlap. (c) The earlier period of the MV12A δ^{18}O chronology, during which time Atlantic SSTA are the most important remote forcing of dry season hydroclimate at Monteverde. (d) The composite δ^{18}O chronology with the overlapping NCEP Reanalysis data (1948 to 2002). Significance levels for 1979 to 2002 are 0.39 ($p < 0.05$) and 0.27 ($p < 0.05$) for 1949 to 2002.).

weather observations from Monteverde (1977 to 2000) and our δ^{18}O chronology, there is no discernable long-term upward trend in annual oxygen isotope values, nor the overall annual maxima (Figure C.5a,c). Instead, the isotope chronology is dominated by the positive δ^{18}O anomalies associated with ENSO years. Large amplitude δ^{18}O cycles in 1983, 1987, and 1998 are associated with an increased number of consecutive dry days and positive local temperature anomalies and correspond to El Niño events. In these years, periods of dry season drought (consecutive dry days) increase and there are temperature anomalies of a degree Celsius or more [*Pounds et al.*, 1999]. On the other hand, two dry season peaks in the isotope chronology in 1993 and 1995 are not obviously anomalous in either the local temperature observations nor dry-day calculations. They do however correspond to late spring weaker zonal winds, and are years of warmer than average temperatures in the Atlantic warm pool [*Wang and Enfield*, 2003] and years of high index values for the NAO [*Wang*, 2002]. This follows from our finding that the climate phenomenon which is most consistently related with dry winters at Monteverde is the slackening of the northeasterly trade winds and a reduction in moisture inputs across the continental divide.

The largest positive δ^{18}O anomalies are also those which correspond to both warm ENSO and large Western Hemisphere Warm Pool SSTAs in 1983, 1986-1987 and 1998 [*Wang and Enfield*, 2001, 2003], as well as other notable events within age model error at $\sim$1958, 1969, 1993, and 1995. Indeed the spatial pattern of δ^{18}O-SSTA correlation over the period from at least the late 1960s to the present suggests the dominant SST forcing on local conditions at Monteverde is related to same-sign anomalies in the WHWP spanning the Central American Isthmus and into the eastern equatorial Pacific cold tongue. However, the weakening in the correlation between WHWP temperatures and dry season conditions prior to that period, which does not appear to be the result of age

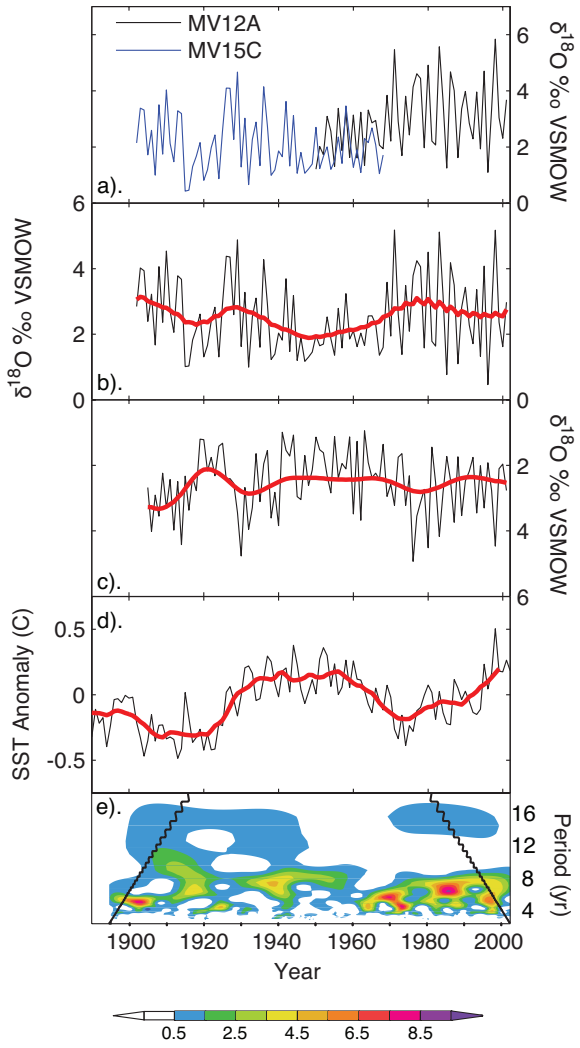

Figure C.9: Composite oxygen isotope chronology from MV12A and MV15C. (a) Dry season amplitude overlap based on radiocarbon dates and crosscorrelation pattern matching between the two chronologies (see also Figure C.5). (b) Composite detrended dry season δ^{18}O amplitude (normalized dry season). Smoothed red line is the leading reconstructed component from Singular Spectrum Analysis (SSA; M = 21) associated with the low-frequency variability and trend (c) Detrended composite annual δ^{18}O amplitude (normalized wet season) series and the leading reconstructed component from SSA, which has a periodicity of $>$40 years. (d) Atlantic Multidecadal Oscillation Index derived from *Kaplan et al.* [1998]. A warm period in the Atlantic between 1940 and 1970 occurs during a cold period in the Pacific, and with a period of decreased amplitude in the composite and MV12 δ^{18}O chronologies from Monteverde. (e) Wavelet analysis [*Torrence and Compo*, 1998] of tropical Pacific SSTA (5^{o}S- 5^{o}N, 110^{o}W- 170^{o}W) [*Kaplan et al.*, 1998]. Time-frequency plot is developed using a Morlet wavelet ($\omega_0 = 6$). Diagonal black lines show the time-frequency region where zero-padding influences the power spectrum.

model error, and the change in the spatial structure of the correlation pattern, may suggest a change in the relationship between the ocean-atmosphere conditions forcing dry season climate at Monteverde. Even more interestingly, the correlation between the δ^{18}O time series and the concurrent zonal wind field retains its spatial pattern and magnitude (Figure C.8), suggesting again that the most stable and proximal control on dry season moisture advection and cloudiness at Monteverde is the strength of the northeasterly trade winds.

The change in the late 1960s and early 1970s in the amplitude of the annual δ^{18}O cycles cycles in MV12A and the resulting upward trend is caused by an increase in the mean annual minimum values of the annual cycles as well as a reduction in the magnitude of the dry season δ^{18}O enrichment. The pairing of the increase in the annual minimum with a smaller difference between wet season δ^{18}O and the subsequent dry season annual minimum in midcentury leads to a rising trend in the annual amplitude (Figure C.9a) in the time series from MV12A and in the composite chronology over the period from the 1930s and 1940s to the present that is caused primarily by the relatively sharp change between 1960 and 1970. According to our heuristic model (Figure C.1), increases in the minimum annual δ^{18}O and a reduction in the annual amplitude is related to an overall drier wet season and a wetter (or cloudier) dry season.

C.5.2 Climate and ecological change at Monteverde

Most of the long-term trend over the last several decades as detected in our isotopic record from *Pouteria* is due to a change in the amplitude of the annual δ^{18}O cycles that occurs around 1970. Variability at the interannual scale dominates the dry season signal during the period of increased ENSO variance since the mid 1970s, with 1983, 1987, and 1998 as the three driest winters in the last three decades. Spectral analysis confirms statistically significant canonical ENSO band power. The period from 1986 to 1988, associated with

the strong El Niño event, appears to be the driest in at least the last 50 years, with reduced cloudiness and moisture inputs during the two dry seasons bracketing an abnormally dry wet season. If the absolute age model of MV15C is correct, this period is among the driest in the last century. This observation from the isotope record is confirmed by the recollections of a field biologist working in Monteverde at the time [*Crump*, 2000]. This suggests that the proximal cause of the well-documented extinction of the Monteverde Golden Toad [*Pounds and Crump*, 1994; *Pounds et al.*, 1999] was the combination of the abnormally strong ENSO-forced dryness and the lethality of the introduced fungus *Batrachochytrium dendrobatidis* which causes chytridiomycosis, and eventually death, in amphibians [*Crump*, 2000; *Lips et al.*, 2003, 2006]. It is possible that the fungus may have already been present in Monteverde prior to 1986 [c.f *Puschendorf et al.*, 2006] and that physical stresses or behavioral changes associated with the anomalous dry conditions during the 1987 ENSO event created the conditions for a nonlinear interactions between environment, disease vectors, and interannual climate [*Pounds and Crump*, 1994; *Bosch et al.*, 2007].

Nair et al. [2003] and *Lawton et al.* [2001] used a regional atmospheric model to demonstrate that deforestation in the tropical lowland upwind from the Monteverde Cloud Forest could potentially result in increased cloud base height. *Pounds et al.* [2006] have subsequently argued that the major period of deforestation in the San Carlos Plains in lowland Atlantic Costa Rica occurred too early and would not in any case have forced sufficient changes in cloud formation to account for the change in dry season moisture inferred from the daily meteorological records during the 1980s and 1990s. Our δ^{18}O chronology is not sufficiently anchored in time to detect potential changes in dry season climate associated with earlier periods of deforestation prior to the $\sim$1950s, and the clearest evidence of climate variability is at interannual time scales associated with

ENSO. However, we interpret the isotope evidence from MV12A to indicate that the most important shift in climate at Monteverde in the last several decades was primarily related to the change in annual amplitude that occurred in the late 1960s and early 1970s. The timing of this change suggests two possible causes. As discussed further below, the rapid shift in δ^{18}O amplitude occurs at approximately the same time as a shift from warm to cold conditions in the tropical Atlantic and just slightly before a change from cold to warm conditions in the Pacific. Alternatively, from the 1960s through the 1970s, deforestation rates in Costa Rica peaked [*Rosero-Bixby and Palloni*, 1998], and could have contributed to mesoscale alterations of boundary layer interactions sufficient to influence downwind montane cloud formation and base heights, as suggested by the simulation modeling by *Nair et al.* [2003].

The relative suddenness of the change is therefore suggestive of either a large-scale, substantial shift in climate or an ecological change (either human-mediated or natural) in the local or regional environment. With our current δ^{18}O chronology, we cannot rule out either cause, nor can we eliminate the possibility that land use or ecological changes in the immediate vicinity of the tree that could have changed its local hydrological conditions. Isotope chronology replication and temporal extension will be necessary to better resolve questions of natural and anthropogenic climate change and variability at Monteverde.

C.5.3 Uncertainty and potential biases

While high resolution oxygen isotope measurements allow us to resolve the annual cycle of water use by cloud forest trees, and therefore to establish chronological control even in the absence of tree-rings, there are a number of limitations and uncertainties in the record that could bias the climatic interpretation from the δ^{18}O time series. Some of the largest uncertainties could be associated with potential errors in the age model. In the

case of MV12A, the use of high-precision, post-bomb radiocarbon measurements helps to constrain the chronology and confirmed the age model established using the annual δ^{18}O cycles. For MV15C, the radiocarbon dates alerted us to the apparent growth hiatus and helped us delimit the most probable time span covered by the isotope time series from the core. However, the limitation of $\Delta^{14}C$ calibration over the recent historical period prevents us from achieving a high-precision chronology from the radiocarbon measurements alone, despite the application of Bayesian statistics.

Our analysis of both local climate variability and its association with broad-scale forcing at Monteverde is necessarily tentative. Our understanding of the physical (climate, hydrology) and biological controls, across a range of spatial and temporal scales, on the eventual δ^{18}O of wood in cloud forest trees is still rudimentary. Moreover, analytical requirements thus far limit the degree of replication and development of multiple overlapping proxy chronologies that is *de rigueur* in traditional approaches to dendrochronology, although tree-ring isotope series typically have a higher signal-to-noise ratio than ring width series [*McCarroll and Pawellek*, 1998; *Gagen et al.*, 2004]. As a consequence, we must assume that age model error exists and could be substantial enough to degrade our high-frequency climatic analysis. There are also potential individual tree-specific responses that are present in our isotope chronology that may not represent either local or global climate and which potentially bias our interpretation of temporal trends in our record. For example, because of the short period of the hypothesized overlap between MV12A and MV15C, it is not possible to definitively establish the extent to which the lower amplitude annual δ^{18}O cycles in the outer portion of MV15 also represents a reduced climate seasonality at that time, or whether it is the result of the relative topographic position, hydrology, or microsite conditions. Similar uncertainties apply to the interpretation of low frequency variability in δ^{18}O amplitude

within MV12A. Analysis of additional samples which span this period can aid in more distinguishing climatological from ecological or biological causality.

Interestingly, our two *Pouteria* cores show quite different behavior approaching the center of each tree. MV12A has a reduction in the amplitude of the annual cycle, which is not apparently related to a reduction in growth rate nor a sampling bias. MV15C shows the opposite behavior, with an increase in annual $\delta^{18}O$ amplitude and a much higher growth rate. In the application of stable carbon isotopes to dendroclimatology, a 'juvenile effect' is often observed, which is characterized by more depleted $\delta^{13}C$ values caused by young subcanopy trees using already depleted CO_2 resulting from organic respiration [*McCarroll and Loader*, 2004]. *Treydte et al.* [2006] identified what they believed to be a juvenile trend in $\delta^{18}O$ in montane forests in Pakistan characterized by enriched oxygen isotope ratios. At Monteverde, and in tropical trees in general, we hypothesize that the juvenile trend might be manifest as an increased annual $\delta^{18}O$ amplitude, as younger trees would not have the fully developed root system of mature canopy trees, and would therefore rely on shallow soil water with short residence times and minimal mixing of distinct meteoric waters. This could be the cause of the large amplitude cycles in the inner most portion of MV15C, and might be reflected in the magnitude of the annual cycle in the *Ocotea tenera* analyzed by *Anchukaitis et al.* [2007b]. The reduced cycles in the deepest part of the core from MV12A, however, appear to be related to an environmental or climatic cause, and are not consistent with a juvenile effect.

The change from low to high amplitude annual cycles which occurs in the 1960s might have several causes, and we cannot rule out a biological or ecological influences unrelated to climate or analytical or sampling bias. However, the change in amplitude is separately observed in both cores, before the composite mean chronology is created. Furthermore, in MBV12A, the reduction in amplitude in the early part of the chronology

is not consistent with a hypothetical juvenile effect. These lines of evidence, in addition to the observed relationships at interannual time scales between climate and δ^{18}O, suggest a potential climatic cause.

C.5.4 Multidecadal dynamics

The timing of the change from low to high amplitude δ^{18}O cycles in the late 1960s coincides with the change from a warm to cold phase of the the Atlantic Multidecadal Oscillation [AMO *Enfield et al.*, 2001; *Dong et al.*, 2006], a decadal-scale oscillation toward an increase in interannual band (ENSO) variance in the tropical Pacific [*Gu and Philander*, 1995; *Wang and Wang*, 1996; *Torrence and Compo*, 1998; *Torrence and Webster*, 1999; *Dong et al.*, 2006], and a change in the seasonality of ENSO [*Mitchell and Wallace*, 1996] (Figure C.9d,e). When the full composite δ^{18}O chronology is considered, a second inflection point marking the change from higher to lower amplitude annual isotope cycles in the earliest part of the 20th century is detectable around ∼1930, which is coincident within age model errors with prior mode shifts in the Pacific and Atlantic. These observations are not inconsistent with an interpretation of the midcentury changes in δ^{18}O amplitude as reflecting the influence of multidecadal changes in the broad-scale forcing in the Atlantic and Pacific affecting the local climate conditions at Monteverde.

Are these temporal patterns in the δ^{18}O chronology consistent with the climatic consequences of a change from a warm (cold) Atlantic (Pacific) to a cold (warm) Atlantic (Pacific)? First, we expect that dry season moisture in the period from 1949 to 1970 in MV12A (or, extended to ∼1930 to 1970 if the composite chronology is considered) should be increased relative to the more recent period, since the dry season δ^{18}O amplitude is reduced. An examination of the differences in February to April 850mb winds (not shown) reveals stronger northeasterly trade winds over Costa Rica and the

central and eastern Pacific in the earlier period compared to the later, consistent with our heuristic model and our analysis of the interannual controls on dry season δ^{18}O. This might also be consistent with that observation that at the interannual scale, a cold Pacific was associated with greater moisture advection via the northeasterly trade winds. When forced by warmer tropical Atlantic SSTs, coarse-resolution fast GCM (FOAM) simulates an increase in precipitation over southern Central America and northern South America at the peak of the dry season (February through April) [*Wu et al.*, 2007], which would also be expected to suppress maximum annual δ^{18}O values in trees at Monteverde.

However, evidence for a climatic cause for the increased δ^{18}O minimum wet season values during the middle part of the century is equivocal. The two climate stations from the Pacific side of northwestern Costa Rica (GHCN: Monteverde and Puntarenas) that span the period of the transition do in fact show an increase in precipitation between 1960 and 1970 [*Fleming*, 1986; *Peterson and Vose*, 1997]. The Monteverde climate station (which is different than the Campbell station, at lower elevation and not in the cloud forest), shows an increase in mean summer precipitation of approximately 200 mm over the period 1965, which would translate into a change in δ^{18}O of up to $\sim$1.2‰, which is slightly larger than is observed in MV12A and in the composite chronology. Gridded precipitation data [*Mitchell and Jones*, 2005], however, show a slight *increase* in late summer precipitation, the opposite of what the isotopes and limited station data suggest. While a decrease in late wet season (September-November) precipitation on the Pacific side of Central America is simulated for warm periods in the tropical North Atlantic using the FOAM climate model [*Wu et al.*, 2007], other general circulation model (GCM) simulations predict a strong increase in summer precipitation over all of Central America and Caribbean in response to a warming of the Atlantic associated with the positive phase of the AMO [*Sutton and Hodson*, 2005]. Different models and different data lead to

different interpretations of midcentury climate in western Costa Rica.

The correlation between the δ^{18}O chronology from MV12A and the SSTA field (Figure C.7) for the period 1949 to 1969 resembles the tripole zonal banding observed in SST and wind fields that are part of the coupled spatial expression of the North Atlantic Oscillation (NAO) [*Seager et al.*, 2000] with SSTA. The warm phase of the AMO is related to patterns similar to the negative phase of the NAO [*Grosfeld et al.*, 2007]. The correlation structure between Monteverde winter dry season climate and Atlantic sea surface temperatures therefore suggests that during the midcentury period coinciding with an observed warm phase of the AMO and the reduction in the interannual SST variability in the eastern tropical Pacific, it was Atlantic Ocean variability that determined the year-to-year changes in winter cloudiness. We hypothesize then that positive (negative) NAO anomalies would result in the weakening (strengthening) of the trade wind flow across Central America and a decrease (increase) of moisture advection to the leeward side of the Monteverde Cloud Forest and a positive (negative) δ^{18}O anomaly in the isotope chronology. Warm subtropical waters in the Atlantic lead to weaker trade winds, which would be reflected in enriched δ^{18}O for that year in the Monteverde isotope record. Following the shift from warm to cold AMO in the 1960s and the increase in equatorial Pacific SSTA variance, interannual variability at Monteverde predominantly reflects ENSO and the tropical Pacific. Mechanistically, at least, this interpretation would not be inconsistent with our model (Figure C.1), our interpretation of the interannual controls on cloud forest tree δ^{18}O, and observed and modeled climate dynamics. However, potential patterns in the chronology not related to climatic causes prevent us from proving these linkages with any great certainty.

Whether variability in the Pacific drives concomitant changes in the Atlantic, or vice versa, remains an open question. The common view has been that ENSO influences the

Atlantic via atmospheric teleconnections [c.f. *Latif*, 2001]. *Wang and Enfield* [2001] have shown that warm ENSO anomalies influence the Western Hemisphere Warm Pool via the connection of the anomalous Walker circulation to changes in the strength of the Atlantic subtropical high. Similarly, *Giannini et al.* [2001] hypothesized that ENSO influenced tropical Atlantic variability through the stabilization of the tropical atmosphere via the propagation of the warming signal through the troposphere. More recent model results focusing on the role of the Atlantic Ocean suggest that changes in the Meridional Overturning Circulation (MOC) in the North Atlantic [*Knight et al.*, 2005] can influence the amplitude of interannual and interdecadal variability in the Pacific. *Dong et al.* [2006] used a coupled ocean-atmosphere GCM with an imposed Atlantic SSTA forcing to mimic the AMO. In these simulations, easterly surface wind anomalies over the central and western Pacific forced by latent heat flux in the tropical North Atlantic deepened the western Pacific themocline, stabilizing the ocean-atmosphere coupled instability in the tropical Pacific and reducing ENSO variance. The relative directional influence of one ocean basin on the other may in fact be time scale dependent. These and numerous other studies point to extant uncertainty regarding the forcing mechanisms for the observed association between Atlantic and Pacific variability at a variety of time scales.

C.5.5 Future applications

Costa Rica, and Central America in general, sit at the very crossroads of the complex and still unresolved interaction between the Atlantic and Pacific Ocean. Our results here suggest that neotropical cloud forests might be sensitive to changes in the ocean-atmosphere interactions across the isthmus and could therefore be optimal locations to develop high-resolution paleoclimate proxies. Climate reconstructions from this region could provide the necessary long-term context for improving our understanding of the

feedbacks and coupling between the two oceans at interannual, decadal, and perhaps multidecadal time scales. The distribution of montane cloud forests along the American cordillera from Mexico through northern Argentina provides climate-sensitive locations at which a network of paleoclimate proxy reconstruction could be developed, in order to understand local and interannual changes in cloud forest hydroclimatology, as well as potential interactions between the tropical Atlantic and the Pacific on multidecadal time scales.

C.6 Conclusions

We have used a high-resolution, annually-resolved δ^{18}O record from tropical trees without rings from Monteverde to reconstruct temporal change in local climate during the last century and identity the relationships between cloud forest hydroclimatology and large-scale modes of ocean-atmophere variability. One sample (MV12A) is securely dated using annual cycles in δ^{18}O and high-precision radiocarbon measurements. A second floating chronology (MV15), relatively dated using Bayesian analysis of multiple radiocarbon dates, likely overlaps with the latter half of our securely dated δ^{18}O chronology, and can be used to tentatively extend our record of climate variability at Monteverde through the 20th century. The results of our analysis suggest the following conclusions:

- Annual δ^{18}O cycles in the radial growth of *Pouteria* (Sapotaceae) at Monteverde can be used to develop chronological control in trees without identifiable annual growth bands.
- Local meteorological data suggest that interannual variability in dry season δ^{18}O variability is positive related to temperature and negatively related to moisture

advection via trade wind strength. As in our previous study [*Anchukaitis et al.*, 2007b], wet season δ^{18}O is related to summer rainfall anomalies.

- El Niño years are associated with anomalously enriched δ^{18}O peaks in the stable isotope chronology. The years of the largest anomalies – 1969, 1983, 1987, 1998, and possibly $\sim$ 1958 – are years in which there were both warm ENSO events and a subsequent positive SSTA anomaly in the Western Hemisphere Warm Pool. The years associated with the 1986-1987 ENSO event are the driest period in our isotope chronology since at least 1949, and potentially one of the driest in the last century, although with considerable uncertainty at the longer timescale. The extinction of the Monteverde Golden Toad therefore appears to have coincided with one of the most severe, extended droughts in the last several decades or more.

- A change in the amplitude of the annual δ^{18}O cycle occurs between 1960 and 1970. There are multiple potential biological, ecological, analytical, and climatic factors that might have contributed to this change. The timing of the change is consistent with the timing of a switch from warm to cool SSTs in the Atlantic and with a change toward increased interannual (ENSO) variance in the Pacific. If the cause of the shift is indeed climatic, this could suggest a relationship between interannual to multidecadal variability in the δ^{18}O chronology of cloud forest trees at Monteverde and patterns of Atlantic and Pacific ocean-atmosphere variability.

- Neotropical cloud forests, situated as they are at the boundary of two oceans and influenced by broad-scale modes of climate variability in each, may be promising sites from which to develop records of past climate in support of research to better understand Pacific interannual variability and perhaps interbasin climate interactions and coupling across a range of time scales. The development of high

resolution stable isotope proxies from the mountains of Central America could help address outstanding uncertainties and provide a validation target for coupled GCM experiments.

C.7 Acknowledgements

We are grateful for comments and suggestions from Julio Betancourt, Malcolm Hughes, Alan Pounds, Mary Gagen, Nat Wheelwright, Julie Cole, Jonathan Overpeck and Tim Shanahan. We benefitted tremendously from excellent laboratory and field assistance from John Buchanan, Mau-Chuang Foo, Lisa Wade, Frank Joyce, Rex Adams, Jim Burns, Arturo Cruz, Eladio Cruz, and Koky Porras. Technical instrumentation support and advice from Bruno Lavettre, David Steinke, and Ben McElhaney. We thank the Organization for Tropical Studies for help with permits and the Tropical Science Center (CCT) for access to the Monteverde Cloud Forest Reserve (Rafael Bolanos and Carlos Hernandez). This research was supported by a graduate training fellowship from the NSF IGERT Program (DGE-0221594) (to KJA), a Graduate Research Environmental Fellowship (to KJA) from the US Department of Energy, grants from the National Science Foundation: NSF/ATM-0349356 (CAREER to MNE) and NSF/ATM-0321348 (MRI), and a pilot grant from the Biogeography Specialty Group of the Association of American Geographers (AAG) to KJA.

C.8 References

Anchukaitis, K. J., M. N. Evans, T. Lange, D. R. Smith, D. P. Schrag, and S. W. Leavitt (2007a), Purity and isotopic results from a rapid cellulose extraction method for high-resolution isotope dendroclimatology, *Analytical Chemistry*, in preparation.

Anchukaitis, K. J., M. N. Evans, N. T. Wheelwright, and D. P. Schrag (2007b), Stable isotope chronology and climate signal in neotropical montane cloud forest trees, *J. Geophysical Research - Biogeosciences*, in preparation.

Barbour, M. M., J. S. Roden, G. D. Farquhar, and J. R. Ehleringer (2004), Expressing leaf water and cellulose oxygen isotope ratios as enrichment above source water reveals evidence of a Peclet effect, *Oecologia*, *138*(3), 426–435.

Bosch, J., L. M. Carrascal, L. Durán, S. Walker, and M. C. Fisher (2007), Climate change and outbreaks of amphibian chytridiomycosis in a montane area of Central Spain; is there a link?, *Proceedings of the Royal Society B: Biological Sciences*, *274*(1607), 253–260.

Bradley, R., M. Vuille, H. Diaz, and W. Vergara (2006), Threats to water supplies in the tropical Andes, *Science*, *312*(5781), 1755 – 1756, doi:10.1126/science.1128087.

Brendel, O., P. P. M. Iannetta, and D. Stewart (2000), A rapid and simple method to isolate pure α-cellulose, *Phytochemical Analysis*, *11*, 7–10.

Bronk Ramsey, C. (1995), Radiocarbon calibration and analysis of stratigraphy: the OxCal program, *Radiocarbon*, *37*(2), 425–430.

Bronk Ramsey, C., and B. van der Plicht, J.and Weninger (2001), 'Wiggle matching' radiocarbon dates, *Radiocarbon*, *43*(2 A), 381–389.

Brown, A. D., and M. Kappelle (2001), Introducción a los bosques nublados del neotrópico: una síntesis regional, in *Bosques nublados del neotrópico*, edited by M. Kappelle and A. D. Brown, pp. 25–40.

Bruijnzeel, L. A. (2001), Hydrology of tropical montane cloud forests: a reassessment, *Land Use and Water Resources Research*, *1*, 1–18.

Clark, K. L., N. M. Nadkarni, D. Schaefer, and H. L. Gholz (1998), Cloud water and precipitation chemistry in a tropical montane forest, Monteverde, Costa Rica, *Atmospheric Environment*, *32*, 1595–1603.

Clark, K. L., R. O. Lawton, and P. R. Butler (2000), The physical environment, in *Monteverde: Ecology and Conservation of a Tropical Cloud Forest*, edited by N. M. Nadkarni and N. T. Wheelwright, pp. 15–38, Oxford University Press, Oxford, United Kingdom.

Crump, M. (2000), *In Search of the Golden Frog*, University of Chicago Press.

Dong, B., R. Sutton, and A. Scaife (2006), Multidecadal modulation of El Niño-Southern Oscillation (ENSO) variance by Atlantic Ocean sea surface temperatures, *Geophys. Res. Lett.*, *8*, 03,405.

Enfield, D. B., A. M. Mestas-Nunez, and P. J. Trimble (2001), The Atlantic Multidecadal Oscillation and its relation to rainfall and river flows in the continental US, *Geophys. Res. Lett.*, *28*, 2077–2080.

Evans, M. N., and D. P. Schrag (2004), A stable isotope-based approach to tropical dendroclimatology, *Geochim. Cosmochim. Acta*, doi:10.1016/j.gca.2004.01.006.

Feild, T. S., and T. E. Dawson (1998), Water sources used by *Didymopanax pittieri* at different life stages in a tropical cloud forest, *Ecology*, *79*, 1448–1452.

Fleming, T. (1986), Secular changes in Costa Rican rainfall: Correlation with elevation, *Journal of Tropical Ecology*, *2*(1), 87–91.

Foster, P. (2001), The potential negative impacts of global climate change on tropical montane cloud forests, *Earth Science Reviews*, *55*, 73–106.

Gagen, M., D. McCarroll, and J. L. Edouard (2004), Latewood width, maximum density, and stable carbon isotope ratios of pine as climate indicators in a dry subalpine environment, French Alps, *Arctic Antarctic Alpine Research*, *36*, 166–171.

Galimberti, M., C. Bronk Ramsey, and S. Manning (2004), Wiggle-Match dating of tree-ring sequences, *Radiocarbon*, *46*(2), 917–924.

Gat, J. R. (1996), Oxygen and hydrogen isotopes in the hydrologic cycle, *Ann. Rev. Earth Planet. Sci.*, *24*, 225–262.

Giannini, A., J. Chiang, M. A. Cane, Y. Kushnir, and R. Seager (2001), The ENSO teleconnection to the tropical Atlantic Ocean: contributions of the remote and local SSTs to rainfall variability in the tropical Americas, *J. Climate*, *14*(24), 4530–4544.

Grissino-Mayer, H. D. (2001), Evaluating crossdating accuracy: a manual and tutorial for the computer program COFECHA, *Tree-Ring Research*, *57*(2), 205–221.

Grosfeld, K., G. Lohmann, N. Rimbu, K. Fraedrich, and F. Lunkeit (2007), Atmospheric multidecadal variations in the North Atlantic realm: proxy data, observations, and atmospheric circulation model studies, *Climate of the Past*, *3*(1), 39–50.

Gu, D. F., and S. Philander (1995), Secular changes of annual and interannual variability in the tropics during the past century, *J. Climate*, *8*(4), 864–876.

Haber, W. A. (2000), Plants and vegetation, in *Monteverde: Ecology and Conservation of a Tropical Cloud Forest*, edited by N. M. Nadkarni and N. T. Wheelwright, pp. 39–70, Oxford University Press, Oxford, United Kingdom.

Holmes, R. (1983), Computer assisted quality control in tree-ring dating and measurement, *Tree-Ring Bulletin*, *44*, 69–75.

Hua, Q., and M. Barbetti (2004), Review of tropospheric bomb ^{14}C data for carbon cycle modeling and age calibration purposes, *Radiocarbon*, *46*(3), 1273–1298.

Hua, Q., M. Barbetti, M. Worbes, J. Head, and V. A. Levchenko (1999), Review of radiocarbon data from atmospheric and tree ring samples for the period 1945-1997 AD, *IAWA Journal*, *20*(3), 261–283.

Ingraham, N. (1998), Isotopic variations in precipitation, in *Isotope tracers in catchment hydrology*, edited by C. K. J. McDonnell, Elsevier Press, Amsterdam, The Netherlands.

Ingraham, N., and R. Matthews (1990), A stable isotopic study of fog - The Point Reyes Peninsula, California, USA, *Chemical Geology*, *80*, 281–290.

Kalnay, E., et al. (1996), The NCEP/NCAR 40-year reanalysis project, *Bull. Amer. Meteorol. Soc.*, *77*(3), 437–471.

Kanamitsu, M., W. Ebisuzaki, J. Woollen, S. Yang, J. Hnilo, M. Fiorino, and G. Potter (2002), NCEP-DOE AMIP-II Reanalysis (R-2), *Bull. Amer. Meteor. Soc*, *83*(11), 1631–1643.

Kaplan, A., M. A. Cane, Y. Kushnir, A. C. Clement, M. B. Blumenthal, and B. Rajagopalan (1998), Analyses of global sea surface temperature 1856-1991, *J. Geophys. Res.*, *103*(C9), 18,567–18,589.

Knight, J., R. Allan, C. Folland, M. Vellinga, and M. Mann (2005), A signature of persistent natural thermohaline circulation cycles in observed climate, *Geophys. Res. Lett.*, *32*.

Lachniet, M. S., and W. P. Patterson (2002), Stable isotope values of Costa Rican surface waters, *Journal of Hydrology*, *260*, 135–150.

Latif, M. (2001), Tropical Pacific/Atlantic Ocean interactions at multi-decadal time scales, *Geophysical Research Letters*, *28*(3), 539–542.

Lawton, R. O., U. S. Nair, R. A. Pielke, and R. M. Welch (2001), Climatic impact of tropical lowland deforestation on nearby montane cloud forests, *Science*, *294*, 584–587.

Lieberman, D., M. Lieberman, G. Hartshorn, and R. Peralta (1985), Growth rates and age-size relationships of tropical wet forest trees in Costa Rica, *Journal of Tropical Ecology*, *1*(2), 97–109.

Lips, K., D. Green, and R. Papendick (2003), Chytridiomycosis in wild frogs from southern Costa Rica, *Journal of Herpetology*, *37*(1), 215–218.

Lips, K. R., et al. (2006), Emerging infectious disease and the loss of biodiversity in a Neotropical amphibian community, *Proc. U. S. Natl. Acad. Sci.*, *103*(9), 3165–3170.

Loope, L. L., and T. W. Giambelluca (1998), Vulnerability of island tropical montane cloud forests to climate change, with special reference to East Maui, Hawaii, *Clim. Change*, *39*, 503–517.

Mann, M. E., and J. M. Lees (1996), Robust estimation of background noise and signal detection in climatic time series, *Clim. Change*, *33*(3), 409–445.

McCarroll, D., and N. J. Loader (2004), Stable isotopes in tree rings, *Quat. Sci. Rev.*, *23*(7-8), 771–801.

McCarroll, D., and F. Pawellek (1998), Stable carbon isotope ratios of latewood cellulose in *Pinus sylvestris* from northern Finland: variability and signal-strength, *The Holocene*, *8*(6), 675–684.

Mitchell, T., and P. Jones (2005), An improved method of constructing a database of monthly climate observations and associated high-resolution grids, *Int. J. Climatol*, *25*(6), 693–712.

Mitchell, T., and J. Wallace (1996), ENSO Seasonality: 1950–78 versus 1979–92, *J. Climate*, *9*(12), 3149–3161.

Nair, U. S., R. O. Lawton, R. M. Welch, and R. A. Pielke (2003), Impact of land use on Costa Rican tropical montane cloud forests: Sensitivity of cumulus cloud field characteristics to lowland deforestation, *J. Geophys. Res.*, *108*.

Peterson, T. C., and R. S. Vose (1997), An overview of the Global Historical Climatology Network temperature database, *Bull. Amer. Meteorol. Soc.*, *78*, 2837–2849.

Pounds, J. A., and M. L. Crump (1994), Amphibian declines and climate disturbance - the case of the golden toad and the harlequin frog, *Conservation Biology*, *8*, 72–85.

Pounds, J. A., M. Fogden, and J. H. Campbell (1999), Biological response to climate change on a tropical mountain, *Nature*, *398*, 611–615.

Pounds, J. A., et al. (2006), Widespread amphibian extinctions from epidemic disease driven by global warming, *Nature*, *439*(7073), 161–167.

Poussart, P. F., M. N. Evans, and D. P. Schrag (2004), Resolving seasonality in tropical trees: multi-decade, high-resolution oxygen and carbon isotope records from Indonesia and Thailand, *Earth Planet. Sci. Lett.*, *218*(3-4), 301–316.

Puschendorf, R., F. Bolanos, and G. Chaves (2006), The amphibian chytrid fungus along an altitudinal transect before the first reported declines in Costa Rica, *Biological Conservation*, *132*(1), 136–142.

Reimer, P., T. Brown, and R. Reimer (2004a), Discussion: reporting and calibration of post-bomb 14 C data, *Radiocarbon*, *46*(3), 1299–1304.

Reimer, P., et al. (2004b), IntCal04 terrestrial radiocarbon age calibration, 0-26 Cal Kyr BP., *Radiocarbon*, *46*(3), 1029–1058.

Rhodes, A. L., A. J. Guswa, and S. E. Newell (2006), Seasonal variation in the stable isotopic composition of precipitation in the tropical montane forests of Monteverde, Costa Rica, *Water Resources Research*, *42*, W11,402, doi:10.1029/2005WR004535.

Robertson, I., C. A. Froyd, R. P. D. Walsh, D. M. Newbery, S. Woodborne, and R. C. Ong (2004), The dating of dipterocarp tree rings: establishing a record of carbon cycling and climatic change in the tropics, *J. Quaternary Science*, *19*, 657–664.

Roden, J. S., G. Lin, and J. R. Ehleringer (2000), A mechanistic model for interpretation of hydrogen and oxygen ratios in tree-ring cellulose, *Geochim. Cosmochim. Acta*, *64*, 21–35.

Rosero-Bixby, L., and A. Palloni (1998), Population and deforestation in Costa Rica, *Population & Environment*, *20*(2), 149–185.

Schmid, S. (2004), Water and ion fluxes to a tropical montane cloud forest ecosystem in Costa Rica, Master's thesis, University of Bern.

Seager, R., Y. Kushnir, M. Visbeck, N. Naik, J. Miller, G. Krahmann, and H. Cullen (2000), Causes of Atlantic Ocean Climate variability between 1958 and 1998, *J. Climate*, *13*, 2845–2862.

Still, C., P. Foster, and S. Schneider (1999), Simulating the effects of climate change on tropical montane cloud forests, *Nature*, *398*, 608–610.

Sutton, R. T., and D. L. R. Hodson (2005), Atlantic Ocean forcing of North American and European summer climate, *Science*, *309*, 115–118, doi:10.1126/science.1109496.

Torrence, C., and G. Compo (1998), A practical guide to wavelets, *Bull. Amer. Meteorol. Soc.*, *79*, 61–78.

Torrence, C., and P. J. Webster (1999), Interdecadal Changes in the ENSO–Monsoon System, *J. Climate*, *12*, 2679–2690.

Treydte, K., G. Schleser, G. Helle, D. Frank, M. Winiger, G. Haug, and J. Esper (2006), The twentieth century was the wettest period in northern Pakistan over the past millennium, *Nature*, *440*(7088), 1179–1182.

Verheyden, A., G. Helle, G. H. Schleser, F. Dehairs, H. Beeckman, and N. Koedam (2004), Annual cyclicity in high-resolution stable carbon and oxygen isotope ratios in the wood of the mangrove tree *Rhizophora mucronata*, *Plant Cell Environment*, *27*, 1525–1536.

Wang, B., and Y. Wang (1996), Temporal structure of the Southern Oscillation as revealed by waveform and wavelet analysis, *J. Climate*, *9*, 1586–1598.

Wang, C. (2002), Atlantic Climate Variability and Its Associated Atmospheric Circulation Cells, *J. Climate*, *15*(13), 1516–1536.

Wang, C., and D. Enfield (2001), The tropical Western Hemisphere Warm Pool, *Geophys. Res. Lett.*, *28*, 1635–1638.

Wang, C. Z., and D. B. Enfield (2003), A further study of the tropical Western Hemisphere Warm Pool, *J. Climate*, *16*, 1476–1493.

Westbrook, J. A., T. P. Guilderson, and P. A. Colinvaux (2006), Annual growth rings in a sample of *Hymenaea courbaril*, *IAWA Journal*, *27*(2), 193–197.

Wheelwright, N. T., and B. A. Logan (2004), Previous-year reproduction reduces photosynthetic capacity and slows lifetime growth in females of a neotropical tree, *Proceedings of the National Academy of Sciences*, *101*(21), 8051–8055.

Wu, L., F. He, Z. Liu, and C. Li (2007), Atmospheric teleconnections of tropical Atlantic variability: Interhemispheric, tropical–extratropical, and cross-basin interactions, *J. Climate*, *20*(5), 856–870.